Coastal Hazards Analysis of the West Basin Municipal Water District Ocean Water Desalination Project

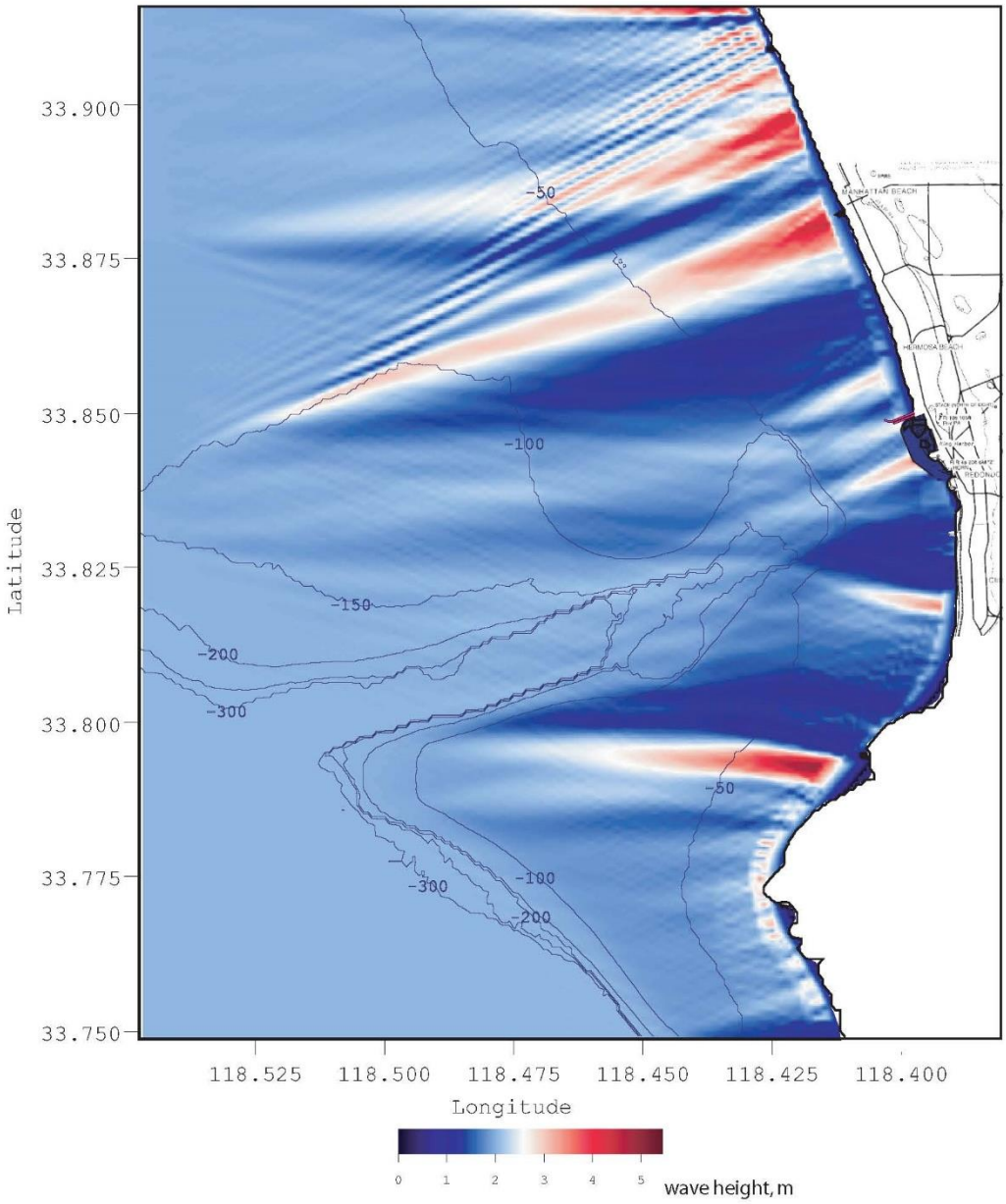

Prepared by:
Scott A. Jenkins, Ph. D.
Michael Baker International

12 July, 2016

Submitted to
Diane Gatza
Desalination Manager
West Basin Municipal Water District.

EXECUTIVE SUMMARY

Extreme wave and tsunami run-up and overtopping were analyzed for the ESGS North and ESGS South sites being proposed for with the West Basin Desalination Project. Hand calculations are given as a lowest order estimate of total water level at both sites, followed up by more exact calculations using the Coastal Evolution Model (CEM) software. Both hand calculations and CEM solutions are given for present sea level and for two extreme scenarios (maximum and minimum) of future sea level rise. Accounting for the spatial complexity of shoaling and run-up on the eroded beach profiles in front of the ESGS North and South sites produced the highest total water levels (TWL) on the bike trail revetment slopes that front both sites for all present and future sea level scenarios. However, the crest elevation of the bike trail is sufficiently high that only minor overtopping of about 0.4 feet (ft) to 1.4 ft occurs, and only then, during the most extreme future sea level rise scenario under CAT-OPC design guidance. The overtopping of the bike trail, however, is blocked by the sea wall at the ESGS North site, whose crest elevation is at h_c = +28 ft to + 29 ft Mean Lower Low Water (MLLW). Similarly, the vegetated berm and slopes at the ESGS South site prevent this small amount of overtopping of the bike trail from reaching the desalination facilities construction pad at +41 ft MLLW. Hence, both sites are protected against overtopping and flooding by the 1 percent extreme wave event, (a.k.a. the 100-year storm) even when superimposed on the highest predicted sea level for the next 50 years.

Site vulnerabilities to extreme tsunami were found to be more problematic, although the modeled tsunami scenario associated with a seismic-induced landslide on the east side of San Clemente Island has never been recorded throughout the Holocene to present. Tsunami run-up and TWL inundation calculations using the CEM software indicate that the bike trail will be overtopped by several feet of tsunami run-up at both sites during both present and future sea levels. At the ESGS North site, the overtopping will be blocked by the sea wall, but the over-pour flows will be free to flow around the southern flank of the sea wall and cause flooding of the pad on which the desalination facility is proposed to be built, which is at elevation +23 ft MLLW. At the ESGS South site, tsunami overtopping of the bike trail will run up on the vegetated slopes and berms that border the facilities construction pad, reaching peak run-up elevations of + 27.9 ft MLLW. However, the facilities construction pad is at + 41 ft MLLW, and hence, the site elevation of the desalination facilities at the ESGS South site will be sufficiently high to avoid flooding by tsunami run-up, even for the highest forecasted sea levels for 2065.

The West Basin Desalination Project proposes no structures that would influence either sediment transport or wave shoaling, breaking, and run-up processes. Therefore, the project causes no impacts to the adjacent shoreline due to sea level rise, or wave-induced erosion from wave diffraction and reflection from the major components of the desalination project and associated structures.

Table of Contents

List of Figures

List of Tables

List of Appendices

Coastal Hazards Analysis of the West Basin Municipal Water District Ocean Water Desalination Project

Prepared by:
Scott A. Jenkins, Ph. D.

1. Introduction

The West Basin Municipal Water District (District) proposes to build and operate a seawater reverse osmosis (SWRO) desalination plant in the southern portion of Santa Monica Bay, which would supplement the District's water resources. The proposed desalination facility site is located at the existing 33-acre NRG El Segundo Generating Station (ESGS). Two potential scales for project build-out at either site are possible:

- A 20 million gallons per day (mgd) project discharging 20.9 mgd of brine at 68 parts per trillion (ppt) from the RO facilities of the desalination plant and 0.1 mgd of West Basin recycled blowdown water at 35 ppt, resulting in a total discharge rate of 21 mgd with 67.84 ppt salinity end of pipe;
- A 60 mgd project discharging 62.7 mgd of brine at 68 ppt from the RO facilities of the desalination plant and 0.3 mgd of West Basin recycled blowdown water at 35 ppt, resulting in a total discharge rate of 63 mgd with 67.84 ppt salinity end of pipe.

Presently, these sites offer existing infrastructure that includes a sea water intake at: 11S 367,576 m E - 3,752,769 m N; and a seawater discharge at: 11S 367,720 m E – 3,752,820 m N (Figure 1.1).

On the ESGS property, two project sites are being considered: 1) the ESGS North site; 2) the ESGS South site. Figures 1.2 and 1.3 show proposed layouts for components of the desalination facility at the ESGS North site for the 20-mgd and 60-mgd scale projects, respectively. The ESGS North site is an approximate 8-acre area located in the middle of the ESGS property which was the previous site for Units 3 and 4 that were recently decommissioned (December 2015). The ESGS North site is bounded on the east by Vista Del Mar, on the west by the Marvin Braude Coastal Bike Trail, on the south by the ESGS South site, and on the north by newly commissioned Units 5, 6, and 7. Due to its previous use for Units 3 and 4, virtually the entire site is a level pad at approximate elevation Z = +23 ft MLLW. The important features with respect to a coastal hazards analysis site is the presence of a sea wall immediately landward from the bike trail. The elevation of the crest of this sea wall ranges from Z = +28 ft MLLW at the north end rising slightly to Z = +29 ft MLLW at the south end which is bounded by a fence along the boundary with the ESGS site. Other significant shoreline fortifications are the bike trail itself which is perched atop a rip-rap revetment at elevation Z = +22 ft MLLW at the

north end of the sea wall and elevation Z = +23 ft MLLW at the south end of the sea wall. The revetment fortifies a low bluff that boarders the back beach.

Figures 1.4 and 1.5 show proposed layouts for components of the desalination facility at the ESGS South site for the 20-mgd and 60-mgd scale projects, respectively. This site is bounded on the east by an existing cutter oil tank which will remain in operation, on the west by the Marvin Braude Coastal Bike Trail, on the south by 45th Street, and on the north by the northern edge of an elevated level pad that was the site of the previous fuel-oil tanks. From this pad, which is at approximately elevation Z = +41 ft, a vegetated slope falls away to the west to a berm at Z = + 25 ft MLLW. The berm then slopes down to the existing bike trail below whose road bed is at Z = +23 ft MLLW. This slope was recently planted and landscaped as part of NRG's redevelopment project for Units 5, 6, and 7. Also as part of that redevelopment project, a landscaped berm at elevation Z = +25 ft MLLW was constructed at the south boundary bordering on 45th Street.

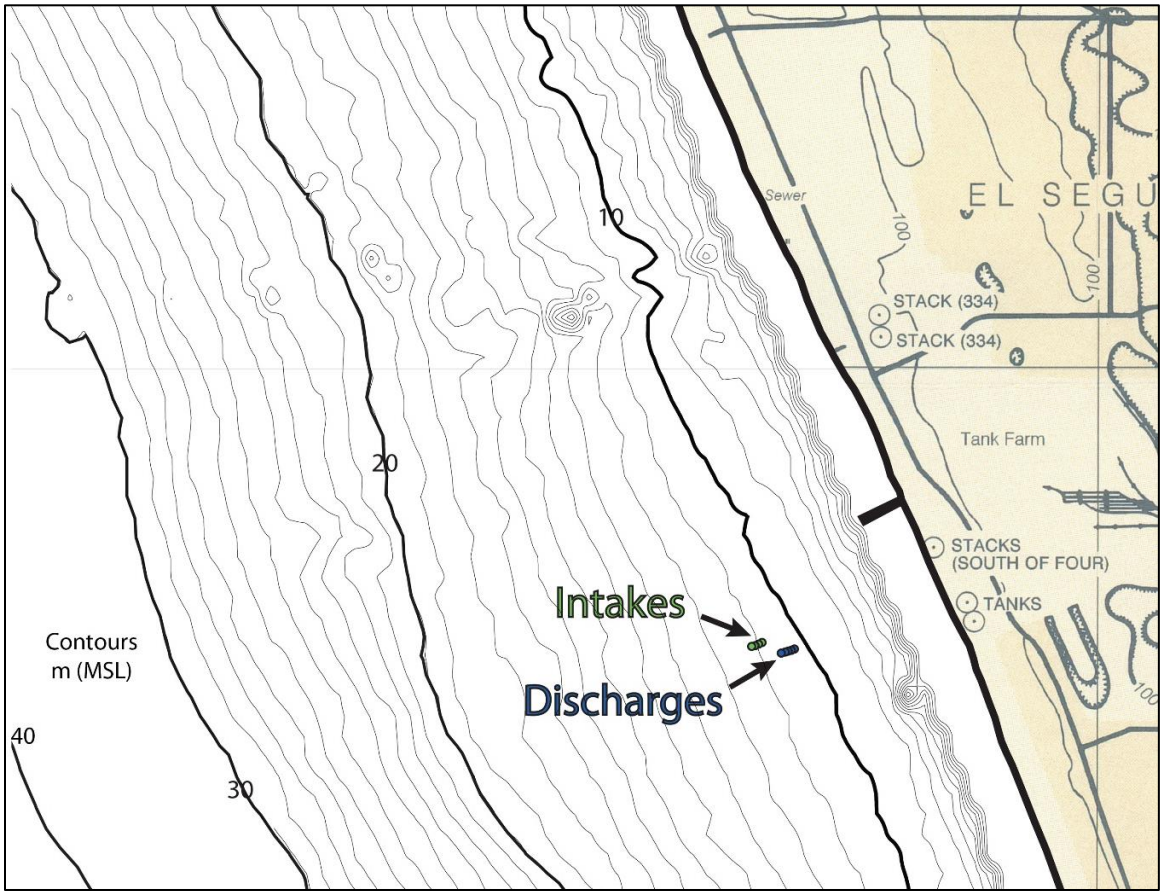

Figure 1.1: Nearfield bathymetric grid centered on the ESGS site for the West Basin Municipal Water District's proposed sea water desalination project. Bathymetry from NOS with survey corrections by Tenera (2007).

El Segundo end of tunnel coordinates in UTM (m) are:

- Intake tunnel: 11S 367,576 m E - 3,752,769 m N
- Discharge tunnel: 11S 367,720 m E – 3,752,820 m N

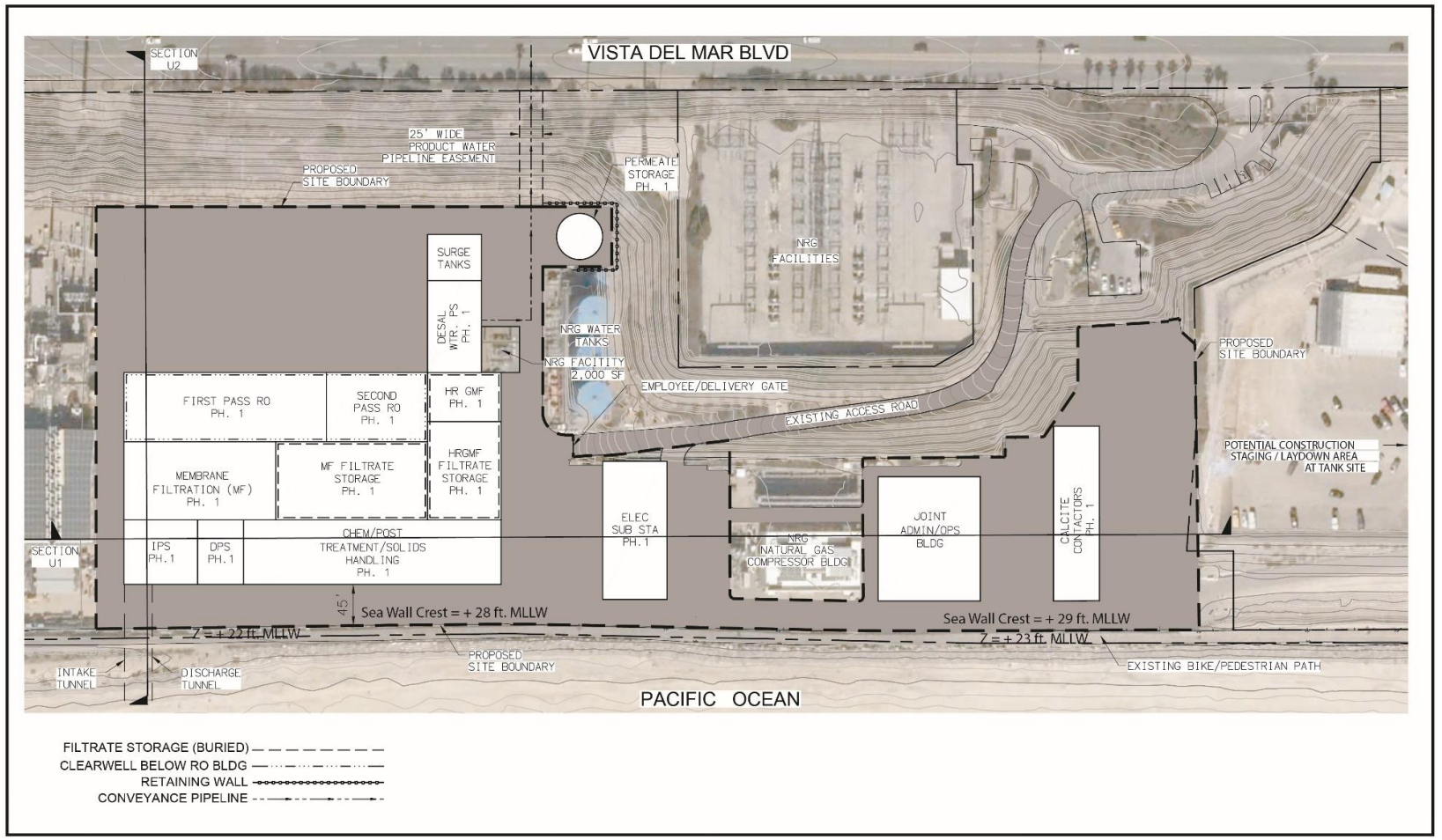

Figure 1.2: Component layout for the 20-mgd scale West Basin Desalination Project at the ESGS North site.

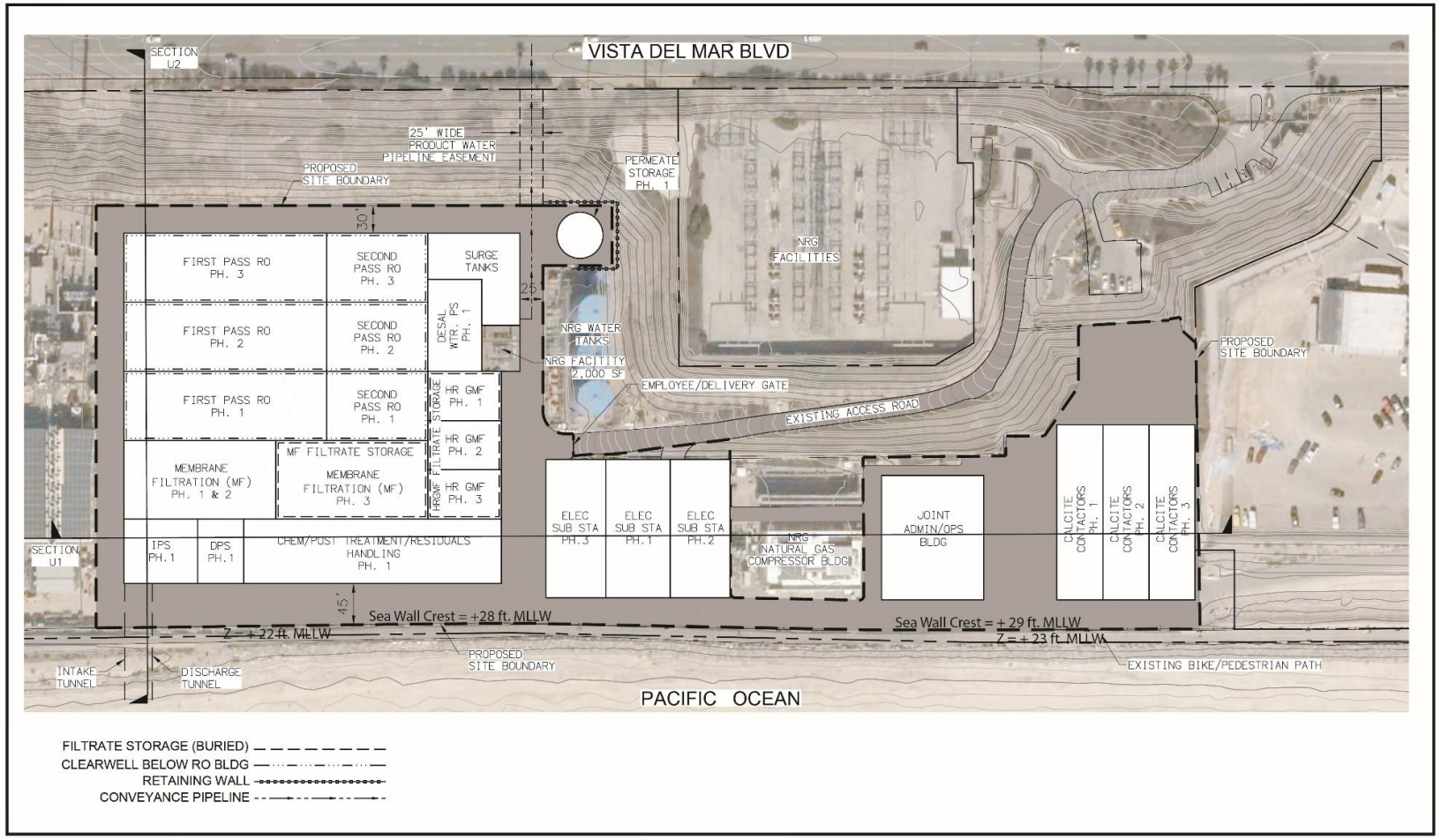

Figure 1.3: Component layout for the 60-mgd scale West Basin Desalination Project at the ESGS North site.

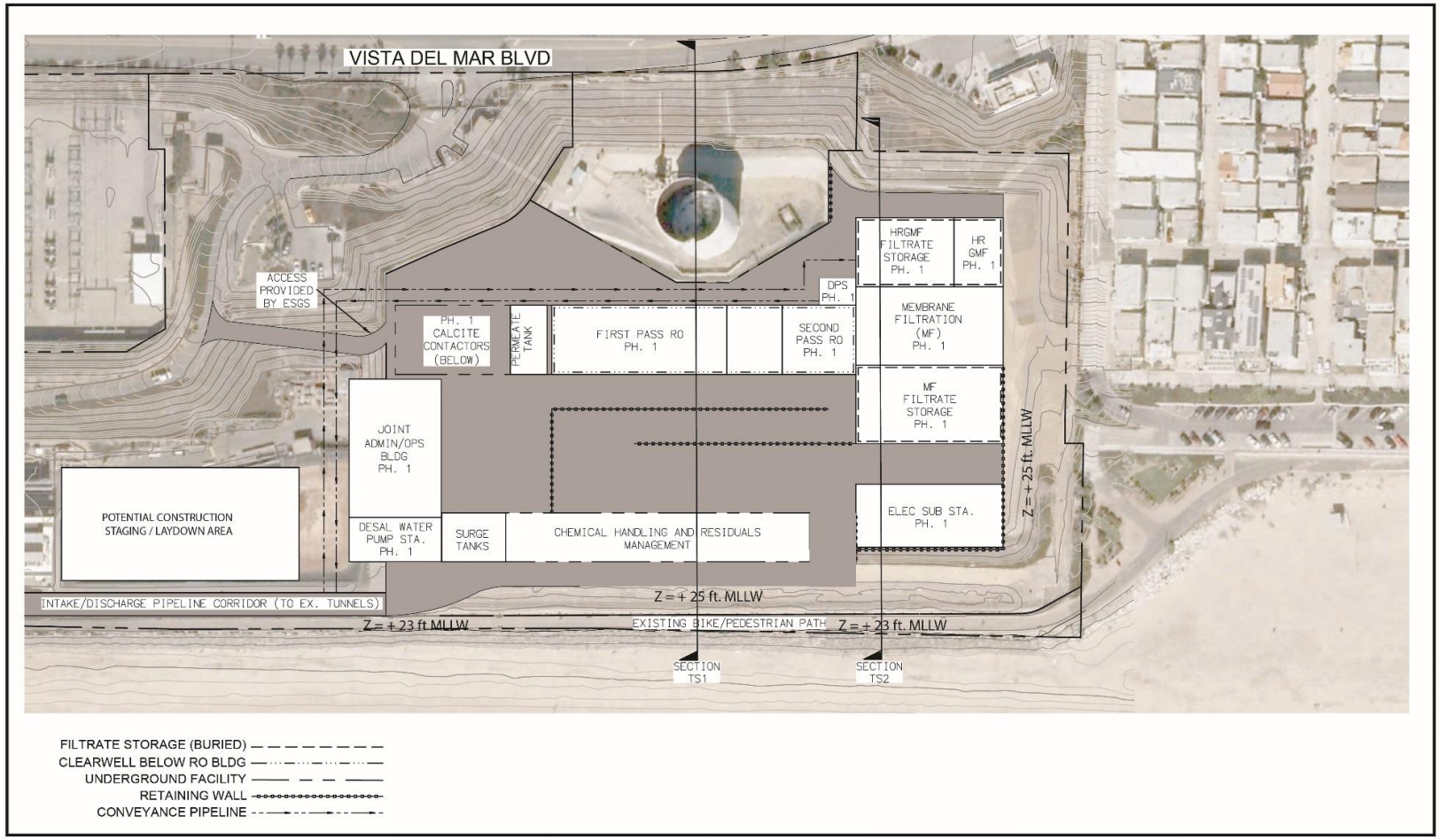

Figure 1.4: Component layout for the 20-mgd scale West Basin Desalination Project at the ESGS South site.

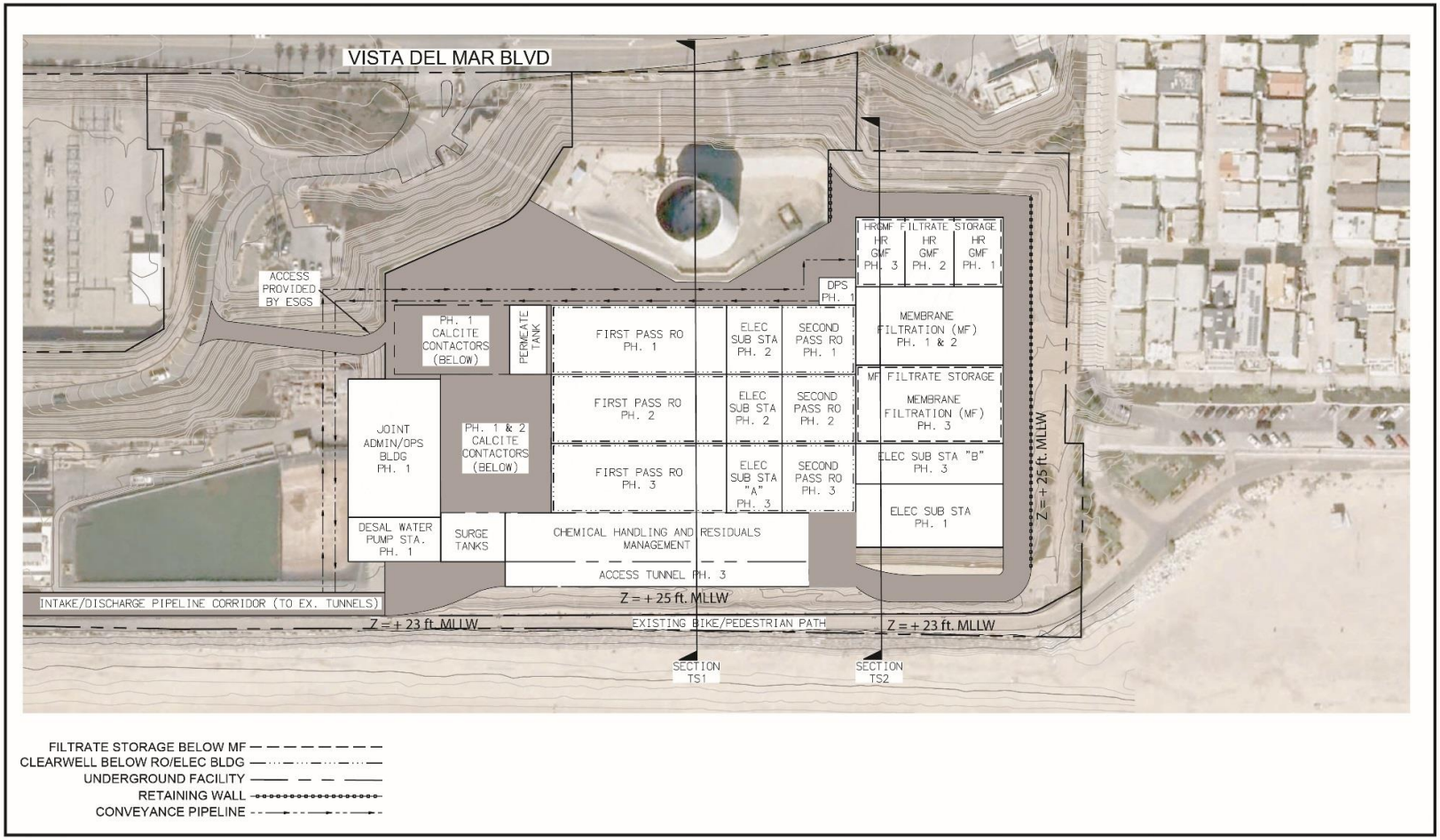

Figure 1.5: Component layout for the 60-mgd scale West Basin Desalination Project at the ESGS South site.

2. Technical Requirements

A coastal hazards analysis begins with assimilation of long-term wave climate databases to evaluate inundation by extreme wave and tsunami run-up that may affect stability and operations of the West Basin Desalination Project at the ESGS North and South sites. The essential requirements for this study, as stated in the California Coastal Commission guidance document for Coastal Development Permits Applications, are:

- Quantify the magnitude and extent to which the desalination facility and associated shore zone structures could be subject to sea level rise, erosion, wave attack or wave run-up due to wave refraction/diffraction over local nearshore and shelf bathymetry over a projected lifespan;
- Quantify the frequency of such events; and
- Evaluate the consequences of such events should they be determined significant, and pose remedial options for avoiding such consequences.

In evaluating these potential hazards for this study, the study will also evaluate potential impacts to the adjacent shoreline due to sea level rise, erosion, or wave diffraction and reflection from the major components of the desalination project and associated structures. The latter requirement entails a sediment budget and transport analysis of both the near- and far-field of the study area.

3. Technical Approach

To quantitatively evaluate potential hazard impacts, we invoke the Coastal Evolution Model applied to the Santa Monica Littoral Cell (Figures 3.1 and 3.2). The Coastal Evolution Model was commissioned by the Kavli Foundation to make forecast predictions of the effects of sea level rise on the coastline of California (see Jenkins and Wasyl, 2005).

3.1 General Description

The Coastal Evolution Model (CEM) is a process-based numerical model. It consists of a Littoral Cell Model (LCM) and a Bedrock Cutting Model (BCM), both coupled and operating in varying time and space domains (Figure 3.2) determined by sea level and the coastal boundaries of the littoral cell at that particular sea level and time. At any given sea level and time, the LCM accounts for erosion of uplands by rainfall and the transport of mobile sediment along the coast by waves and currents, while the BCM accounts for the cutting of bedrock by wave action in the absence of a sedimentary cover.

In both the LCM and BCM, the coastline of the Santa Monica Littoral Cell (the region of coastline between Point Dume and Palos Verdes, Figure 3.1) is divided into a series of coupled control cells (Figure 3.3). Each control cell is a small coastal unit of

uniform geometry where a balance is obtained between shoreline change and the inputs and outputs of mass and momentum. The model sequentially integrates over the control cells in a down-drift direction so that the shoreline response of each cell is dependent on the exchanges of mass and momentum between cells, giving continuity of coastal form in the down-drift direction. Although the overall computational domain of the littoral cell remains constant throughout time, there is a different coastline position at each time step in sea level. For each coastline position, there exists a similar set of coupled control cells that respond to forcing by waves and current. Time and space scales used for wave forcing and shoreline response (applied at six-hour intervals) and sea level change (applied annually) are very different. To accommodate these different scales, the model uses multiple nesting in space and time, providing small-length scales inside large, and short time scales repeated inside of long time scales.

The LCM (Figure 3.2, upper) has been used to predict the change in shoreline width and beach profile resulting from erosion, accretion, and longshore transport of sand by wave action where sand source is from river runoff or from tidal exchange at lagoon and bay inlets (e.g., Jenkins and Inman, 1999). More recently, it has been used to compute the sand level change (far-field effect) in the prediction of mine burial (Jenkins and Inman, 2002; Inman and Jenkins, 2002). Time-splitting logic and feedback loops for climate cycles and sea level change were added to the LCM, together with long run time capability, to give numerically stable long term predictions. In the LCM, the variation of the sediment cover with time is modeled by time-stepped solutions to the sediment continuity equation (otherwise known as the *sediment budget*) applied to the boundary conditions of the coupled control cell mesh diagramed schematically in Figure 3.3. The sediment continuity equation is written (Jenkins, et al, 2007):

$$\frac{\partial q}{\partial t} = \frac{\partial}{\partial y}\left(\varepsilon \frac{\partial q}{\partial y}\right) - V_l \frac{\partial q}{\partial y} + J(t) - R(t) \tag{1}$$

Where q is the sediment volume per unit length of shoreline (m^3/m) and *dq/dt* is the sediment volume flux ($m^3/m/day$), ε is the mass diffusivity, V_l is the longshore current, *J(t)* is the flux of new sediment into the littoral cell from watersheds or beach disposal of dredge material, and *R(t)* is the flux of sediment lost to sinks, in this case, the Redondo Submarine Canyon.

The first term in Equation (1) is the surf diffusion term, while the second is the advective term due to the longshore current. For any given control cell inside the reach from Point Dume to the Redondo King Harbor, Equation (1) may be discretized in terms of the rate of change of "beach volume," Λ, in time increment Δt, given by:

$$\frac{d\Lambda}{dt} = J(t) + \frac{q_{in} + q_{out}}{\Delta t} \tag{2}$$

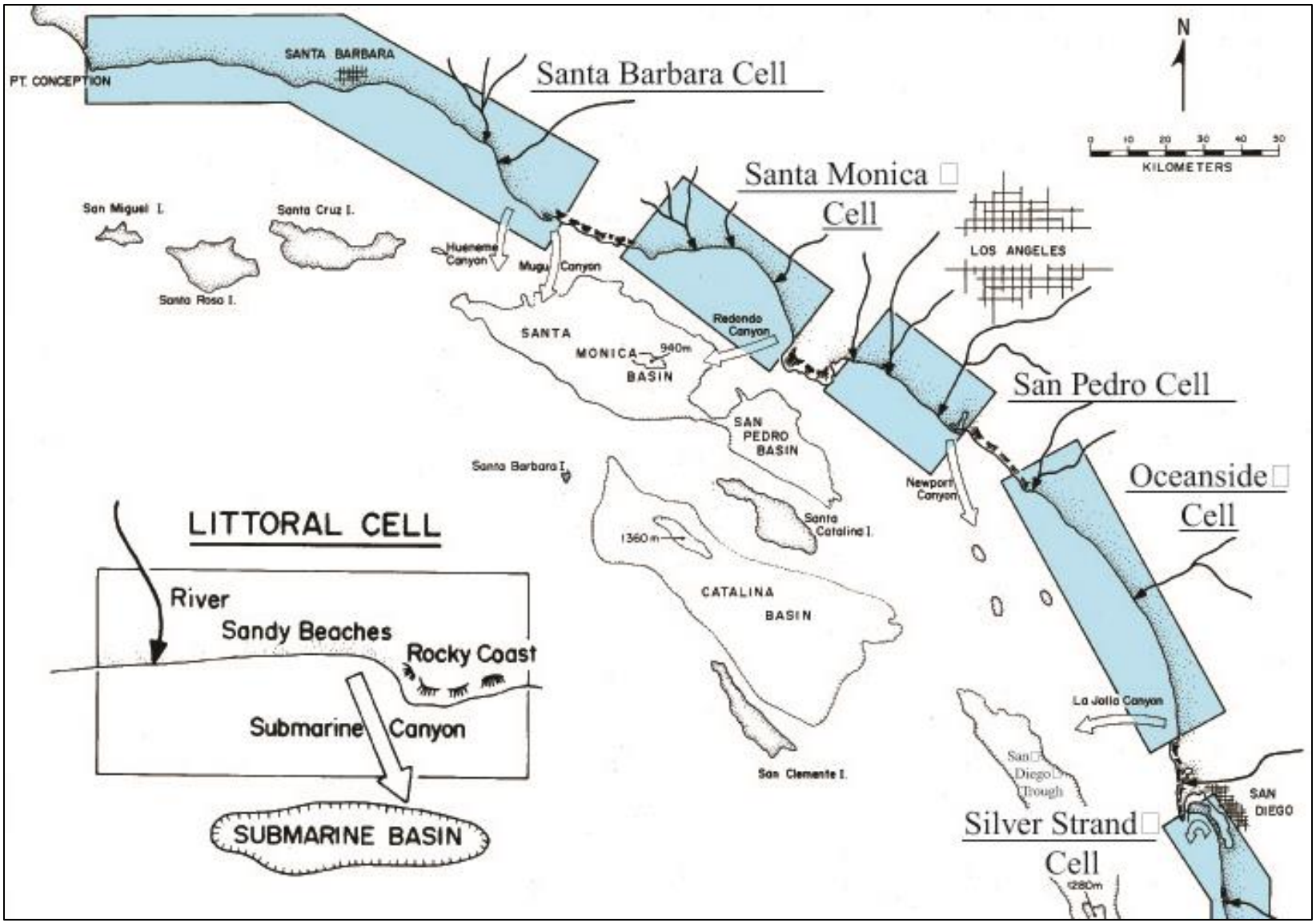

Figure 3.1: The five littoral cells along the Southern California coast. Each cell contains a complete sedimentation cycle. Most sand is brought to the coast by streams, carried along the shore by waves and currents, and lost through submarine canyons to offshore basins [after Inman and Frautschy, 1965].

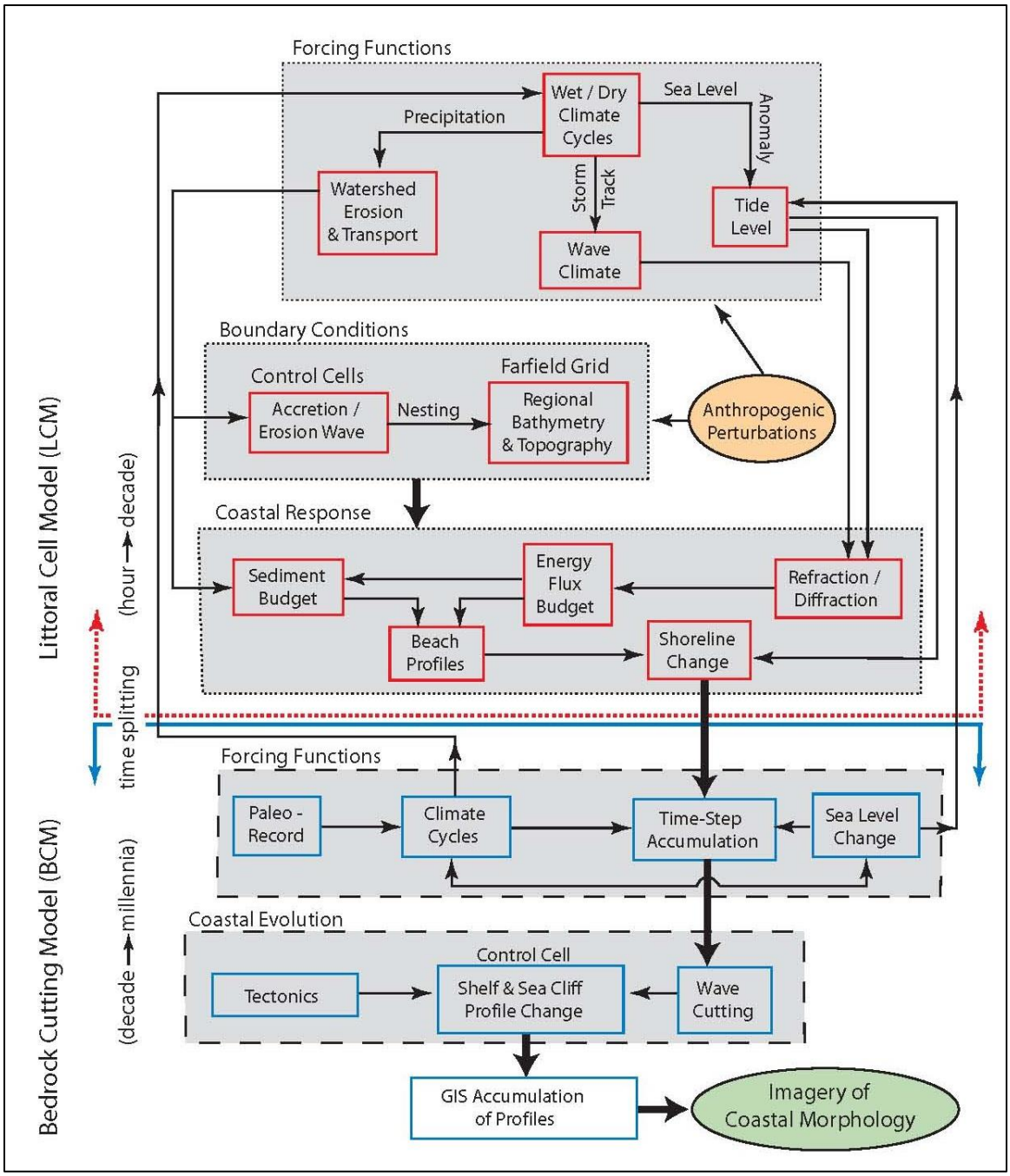

Figure 3.2: Architecture of the Coastal Evolution Model consisting of the Littoral Cell Model (above) and the Bedrock Cutting Model (below). Modules (shaded) are formed of coupled primitive process models. (from Jenkins and Wasyl, 2005).

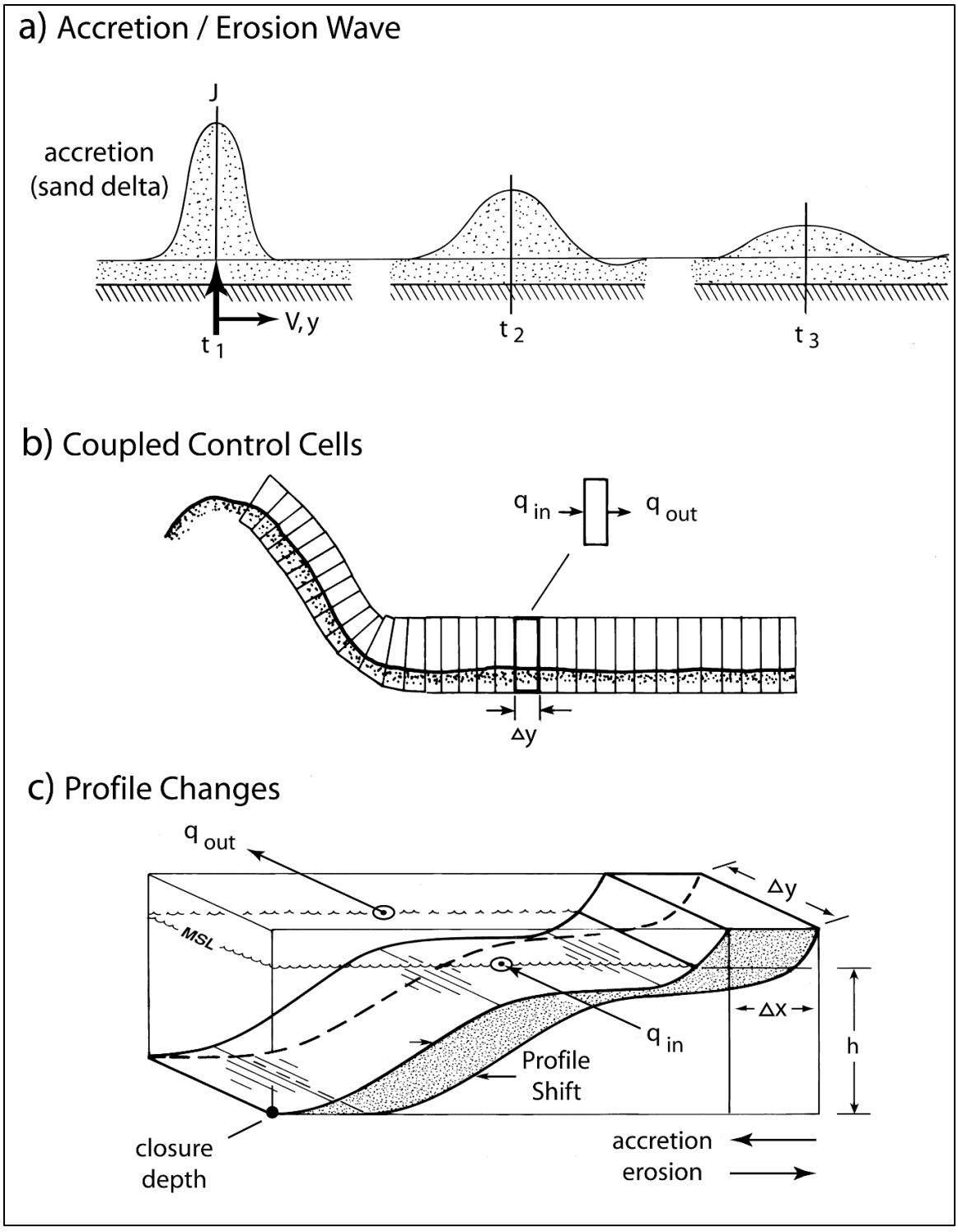

Figure 3.3: Computational approach for modeling shoreline change after Jenkins, et. al., (2007).

Sediment is supplied to the control cell by the sediment yield from the rivers and beach nourishment, *J(t)* by the influx of sediment volume due to littoral drift from up-coast sources, q_{in} (beach-fill). Sediment is lost from the control cell due to the action of wave erosion and expelled from the control cell by exiting littoral drift, q_{out}. Here, fluxes into the control cell (*J(t)* and q_{in} /Δt) are positive, and fluxes out of the control cell (q_{out} /Δt) are negative.

The beach and nearshore sand volume change, *dq/dt*, is related to the change in shoreline position, *dX*/*dt*, according to:

$$\frac{dV}{dt} \cong \frac{d\Lambda}{dt} = \frac{dX}{dt} \cdot Z \cdot l \tag{3}$$

where

$$Z = Z_1 + h_c \tag{4}$$

Here, *Z* is the height of the shoreline flux surface equal to the sum of the closure depth below mean sea level, h_c, and the height of the berm crest, Z_1, above mean sea level; and *l* is the length of the shoreline flux surface. Hence, beaches and the offshore bottom profile out to closure depth remain stable if a mass balance is maintained such that the flux terms on the right-hand side of Equation (2) sum to zero; otherwise, the shoreline will move during any time step increment as:

$$\Delta x(t) = \frac{1}{\Delta y(Z_1 + h_c)} \int \left(\frac{\partial}{\partial y} \left(\varepsilon \frac{\partial q}{\partial y} \right) - V \frac{\partial q}{\partial y} + J(t) \right) dt \tag{5}$$

where ε is the mass diffusivity, *V* is the longshore drift , *J* is the flux of sediment from river sources, Δy is the alongshore length of the control cell, and Z_1 is the maximum run-up elevation from Hunt's Formula. River sediment yield, *J*, is calculated from streamflow, *Q*, based on the power law formulation of that river's sediment rating curve after Inman and Jenkins, (1999), or

$$J = \xi \, Q^{\omega} \tag{6}$$

where ξ, ω are empirically derived power law coefficients of the sediment rating curve from best fit (regression) analysis (Inman and Jenkins, 1999). When river floods produce large episodic increases in *J*, a river delta is initially formed. Over time, the delta will widen and reduce in amplitude under the influence of surf diffusion and advect (move) down-coast with the longshore drift, forming an accretion erosion wave (Figure 3a). The local sediment volume varies in response to the net change of the volume fluxes, between any given control cell and its neighbors, referred to as divergence of drift = q_{in} - q_{out}, see Figures 3b and 3c. The mass balance of the control cell responds to a non-zero divergence of drift with a compensating shift, Δx , in the position

of the equilibrium profile (Jenkins and Inman, 2006). This is equivalent to a net change in the beach entropy of the equilibrium state. The divergence of drift is given by the continuity equation of volume flux, requiring that *dq/dt* is the net of advective and diffusive fluxes of sediment plus the influx of new sediment, *J*. The rate of change of volume flux through the control cell causes the equilibrium profile to shift in time according to Equation (5).

It is well known that beach and nearshore bottom profiles change seasonally in response to seasonal wave climate variations as shown in Figure 3.4, (cf: Inman et al, 1993; Jenkins and Inman 2006); and that seasonal transitions between summer and winter equilibrium states cause seasonal changes in the mean shoreline (Equation (7)).

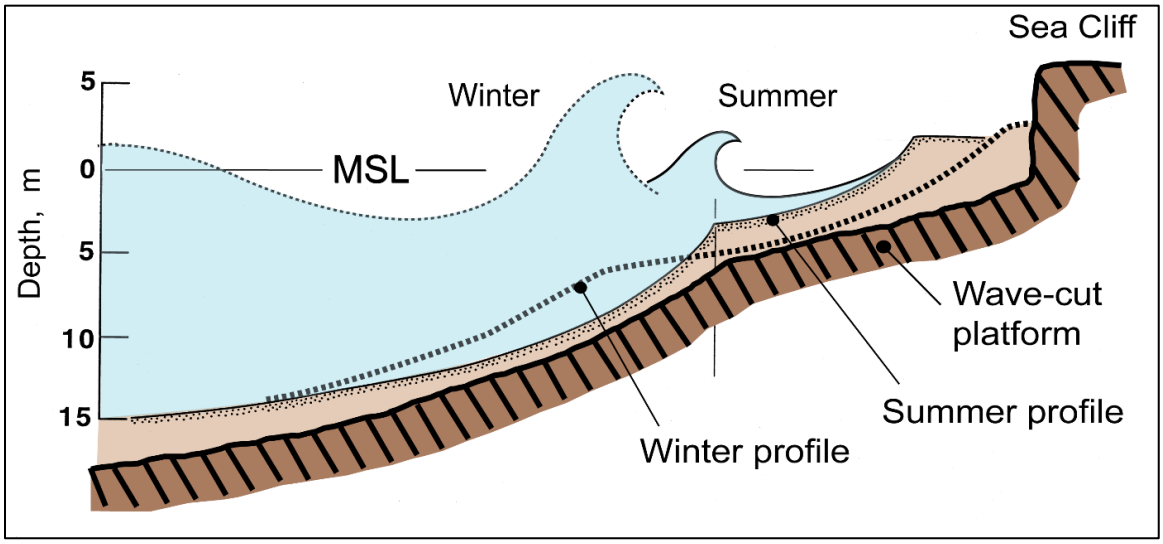

Figure 3.4: Schematic of summer and winter equilibrium beach profiles, from Inman, et al (1993).

Short period waves during summer (from the spin up of winds from the local North Pacific High) cause the inner bar-berm section of the beach profile to build up and steepen; while long period storm swells during winter from the Aleutian Low cause the bar-berm profile to flatten, and transfer beach sand to the outer shore-rise profile. These changes between summer and winter equilibrium states are predicted from long-term wave records applied to the well-tested elliptic cycloid solutions published in Jenkins and Inman (2006).

With a long-term collection of summer and winter beach equilibrium profiles for a broad range of wave heights, a well-defined envelope of variability becomes apparent as illustrated in Figure 3.5 and 3.6a. Figure 3.5 combines 12 measured bottom profiles over a 37-year period from two adjacent beaches near Oceanside, CA. These beaches have geomorphic similitude with the beaches near Redondo King Harbor and are shown here to illustrate a fundamental principle. In Figure 3.5, elliptic cycloid solutions for equilibrium profiles are also overlaid as colored traces to further define this envelope of variability.

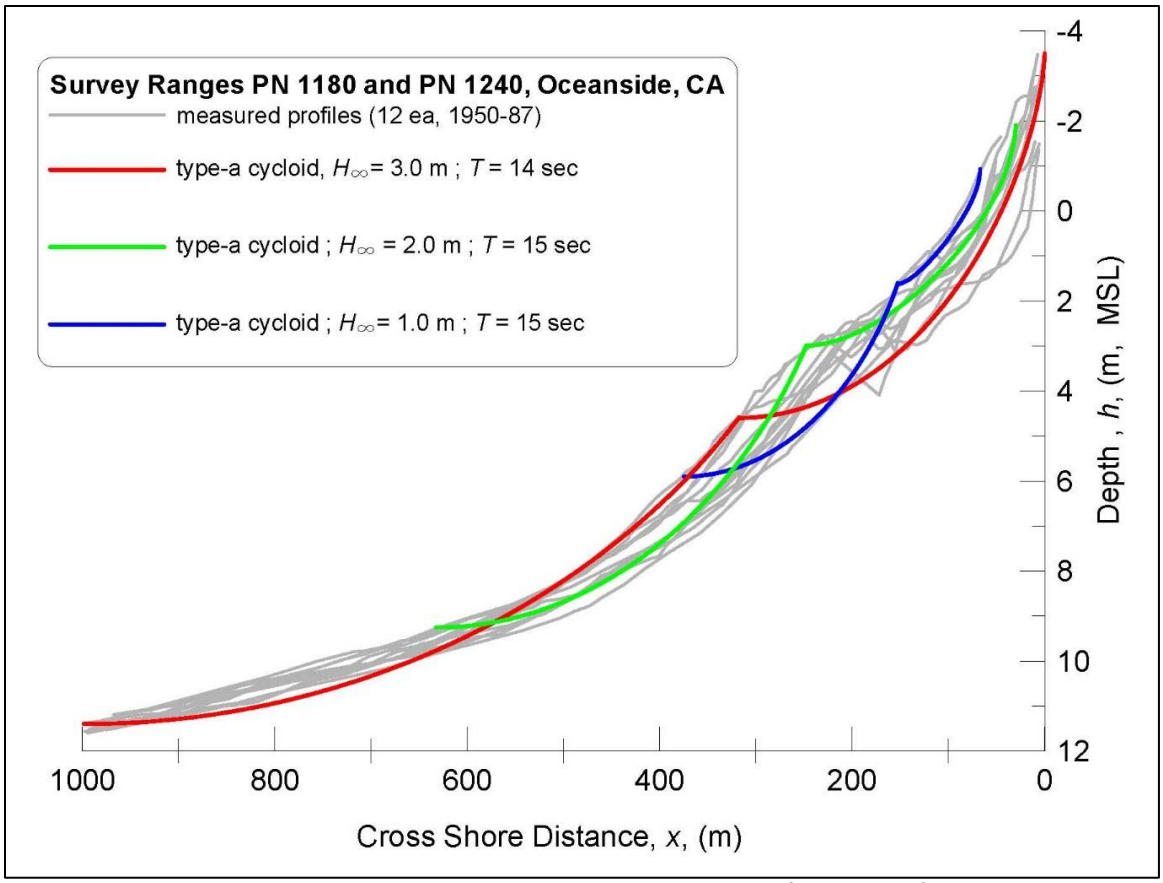

Figure 3.5: Envelope of variability of measured beach profiles (1950-1987) at Oceanside, CA (shown in grey), compared to an ensemble of elliptic cycloid solutions (colored) for selected wave heights and periods for average summer and winter wave climate; (from Jenkins and Inman, 2006)

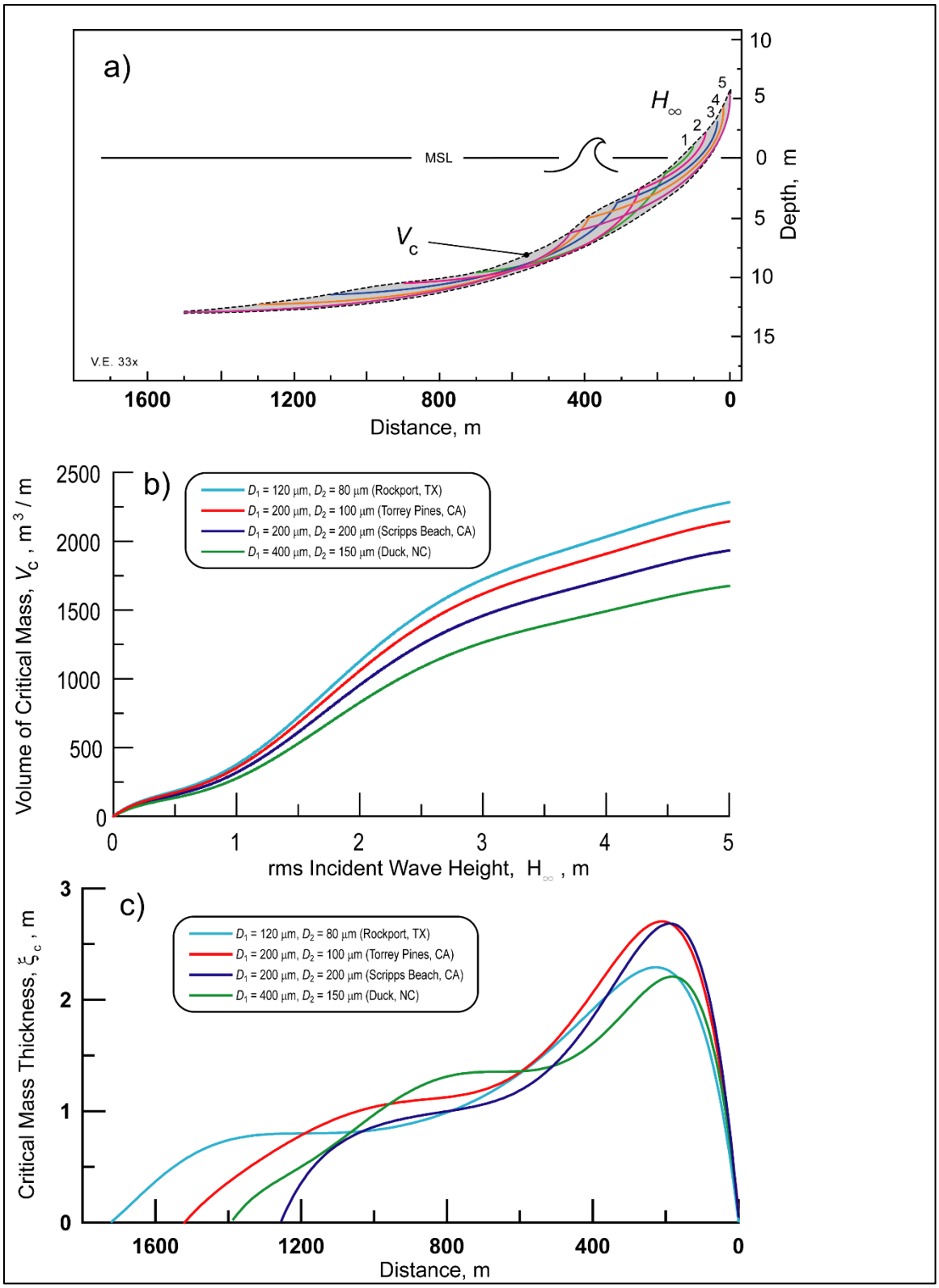

Figure 3.6: Features of the critical mass of sand: a) critical mass envelope for waves of 1m to 5m in height; b) volume of critical mass as a function of wave height and sediment grain size; c) variation in the thickness of the critical mass as a function of distance offshore.

The cycloid solutions are from Jenkins and Inman, 2006, and are based on average summer and winter wave heights and periods. Comparison of the measured profiles in grey with the cycloid solutions indicates that the volume of sand associated with long-term beach profile variations are directly calculable by integration of the cycloid solutions between the limits of wave climate. This integration is shown in Figure 3.6b, and the volume of sand is referred to as the *critical mass*. The critical mass represents the minimum volume of sediment cover required to maintain equilibrium bottom profiles and a stable seabed over the long term, (where long term is on the order of decades). Figure 3.6b indicates that the critical mass increases with wave height and decreases with sediment grain size. Thus, the critical mass requirements become very large for finer-grained sediments in high energy wave climate environments.

Furthermore, the total mass of sand in the littoral cell, (as specified by the sediment budget in Equation (4), must exceed the critical mass in order for the beach and nearshore sediment cover to remain sustainable over time. If the sediment budget declines to less than the critical mass, then the beach and nearshore will denude down to bedrock, and all the sediment cover is quickly lost. This occurred in many places in Southern California during the El Niño winter of 1983 (Inman and Jenkins, 1993, 2004) and would be disastrous for a SIG or BIG intake system if it happened at the RBGS or ESGS sites in the future. Only the Neodren™ technology would be able to survive a repeat of the 1983 El Niño winter conditions due to its ability to be placed below the critical mass envelope by means of horizontal directional drilling (HDD).

3.2 Closure Depth

This is the most important parameter in the optimal siting of shallow sub-seabed intake technology. Closure depth represents the closest point to the shoreline where a stable seabed can be found, because it is the point beyond which all changes in the beach profiles cease. It also represents the outer limit of the critical mass. If a SIG were located inshore of closure depth, the engineered fill would suffer seasonal or episodic erosion, and subsequently be replaced by seasonal or episodic deposition of native sediments whose grain size may or may not be compatible with the fill material.

Hallermeier [1978, 1981] derived a relation for closure depth, by assuming a relationship for the energetics of sediment suspensions based on a critical value of the Froude number, giving:

$$h_c \cong 2.28 H_{ss} - 6.85 \left(H_{ss}^2 / gT^2 \right) \tag{7}$$

Where H_{ss} is the nearshore storm wave height that is exceeded only 12 hours each year and T is the associated wave period.

Birkemeier [1985] suggested different values of the constants and found that the simple relation $h_c = 1.57\ H_{ss}$ provided a reasonable fit to his profile measurements at Duck, North Carolina. Cowell et al. [1999] reviews the Hallermeier relation for closure

depth h_c and limiting transport depth h_i and extends the previous data worldwide to include Australia. Their calculations indicate that h_c ranges from 5 m (Point Mugu, California) to 12 m (SE Australia), while h_i ranges from 13 m (Netherlands) to 53 m (La Jolla, California). They conclude that discrepancies in data and calculation procedures make it "pointless to quibble over accuracy of prediction" in h_c and h_i. In the context of planning for beach nourishment, Dean [2002] observes that "although closure depth… is more of a concept than a reality, it does provide an essential basis for calculating equilibrated… beach widths."

While it may be reasonable to apply the Hallermeier relation or its simpler form after Birkemeier [1985] to the shore-rise boundary condition, comparisons with the Inman et al. [1993] beach profile data set show that these relations tend to underestimate closure depth. An alternative closure depth relation is proposed. This relation is based on two premises: 1) closure depth is the seaward limit of non-zero net transport in the cross-shore direction; and, 2) closure depth is a vortex ripple regime in which no net granular exchange occurs from ripple to ripple. Inman [1957] gives observations of stationary vortex ripples in the field, and Dingler and Inman [1976] establish a parametric relationship between dimensions of stationary vortex ripples and the Shield's parameter $\widetilde{\Theta}$ in the range $3 < \widetilde{\Theta} < 40$. Using the inverse of that parametric relation to solve for the depth gives (Jenkins and Inman, 2006):

$$h_{\mathrm{c}} = \frac{K_{\mathrm{e}} H_{\infty}}{\sinh k h_{\mathrm{c}}} \left(\frac{D_{\mathrm{o}}}{D_2} \right)^{\Psi} \tag{8}$$

Where K_e and Ψ are non-dimensional empirical parameters, D_2 is the shore-rise median grain size; and D_o is a reference grain size. With $K_e \sim 2.0$, $\Psi \sim 0.33$ and $D_o \sim 100$ μm, the empirical closure depths reported in Inman et al. [1993] are reproduced by Equation (8). From Equation (8), we find closure depth increases with increasing wave height and decreasing grain size, as shown in Figure 3.7. Because of the wave number dependence of Equation (8), closure depth also increases with increasing wave period. Using Equation (8), the distance to closure depth X_{c2} can be obtained from (Jenkins and Inman, 2006):

$$X_{\mathrm{c2}} = \frac{h_{\mathrm{c}} I_{\mathrm{e}}^{(2)}}{\varepsilon} \cong \frac{\pi \, h_{\mathrm{c}}}{2\varepsilon} \sqrt{\frac{2 - e^2}{2}} \tag{9}$$

Where X_{c2} is measured from the origin of the shore-rise located a distance X_2 from the berm and a distance X_3- X_2 inside the breakpoint (Figure 3.8a), $I_e^{(2)}$ is the elliptic integral of the second kind, and ε is a stretching factor proportional to the Airy wave mild slope factor N, and

$$\varepsilon = \frac{\sigma}{N} \left(\frac{H_{\mathrm{b}}}{\gamma \, g} \right)^{1/2} \cong \frac{\sigma^{4/5}}{2^{1/5} N} \left(\frac{H_{\infty}}{g \gamma} \right)^{2/5}$$

3.3 Elliptic Cycloid Solutions for the Shore-rise and Beach Profiles

The elliptic cycloid was proven to be the mathematical representation of a shore-rise or bar-berm beach profile by Jenkins and Inman, 2006. This mathematical relation is embedded in the algorithms of the CEM and used to calculate the bottom profile of the beach and seabed offshore of the RBGS and ESGS for any given point in time based on the incident wave height, period, direction, and sediment grain size.

The elliptic cycloid solutions were developed for beach profiles by Jenkins and Inman (2006) using equilibrium principles of thermodynamics applied to very simple representations of the nearshore fluid dynamics. Equilibrium beaches are posed as isothermal shorezone systems of constant volume that dissipate external work by incident waves into heat given up to the surroundings. By the maximum entropy production formulation of the second law of thermodynamics (the law of entropy increase), the shorezone system achieves equilibrium with profile shapes that maximize the rate of dissipative work performed by wave-induced shear stresses. Dissipative work is assigned to two different shear stress mechanisms prevailing in separate regions of the shorezone system, an outer solution referred to as the *shore-rise* and a *bar-berm* inner solution. The equilibrium shore-rise solution extends from closure depth (zero profile change) to the breakpoint, and maximizes dissipation due to the rate of working by bottom friction. In contrast, the equilibrium bar-berm solution between the breakpoint and the berm crest maximizes dissipation due to work by internal stresses of a turbulent surf zone. Both shore-rise and bar-berm equilibria were found to have an exact general solution belonging to the class of elliptic cycloids.

The elliptic cycloid solution is a curve allows all the significant features of the equilibrium profile to be characterized by the eccentricity and the size of one of the two ellipse axes. These two basic ellipse parameters are related herein to both process-based algorithms and to empirically based parameters for which an extensive literature already exists. The elliptic cycloid solutions reproduce realistic and validated wave height, period, and grain size dependence and demonstrated generally good predictive skill in point-by-point comparisons with measured profiles (Jenkins and Inman, 2006 display).

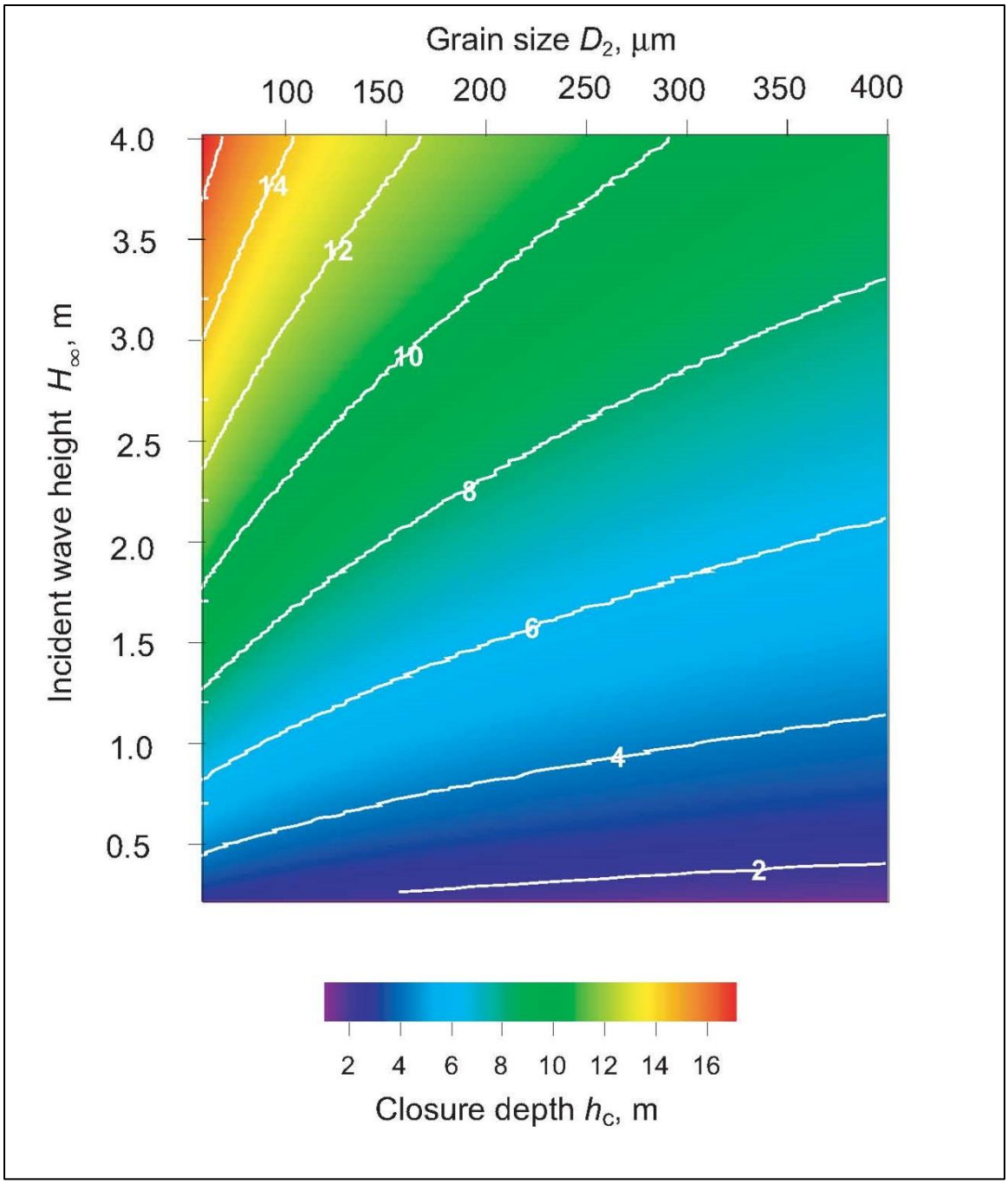

Figure 3.7: Closure depth contoured versus incident wave height and sediment grain size for waves of 15-second period, with $K_e \sim 2.0, \psi \sim 0.33$ and $D_o \sim 100\mu m$. D_2 is the shore-rise median grain size; and D_o is a reference grain size.

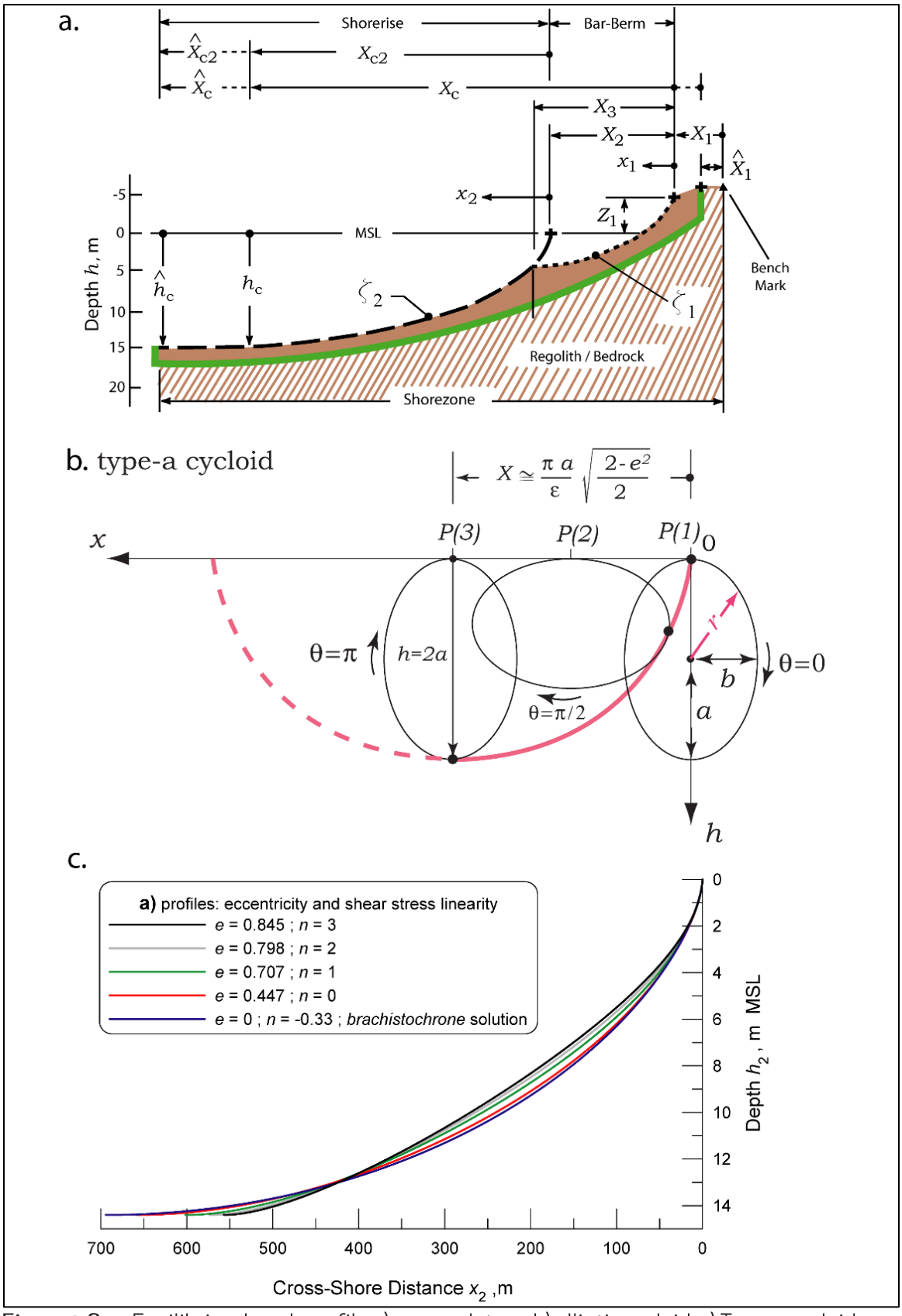

Figure 3.8: Equilibrium beach profile a) nomenclature, b) elliptic cycloid, c) Type-a cycloid solution.

To understand the formulation of the elliptic cycloid representation of the nearshore bottom profile and sensitivity to ocean conditions, we first review the nomenclature of the shorezone as shown schematically in Figure 3.8. The seaward boundary of the shorezone is a vertical plane at the critical closure depth $\hat{h}_c$ (Figure 8a) corresponding to the maximum incident wave [e.g., Kraus and Harikai, 1983]. The landward boundary is a vertical plane at the berm crest (cross), a distance $\hat{X}_1$ from a benchmark. The cross-shore length of the system from the berm crest to closure depth is $\hat{X}_c$. The distance from the point of wave breaking to closure depth is $\hat{X}_{c2}$ such that $\hat{X}_c = \hat{X}_{c2} + \hat{X}_2$, where $\hat{X}_2$ is the distance from the berm crest to the origin of the shore-rise profile near the wave breakpoint. We consider equilibrium over time scales that are long compared with a tidal cycle and profiles that remain in the wave-dominated regime where the relative tidal range (tidal range/*H*) < 3 [Short, 1999]. Under these conditions, the curvilinear solution to the bottom profile which satisfies the maximum entropy production formulation of the Second Law of Thermodynamics can be expressed in polar coordinates (*r*, θ) as:

$$x = x_2 = \frac{2r\, I_e^{(k_{1,2})}}{\pi\, \varepsilon}\,(\theta - \sin\theta) \tag{10}$$

Where *r* is the radius vector measured from the center of an ellipse whose semi-major and semi-minor axes are *a*, *b*, and $I_e^{(k)}$ is the elliptic integral of the first or second kind. This curve is what a point on the circumference of an ellipse would trace by rolling through some angle θ (Figure 3.8b); hence, the name elliptic cycloid. The polar equivalent of the type-a cycloid shown in Figure 3.8b has a radius vector whose magnitude is:

$$r = r_a = \left[\frac{a^2 b^2}{a^2 \sin^2\theta + b^2 \cos^2\theta}\right]^{1/2} = \frac{a\sqrt{1-e^2}}{\sqrt{\sin^2\theta + (1-e^2)\cos^2\theta}} \tag{11}$$

Where *e* is the eccentricity of the ellipse given by $e = \sqrt{1-(b^2/a^2)}$. The polar form of the type-a cycloid in Figure 3.8b is based on the elliptic integral of the second kind that has an analytic approximation, $I_e^{(2)} = (\pi/2)\sqrt{(2-e^2)/2}$, see Hodgman [1947]. The inverse of Equation (11) for the type-a elliptic cycloid gives the companion solution in terms of local water depth, *h*, as:

$$h = h_2 = \frac{\pi\varepsilon\ x_2}{2I_e^{(k_{1,2})}}\left(\frac{1-\cos\theta}{\theta - \sin\theta}\right) = r\,(1-\cos\theta\ ) \tag{12}$$

The depth of water at the seaward end of the profile ($\theta = \pi$) is *h = 2a* in the case of the type-a cycloid. The length of the profile *X* is equal to the semi-circumference of the ellipse:

$$X = \frac{2aI_e^{(2)}}{\varepsilon} \cong \frac{\pi\ a}{\varepsilon}\sqrt{\frac{2-e^2}{2}} \text{ at } \theta = \pi \text{ (type-a cycloid)} \quad (13)$$

3.4 Critical Mass

The critical mass determines the volume of sediment that can be potentially eroded, and the depth below existing grade that erosion might extend, due to extreme storms and seasonal change or shoreline recession. The critical mass of sand on a beach is that required to maintain equilibrium beach shapes over a specified time, usually ranging from seasons to decades. The critical mass for a seasonal beach is determined from the volume of the envelope of sand necessary to maintain continuous beach forms during the many changes in shape from one equilibrium state to another over a period of seasons (Jenkins and Inman, 2003). Generally, changes in profile shape between equilibrium states involve transitional shapes that are non-equilibrium in form. However, as a first order approximation, it is assumed the critical mass envelope consists of a set of incremented equilibrium profiles, and the associated set of transitional profiles occurring between successive equilibrium states. Each profile in this set corresponds to a particular rms breaker height H_b that varies between some seasonal minimum H_{bo} and the critical wave height $\hat{H}_b$, the highest wave condition for which the existing sand supply can accommodate equilibrium and transitional profile adjustments. The equilibrium profiles are incremented by infinitesimal changes in wave height, $H_{bo} \le H_b + dH_b \le \hat{H}_b$, giving a continuous envelope of beach profile change. The volume of this envelope can be calculated from the thermodynamic solutions for the bar-berm profile, ζ_1, and the shore-rise profile ζ_2 to solve for the volume of critical mass V_c per meter of shoreline (m^3/m):

$$V_c = \int_{H_\infty}^{\hat{H}_b}\int_{X_1}^{X_3}\frac{\partial\zeta_1}{\partial H_b}dxdH_b + \int_{H_\infty}^{\hat{H}_b}\int_{X_3}^{X_c}\frac{\partial\zeta_2}{\partial H_b}dxdH_b \quad (14)$$

Analytic solutions to V_c are difficult because the thermodynamic solutions for the curvilinear coordinates (ζ_1, ζ_2) using elliptic cycloids are transcendental. Therefore, solutions for the V_c envelope are obtained by numerical integration of Equation (14) based on long-term wave climate (cf. Section 5). The number-crunching capabilities of the CEM are used for this purpose. Figure 3.9 gives the critical mass solution resulting from numerical integrations of Equation (14). Because equilibrium and transitional profiles are grain-size dependent through the closure depth condition, the volume of critical mass has a certain degree of sensitivity to grain size. Sensitivity analyses of Equation (14) based on numerical integration show that finer grain sizes, particularly in the shore-rise, tend to result in larger volumes of critical mass. This is shown in Figure

3.10 with the wave period fixed. Longer curvilinear length ζ_1, ζ_2 and deeper closure depths h_c arise from finer-grained sediment, thus resulting in physically larger critical mass envelopes. However, the sensitivity of the volume of critical mass to grain size is second order relative to the dependence on wave height and period. A polynomial fit to the wave height dependence averaged over all grain sizes gives the following analytic approximation:

$$V_c \cong 500 H_b^{0.9} \tag{15}$$

Where H_b is in meters, giving V_c in m^3 per meter of beach length.

3.5 Wave Setup and Run-up

Wave setup is an increased elevation of the water level due to the effects of wave momentum being transferred to the surf zone. In wave systems composed of more than one wave component, as occurs in the Pacific Ocean, the setup oscillates and comprises a static and a dynamic component. Wave run-up is the culmination of the wave breaking process, whereby the wave surges up the beach, bluff, or structure face along the shoreline. Overtopping occurs when the wave run-up exceeds the profile crest elevation, which can result in flooding landward of the crest. Run-up is a function of several key parameters. These include the wave height, H; the wave period, T; the wave length, L; the profile slope, m; and the surf similarity parameter (Iribarren number), ξ defined as: $\xi = m/\sqrt{H/L}$. The total water level (TWL) is defined as the sum of the total run-up and the SWL, referenced to an established vertical datum. The results for this study are referenced to the North American Vertical Datum of 1988 (NAVD88) vertical datum. The total run-up, R, is composed of three main components: Static wave setup, $\overline{\eta}$; Dynamic wave setup, η_{rms}; Incident wave run-up, R_{inc}.

Wave setup and run-up are typically computed at hourly time steps from an historic record of wave monitoring (see Section 4.0). Wave setup and run-up are combined with coincident water level values (from hydroperiod functions, see Jenkins, 2015) to develop the TWL values. It should be noted that the increase in sea level for future scenarios should be added to each hourly SWL over the 50-year hindcast for the analysis of TWLs, with the 1-percent-annual-chance results derived statistically from the resultant 50 annual maxima as explained in Section 3.10.

Annual maxima TWLs are computed for each sea level rise (SLR) scenario, and a statistical Generalized Extreme Value (GEV) analysis is performed on these values to determine the 1-percent-annual-chance TWL for two example problems. The overtopping rate is calculated for instances where the TWL exceeded the engineered barrier crest and overtopping occurred. Each step used to evaluate hazards is described in detail in the following subsections.

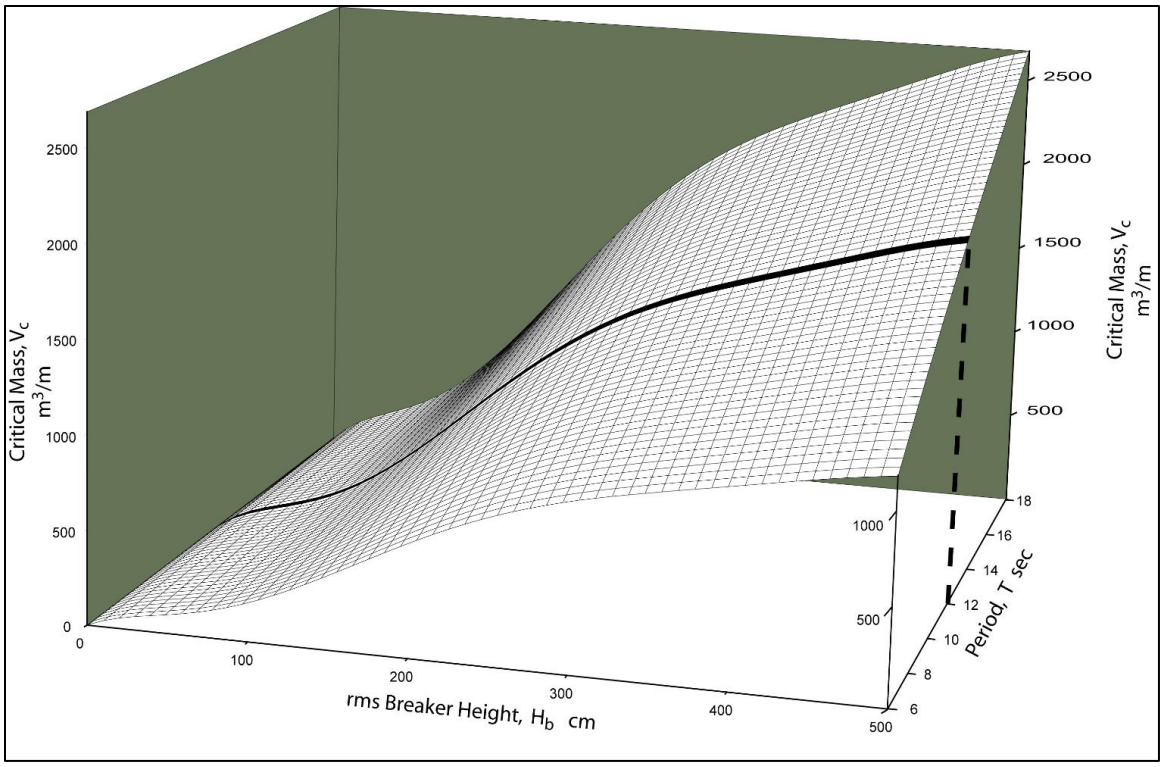

Figure 3.9: Three-dimensional rendering of the total solution space of the critical mass. Black line corresponds to the solution in Figure 10 for D_1 = 225 microns and D_2 = 125 microns.

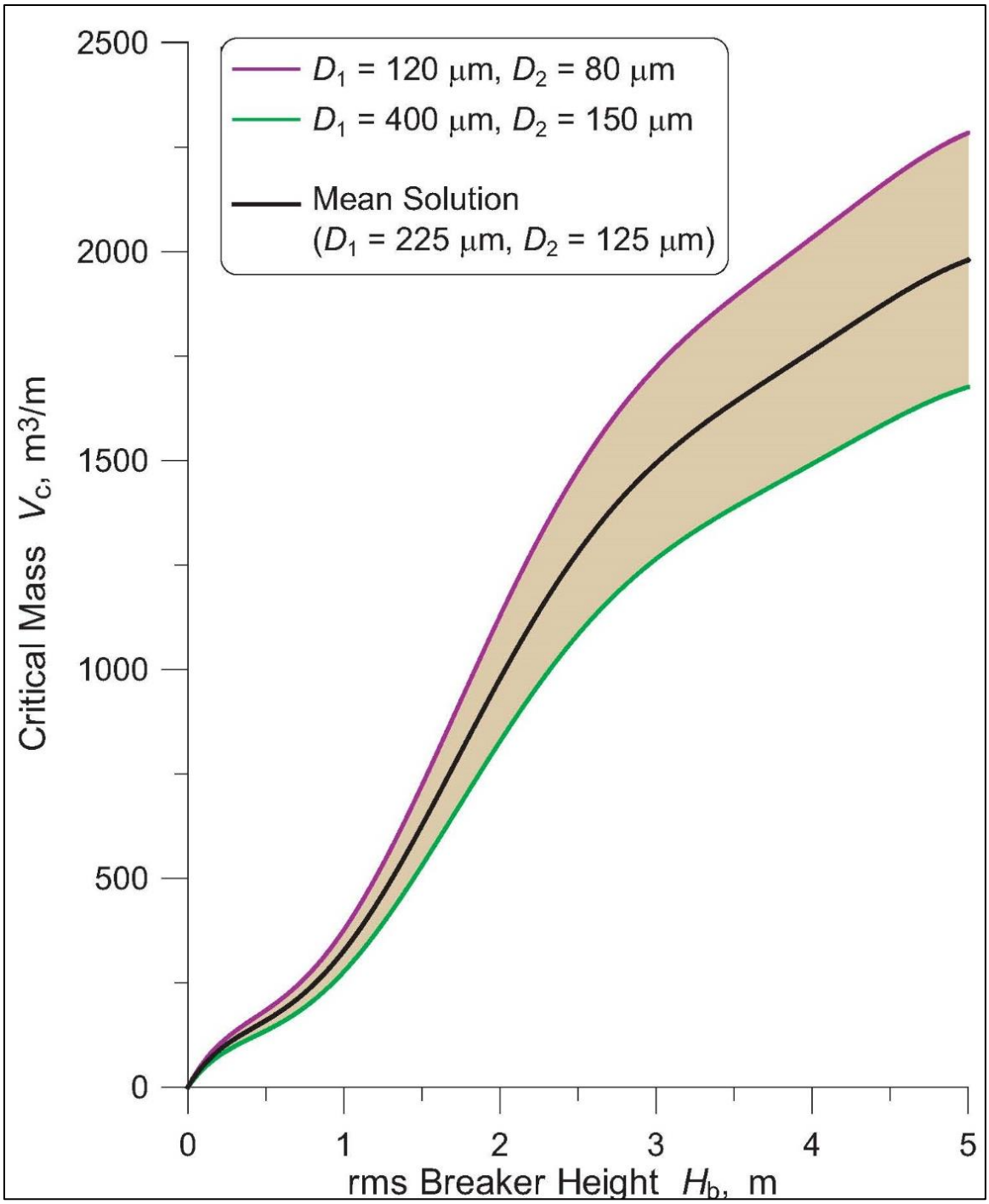

Figure 3.10: Critical mass solution as a function of rms breaker height for 12 sec waves breaking on variable sediment grain size in the bar-berm D1 and shore-rise D2 portions of the seabed profile. Curves generated from numerical integration of elliptic cycloid solutions.

3.6 Static and Dynamic Wave Setup

Both static and dynamic components of wave setup were calculated using the Direct Integration Method (DIM) which uses a parameterized set of equations that consider wave and bathymetric characteristics, specifically the shape of the wave energy spectrum and the nearshore shore-rise and bar-berm beach slope (m_{DIM}). The wave setup equations include factors for wave height (F_H and G_H), wave period (F_T and G_T), JONSWAP spectral narrowness factor (F_{Gamma} and G_{Gamma}), and nearshore slope (F_{Slope} and G_{Slope}).

Static wave setup is calculated as:

$$\overline{\eta} = 4.0 F_H F_T F_{Gamma} F_{Slope} = 4.0 \left(\frac{H_0'}{26.2} \right)^{0.8} \left(\frac{T_P}{20.0} \right)^{0.4} \left(\frac{m_{DIM}}{0.01} \right)^{0.2} \quad (16)$$

Dynamic wave setup is calculated as:

$$\eta_{rms} = 4.0 G_H G_T G_{Gamma} G_{Slope} = 4.0 \left(\frac{H_0'}{26.2} \right)^{0.8} \left(\frac{T_P}{20.0} \right)^{0.4} (Gamma)^{0.16} \left(\frac{m_{DIM}}{0.01} \right)^{0.2} \quad (17)$$

The wave parameters required as input for DIM are the deep water equivalent significant wave height, in feet, (H'_0) and the spectral peak wave period (T_P), as well as a measure of the spectral shape (*Gamma*). The spectral peak parameter, *Gamma*, was computed via a polynomial fit between the spectral width parameter, ν , and *Gamma,* according to:

$$Gamma = 2047\nu^4 - 3083\nu^3 + 1782\nu^2 - 4769.9\nu + 507.1 \quad (18)$$

Values of the spectral width parameter are computed directly from the standard deviation of the incident wave oscillation, σ_2 , based on the Longuet-Higgins (1973) definition of the spectral narrowness:

$$\nu = \left[\frac{2\sigma_2}{H_0'} \right]^{1/2} \quad (19)$$

Gamma values are limited from 1 to 38, based on the range of wave data used (Section 4) to relate the spectral narrowness, ν , to the peak parameter, *Gamma*, as shown in Figure 3.11.

The deep water equivalent significant wave height, H'_0 , and the peak wave period, T_P , are provided as output from the CDIP wave monitoring data (CDIP, 2015) and from Graham (2003) and are input directly into Equations (16) and (17). The nearshore slope, m_{DIM} , is taken as the average slope between the landward limit of wave run-up and the location offshore where the water depth is two times the depth at which the deep water significant wave height would be subject to depth-limited

breaking (van der Meer, 2002). The landward limit of wave run-up is calculated iteratively, with the initial approximation being the SWL.

3.7 Wave Run-up

Wave run-up was calculated using either the DIM or the Technical Advisory Working Group (TAW) method (van der Meer, 2002), depending upon the dynamic water level relative to the toe of the coastal structure and the shoreline (bar-berm) slope, m_{TAW} , calculated iteratively across the surf zone. The DIM is used to calculate run-up for transects with natural, gently sloping (m_{DIM} < 0.125) profiles. For shorelines with shore protection structures and steeply sloping (m_{TAW} ≥ 0.125) natural shorelines where the dynamic water level exceeds the toe of the structure, the TAW method was used to calculate run-up. If the dynamic water level does not reach the toe of the structure or bluff face, the DIM is used. The total run-up, including wave setup and incident wave run-up, is added to the *still water level* (SWL) to determine the *total water level* (TWL) (see Figure 3.12). Each of these methods is described in detail in the following subsections.

3.8 DIM Run-up Calculations

Run-up on gently sloping, natural shorelines, with structures or bluffs with slopes less than 12.5 percent, is calculated using the DIM. The run-up calculation is based on the standard deviations of the oscillating wave setup and the incident wave run-up components, and is a continuation of the DIM approach for wave setup. The dynamic setup η_{rms} is defined as the standard deviation of setup fluctuations, calculated from Equation (2). The standard deviation of the incident wave oscillations (wave run-up), σ_2 , on natural beaches is:

$$\sigma_2 = 0.3\xi_0 H'_0 \tag{20}$$

Where, H'_0 is the deep water significant wave height, m_{DIM} is the nearshore (shore-rise) bottom slope, $L_0 = gT_P^2 / 2\pi$ is the deep water wave length, and ξ_0 is the Iribarren number:

$$\xi_0 = \frac{m_{DIM}}{\sqrt{H'_0 / L_0}}$$

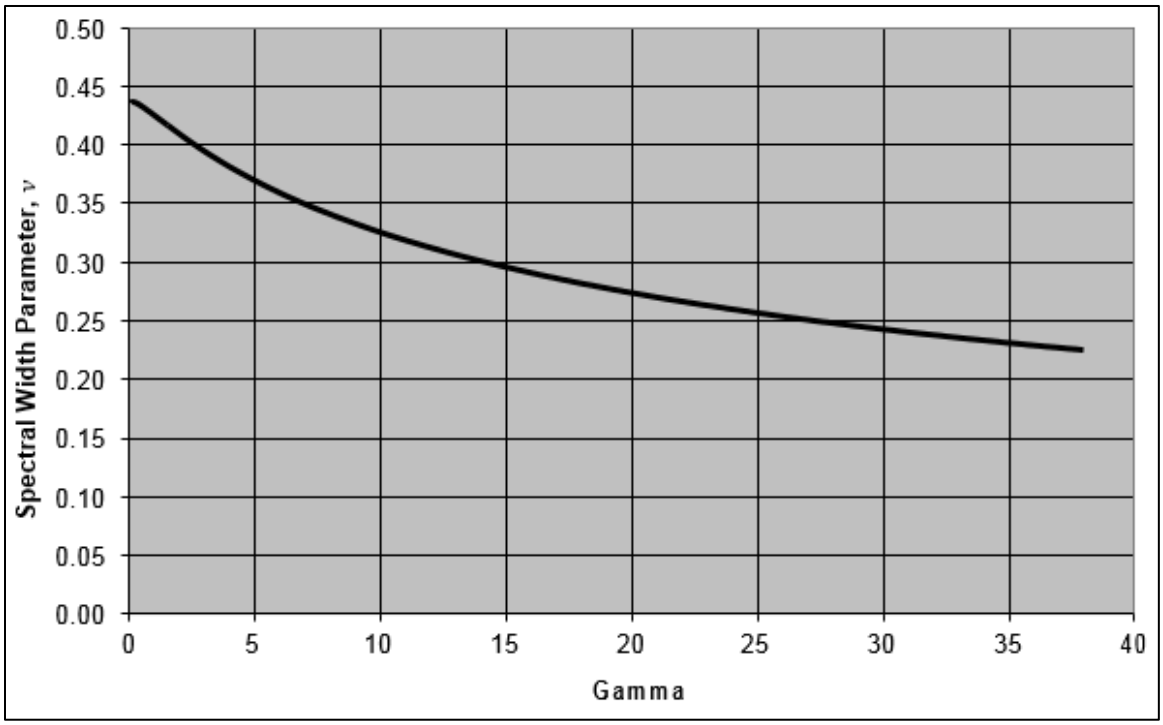

Figure 3.11: Spectral Width Parameter versus Spectral Peak Parameter. Note Gamma ≥ 1.0

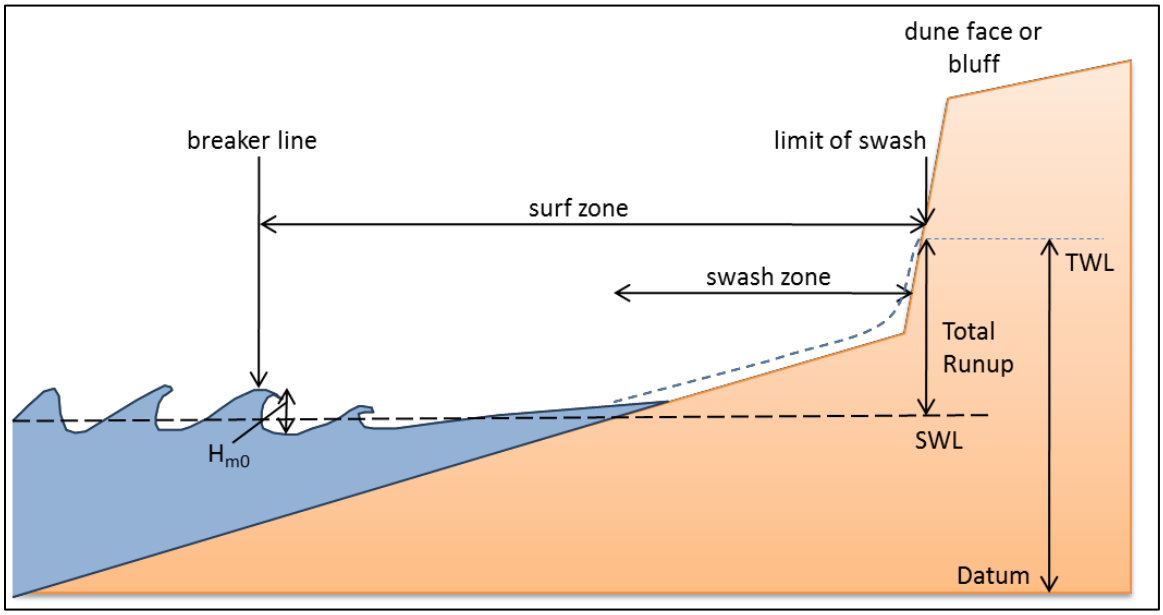

Figure 3.12: Conceptual Model Showing the Components of Wave Run-up Associated with Incident Waves

The oscillating component of the total wave run-up, $\hat{\eta}_T$, is determined from the combination of the two standard deviations of the fluctuating components:

$$\hat{\eta}_T = 2.0\sqrt{\eta_{rms}^2 + \sigma^2} \tag{21}$$

Combining the results from Equations (1) and (6) yields the total wave run-up, which when superimposed with the SWL yields the total water level, TWL:

$$TWL = \overline{\eta} + \hat{\eta}_T + SWL \tag{22}$$

Where SWL is the still water level derived from the hydroperiod function given by the companion guidance document, Jenkins, (2015), and is entered in Table 1 of Section 3.5.

3.9 TAW Run-up Calculations

Run-up on barriers, including steep (m_{TAW} > 0.125) dune features, bluffs, and coastal armoring structures such as revetments, are calculated using the TAW method (van der Meer, 2002). Wave run-up on barriers is a function of the geometry and roughness of the structure, as well as the height and steepness of the incident wave. The TAW method provides a mechanism for calculating wave run-up with adjustments made through reduction factors to account for surface roughness and the effects associated with the angle of wave approach.

With the TAW methodology the wave setup component of the TWL is calculated at the toe of the structure, and wave setup landward of the toe of the structure is not included. Wave setup seaward of the toe of the structure is computed with the DIM, using the nearshore slope, m_{DIM} .Wave setup is not included for cases where waves would not have broken prior to reaching the toe of the structure.

The reference water level at the toe of the structure for run-up calculations using the TAW method is defined as the 2-percent Dynamic Water Level ($DWL_{2\%}$). The dynamic water level is the sum of the measured SWL, the static wave setup, $\overline{\eta}$, and the dynamic wave setup, η_{rms} . Because DIM provides the static setup at the shoreline and not the barrier toe, and the magnitude of static wave setup varies significantly with depth across the surf zone, from a maximum at the shoreline to approximately zero seaward of the breaking point, a reduction to the static setup component is applied for cases where the barrier toe elevation is inundated by the SWL and the TAW method is used for computing wave run-up. The dynamic setup, however, varies insignificantly across the surf zone and requires no adjustment.

This procedure involves computing the static wave setup at the shoreline and at the toe location to determine a static setup reduction factor to be applied to the static wave setup calculated using DIM. The wave setup at the shoreline and toe location and subsequent reduction factor are based on the root mean square of the breaking

significant wave height $(H_b)_{rms}$, and the local water depth, h, at the toe of the barrier relative to SWL. The $(H_b)_{rms}$ is determined using the deep water equivalent significant wave height, H'_0, and the peak wave period, T_P, according to:

$$(H_b)_{rms} = 0.714\left(\frac{\kappa}{g}\right)^{1/5}\left(\frac{H_0'^2 C_0}{2}\right)^{2/5} \quad (23)$$

Where κ is the breaker criterion equal to 0.78 and C_0 is the deep water wave celerity, $C_0 = gT_P / 2\pi$. The static wave setup at the SWL shoreline is:

$$\overline{\eta}_0 = 0.189(H_b)_{rms} \quad (24)$$

And the static wave setup at the toe of the engineered barrier is:

$$\overline{\eta}(h) = 0.189(H_b)_{rms} - 0.186h \quad (25)$$

The static wave setup reduction factor, γ_η is then a ratio of the static wave setup at the toe to the static wave setup at the SWL shoreline, or:

$$\gamma_\eta = \frac{\overline{\eta}(h)}{\overline{\eta}_0} \quad (26)$$

This reduction factor is then applied to the DIM static wave setup to compute a depth-adjusted static wave setup at the toe of the engineered barrier,

$$\overline{\eta}' = \gamma_\eta \overline{\eta} \quad (27)$$

The 2-percent Dynamic Water Level ($DWL_{2\%}$) is thus calculated as:

$$DWL_{2\%} = \overline{\eta}' + 2\eta_{rms} + SWL \quad (28)$$

The next step is to compute the wave height at the toe of the barrier and the resultant wave run-up on the barrier. Let H_{m0} represent the spectral significant wave height at the toe of the structure. If the *DWL*$_{2\%}$ depth at the structure toe is found to be too shallow to support the calculated wave height, the wave was assumed to be depth-limited and the incident wave height was calculated using a breaker index of 0.78, whence $H_{m0} = 0.78h_{toe}$. The average slope for use in the TAW methodology, m_{TAW}, is calculated iteratively across the surf zone between the still water line minus $1.5H_{m0}$ and the run-up limit. The lower slope point must never be below the toe, however, even if SWL - $1.5H_{m0}$ falls below the toe (van der Meer, 2014). In these cases, the lower slope point is set at the toe. Since the run-up limit is initially unknown, the still water level plus $1.5H_{m0}$ is chosen as a first estimate (Figure 3.13). If the run-up limit exceeded the selected crest, the run-up limit was set at the crest. The general formula of TAW for calculating the 2-percent wave run-up on barriers is

$$R_{2\%} = 1.77 H_{m0} \gamma_r \gamma_b \gamma_\beta \xi_{0m} \text{ if: } 0.5 \le \gamma_\beta \xi_{0m} < 1.8$$

Or: (29)

$$R_{2\%} = H_{m0} \gamma_r \gamma_b \gamma_\beta \left(4.3 - \frac{1.6}{\sqrt{\xi_{0m}}} \right) \text{ if: } 1.8 \le \gamma_\beta \xi_{0m}$$

Where, $R_{2\%}$ is the wave run-up height exceeded by 2 percent of the incoming waves; H_{m0} is the spectral significant wave height at the structure toe; γ_r is the influence coefficient for roughness element of slope; γ_b is the influence coefficient for a berm; γ_β is the influence coefficient for oblique wave attack; $\xi_{0m} = m_{TAW} / (H_{m0} / L_m)^{0.5} = m_{TAW} T^{1/2} g^{1/2} / (0.883 h_{toe}^{1/2})$ is the Iribarren number based on wave parameters at the toe of the structure. For the purposes of worst-case assessments, we smooth run-up surfaces, normally incident waves, and plane sloping beaches, whence we assume these influence coefficients approach unity, $\gamma_r = \gamma_b = \gamma_\beta \rightarrow 1.0$.

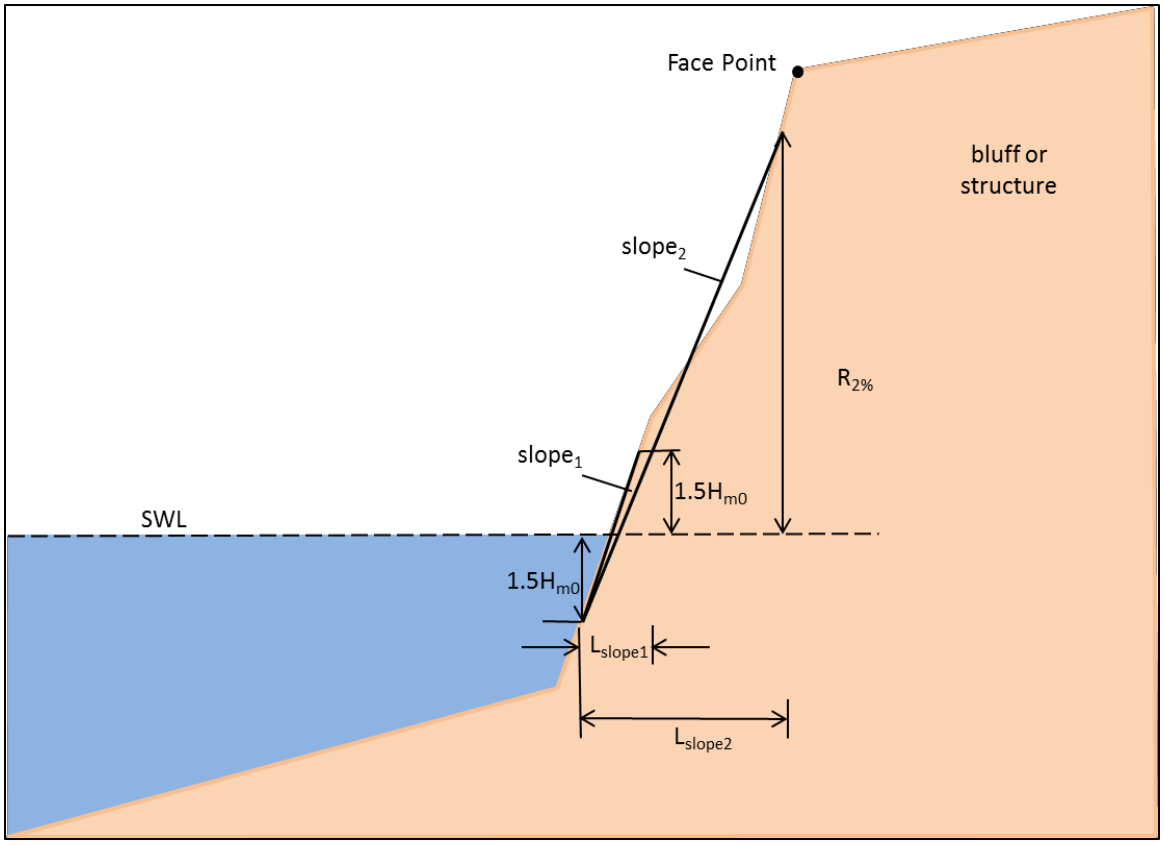

Figure 3.13: Determination of an Average Slope Based on an Iterative Approach (Corrected from van der Meer, 2002)

For assessments based on conditions other than worst-case, influence factors for roughness, the presence of a berm, and oblique wave attack are selected according to Table D.4.5-3 in the Final Draft *Guidelines for Coastal Flood Hazard Analysis and Mapping for the Pacific Coast of the United States* (FEMA, 2005), hereafter referred to as the Pacific Guidelines. The roughness reduction factor is set to 1.0 for a smooth concrete sea wall or sheet pile barrier.

When using software in Appendix-C, the influence factor for oblique wave attack is calculated at each time step in the CDIP wave record (see Section 4). The spectral significant wave height H_{m0} is shoaled and refracted from a deep water point to the structure toe using the oceanrds_raster.f computer code. The wave direction at the toe is compared to the transect orientation, perpendicular to the shoreline, to determine the angle of wave attack. For cases in which waves break seaward of the structure toe, the wave direction is taken from the point of breaking; i.e., where the incident wave height at the toe is depth-limited and calculated using a breaker index of 0.78, whence $H_{m0} = 0.78 h_{toe}$.

Ultimately, incident wave run-up using TAW, $R_{2\%}$, is statistically combined with the reduced dynamic wave setup, and added to SWL and static wave setup to yield the total water level, TWL, or:

$$TWL = SWL + \overline{\eta}' + 2.0\sqrt{\eta_{rms}^2 + \left(\frac{R_{2\%}}{2}\right)^2} \tag{30}$$

For non-vertical structures with slopes greater than 1:1, the TAW manual after van der Meer (2002) suggests using the TAW method with an additional vertical wall reduction factor, γ_v , to account for run-up on very steep (but not vertical) slopes. With steep slopes, the Iribarren number $\xi_{0m} = m_{TAW} / \left(H_{m0} / L_m\right)^{0.5}$ becomes large. To keep the relationship between the type of breaking and the Iribarren number, the vertical wall must be schematized as a 1:1 slope. Therefore, the barrier slope was set to 1:1 for the Iribarren number calculation, and a vertical wall reduction factor for steep slopes was applied:

$$\gamma_v = 1.35 - 0.0078 \tan^{-1} m_{face} \tag{31}$$

where the face slope, m_{face} measured between the selected toe and face locations, is the angle of the actual slope in degrees (van der Meer, 2002). While this approach is based on work done for vertical walls atop dikes, sensitivity testing showed that it compared well with the TAW method and the Shore Protection Method (SPM) (USACE, 1984) for vertical walls as an intermediate approach to calculating run-up on steep slopes. The use of this vertical wall reduction factor accounts for wave reflection expected on slopes greater than 45 degrees, and this approach generates results that fall between those for a 45-degree slope and those for a vertical wall.

Wave overtopping occurs when a potential run-up elevation exceeds a structure's profile crest elevation. When wave run-up is shown to exceed the barrier crest, the severity of wave overtopping is evaluated based on the mean overtopping rate, *q*. The required input parameters for computing the mean overtopping discharge are the wave height and freeboard, defined as the difference between the $DWL_{2\%}$ and the structure crest. The 1-percent-annual-chance TWL available from the wave run-up and extreme value analyses is a statistical value and is not associated with either a specific wave height or $DWL_{2\%}$. Therefore, the maximum wave height at the structure toe and the maximum and average $DWL_{2\%}$ associated with the 50 annual maximum TWLs were chosen for use with the 1-percent TWL to estimate the 1-percent overtopping hazard.

Mean overtopping rates, *q*, were computed following Table VI-5-13 in the Coastal Engineering Manual (USACE, 2006) which presents an overtopping formula for impermeable and permeable vertical walls according to:

$$q = 0.082\sqrt{g\hat{\eta}_T^3}\exp\left(-\frac{3.0R_c}{\hat{\eta}_T\gamma_\beta\gamma_s}\right) \quad (32)$$

Where R_c is the freeboard, $R_c = h_c - SWL$, γ_β is the influence factor for oblique wave attack, and γ_s is the influence factor for porosity. To conservatively maximize the overtopping potential, the designer should assume normally incident waves on non-porous surfaces, whence $\gamma_\beta = \gamma_s \rightarrow 1.0$. This maximum overtopping potential is based on a single hourly 1% design wave measurement and likely exceeds the 1-percent overtopping hazard. For comparison, the maximum wave height at the structure is also paired with the freeboard between the average $DWL_{2\%}$ from the 50 annual maxima and the crest elevation to estimate the overtopping rate expected over a full tidal cycle during a peak storm event.

3.10 Statistical Analysis

The preferred approach for determining the X-percent-annual-chance wave-induced flood elevation involves utilizing a reasonably long observational (or continuous model) record to establish a probability distribution that can be used to evaluate the flood elevation for any frequency. A general rule of thumb is that a historical record at least one-third the length of the return period of interest is the minimum record needed to produce statistically reliable results. The extremal probability distribution can be used to establish any flood elevation frequency, but the levels of confidence in the values decrease with the length of record. In this case, a modeled continuous record of 50 years of offshore and nearshore wave conditions are used to derive estimates of TWLs. This hindcast period is long enough that an extreme value distribution can be applied to it, in order to estimate the TWL elevation for a 1-percent-annual-chance condition. An annual maxima/Generalized Extreme Value (GEV) fit is used in the extreme value

analysis to determine the 1-percent-annual-chance event for existing conditions and for two sea level rise example scenarios.

The cumulative distribution function of the GEV family of distributions is given by:

$$F(z)=\exp\left\{-\left[1+\xi\left(\frac{z-\mu}{\sigma}\right)\right]^{-1/\xi}\right\} \quad (33)$$

The GEV model has three parameters: μ is the mode of the extreme value distribution (referred to as location parameter); σ is the dispersion (also known as the scale parameter), and ξ , (not to be confused with the Iribarren number in wave run-up equations), is a shape parameter that determines the type of extreme value distribution. These parameters were determined using routines for GEV statistical analysis within the Wave Analysis for Fatigue and Oceanography, Version 2.1.1 (WAFO) toolbox for Matlab, which contains tools for fatigue analysis, sea state modeling, statistics, and numerics (WAFO-group, 2000). The three parameters, μ , σ , ξ and the fit of the resulting cumulative distribution function to the annual maxima are evaluated for the maximum likelihood solutions.

The "Standard Method" used in the design calculations for coastal flooding by extreme event total water levels from combinations of extreme wave run-up and set-up atop extreme ocean water levels requires that the design frequency (one percent recurrence interval) must equal the compound frequency of the wave height and the ocean water level or:

$$P\left[H_T,\eta\right]=P(H_T)\bullet P(\eta)=\frac{1}{100} \quad (34)$$

Where H_T is the wave height with return period of T years, η is the ocean water level, $P(H_T)=1/T$ is the probability of wave occurrences with return frequency of once every T years; and $P(\eta)$ is the annualized probability of ocean water levels reaching an elevation of η feet NAVD 88. Implementation of this method uses the NOAA California tide gage data in the design process that are formatted in a type of stage frequency curve called a "*hydroperiod function."* The hydroperiod function provides a continuous relationship between ocean water levels measured at 6-minute time intervals and the recurrence probability (percent time wet) for each observed water level increment. The computations involves N_0 time steps, each 6 minutes in length, in order to sweep through the NOAA period of record for the tide gage station in Section 4.6. Conditional if statements and counting loops calculate the number time steps, $N(\eta)$, for which the ocean water level was greater than a particular elevation, Z_i representing a possible culvert design elevation. The percent time that elevation Z_i was wet due to ocean inundation over the period of record was calculated as:

$$E_i = \frac{100\%}{N_o} \sum N(\eta \geq Z_i) \tag{35}$$

An example of a hydroperiod function calculated for the for outer San Francisco Bay is shown in Figure 1 measured at the Golden Gate Bridge, giving the percent time that bay water levels caused wetting at elevations up to the extreme high water level for the period of record June 30, 1854 to present. The tidal datums used in the Standard Method (Equations (2) and (3)) are indicated by dashed colored lines according to tidal epoch 01/01/1983 - 12/31/2001, which is the last time that NOAA leveled the tide gages and verified water levels for the continental United States. The hydroperiod function must be annualized before it can be applied to Equation (1), because it represents probabilities of wetting in 6 minute intervals at various elevations between the extreme low water (ELW) and the extreme high water (EHW). In addition, the Standard Method protocols with the Draft 821.5 updates only admit to ocean water levels at or above mean sea level (MSL); otherwise the 100-year flood would be combined with ELW when applying Figure 1 water level probabilities to Equation (1). Therefore, we modify Equation (4) to consider only culvert elevations, Z_i, at or above MSL :

$$\hat{E}_i = \frac{100\%}{\hat{N}_o} \sum N(\eta \geq Z_i \geq MSL) \tag{36}$$

where:

$$\hat{N}_0 = \sum_i N_i(\eta \geq MSL)$$

Time averaging Equation (5) over yearly increments and then ensemble averaging the yearly increments gives an *annualized hydroperiod function* $H_{i,j}$ that represents the annualized probability of ocean water levels reaching a particular culvert elevation Z_i

$$H_{i,j} = \frac{1}{k} \sum_{j=1}^{j=k} \left[\frac{1}{\tau_j} \int_0^{\tau_j} \hat{E}_i \, dt \right] \tag{37}$$

Here τ_j is the length of tidal record in *year-j* and k is the number of years in the period of record at a particular tide gage station.

The one-percent compound frequency curve (34) is based on two annualized independent probability functions, $P(H_T)$, $P(\eta)$ and has units of reciprocal years, (years $^{-1}$), based on the wave height recurrence period, T . Although dimensionless, the annualized probability of ocean water levels, $P(\eta)$, is numerically equivalent to the wave height recurrence interval when expressed as an annualized hydroperiod function (37). This is apparent from the Standard Method, whereby it can be shown, for example, that the annualized probability of wetting for a particular ocean water elevation, e.g. $P(MHW)$ = 25% $\Leftrightarrow$ 25/100, combines exactly with a wave height recurrence interval of

the same numeric value $P(H_{25})$ = 1/25, to give a one-percent compound frequency from Equation (34). This fact (unique to the one-percent frequency calculus) allows the annualized hydroperiod from (37) be transposed into a *One-Percent Compound Frequency Curve* that establishes a direct relationship between the wave height recurrence period and the still water level, η =*SWL* , component of TWL (Equations (22) and (30)) such that there is only a 1% chance of high ocean water levels and extreme wave heights occurring once every *T* years.

4. Model Initialization and Calibration

Implementation of the CEM to evaluate coastal hazards questions requires comprehensive data bases to populate the input files and arrays. Those data bases were harvested from the existing literature and include bathymetry, beach and shore-rise profiles, sediment grain size, river sediment flux, and nearshore, tides, waves, and currents. Long-term monitoring of ocean properties in the coastal waters surrounding ESGS has been ongoing for about 30 years as required for compliance with NPDES permits for the AES Redondo Beach Generating Station thermal discharges (CRWQCB, 1999, 2000; MBC, 2002-2006). These data were accessed from the NPDES monitoring reports that are periodically released and filed with the Regional Water Quality Control Board. In attempting to reconstruct 24-year long, continuous, unbroken records of all eight controlling variables for the dilution and dispersion modeling problem, certain gaps were found in some of the data bases. These gaps were filled by using ocean data measured at CDIP monitoring sites in Santa Monica Bay, San Pedro, Sunset Beach, Huntington Beach, Begg Rock and San Clemente, CA, see CDIP (2004). Any remaining gaps that could not be filled by these most immediate neighbors were filled by monitoring data from the Scripps Pier in La Jolla, about 90 miles to the southeast of RBGS and King Harbor. Only about 1% of the total record length contained gaps filled by the Scripps Pier proxy records. None the less, the Scripps Pier site has many physical features in common with the nearshore area around RBGS and King Harbor. Both sites have a submarine canyon nearby. Consequently, internal waves are an active mechanism at both sites in causing daily (diurnal) variations in salinity, temperature, and other ocean properties. The longer period variations at seasonal and multiple year time scales are the same at both sites due to their proximity. Consequently, the Scripps Pier Shore Station data (SIO, 2005) and the Coastal Data Information Program monitoring at Santa Monica Bay, San Pedro, Sunset Beach and Huntington Beach, (CDIP, 2004) are reasonable surrogates to fill gaps in the NPDES data for the RBGS and King Harbor and Hyperion outfalls. These properties will be shown to exhibit considerable natural variability over the period of record from 1980 to mid-2004 due to daily and seasonal changes, but most especially due to climate changes of global scale.

4.1 Bathymetry

Bathymetry provides a controlling influence on all of the coastal processes that affect sediment transport. The bathymetry consists of two parts: 1) a stationary

component in the offshore where depths are roughly invariant over time; and 2) a non-stationary component in the nearshore where depth variations do occur over time. The stationary bathymetry generally prevails at depths that exceed closure depth which is the depth at which net on/offshore transport vanishes. Closure depth is typically -12 m to -15 m MSL in the Santa Monica Littoral Cell, [Inman et al. 1993]. The stationary bathymetry was derived from the National Ocean Survey (NOS) digital database. Gridding is by latitude and longitude with a 1 x 1 arc second grid cell resolution yielding a computational domain of 30.9 km x 18.5 km, (Figure 4.1). Grid cell dimensions along the x-axis (longitude) are 25.7 meters and 30.9 meters along the y-axis (latitude).

For the non-stationary bathymetry data inshore of closure depth (less than -15 m MSL) nearshore and beach surveys were conducted by the US Army Corps of Engineers in 1985, 1990, 1996 and have been compiled in Everts, 1997. These nearshore and beach survey data were used to update the NOS database for contemporary nearshore and shoreline changes that have occurred following the most recent NOS surveys. In the very nearfield of the RBGS an ESGS intakes and discharge, Tenera (2007) performed high resolution bathymetric survey on 5 m grid cell resolution. These data were incorporated in the nearfield grid and co-registered with the NOS data along the deep water boundary (Figures 4.2).

To perform both the required wave shoaling and transport computations in the far-field of RBGS and ESGS, resolution of the bottom bathymetry must be sufficient to provide at least two grid points per wavelength of the highest frequency wave to be shoaled. The far-field grid computes the effects of island sheltering and regional scale refraction and circulation due to the shallow banks of the continental margin (Figure 4.3). Nearfield grids (Figures 4.1 and 4.2) are nested inside the far-field grid and is used to calculate the broad scale littoral sediment transport in the Santa Monica Littoral Cell between Marina Del Rey and Redondo King Harbor.

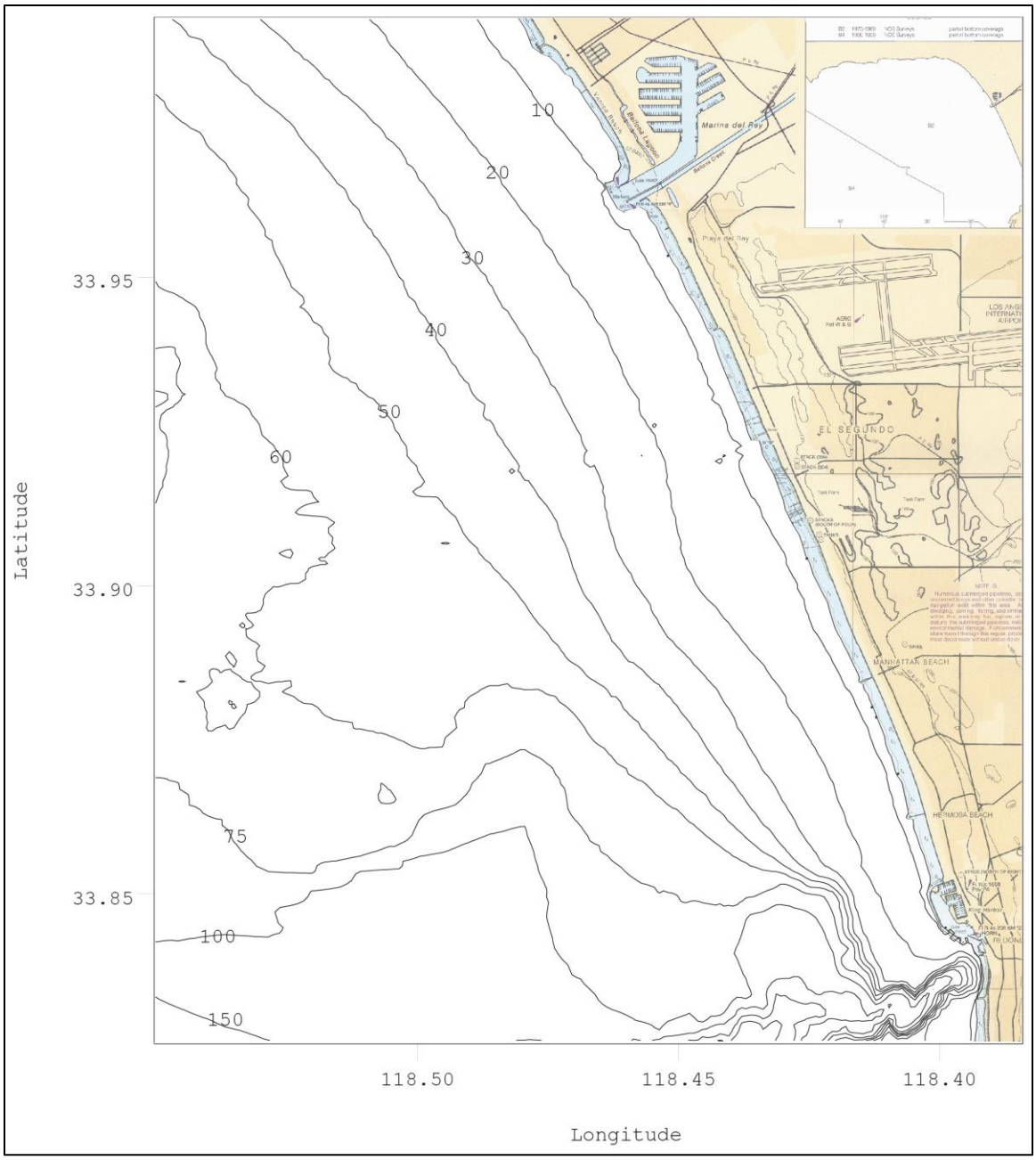

Figure 4.1: Nearfield grid derived from NOS bathymetry used for divergence of littoral drift, erosion/accretion and critical mass computations. Depth contours in meters MSL. Note *Redondo Submarine Canyon* in the bottom right hand corner of the figure.

4.2 Sediment Grain Size and Stratigraphy

Grain size of the sediments in the nearshore domain, and their variability with depth in the seabed (stratigraphy) is a leading order variable in both the closure depth and beach/shore-rise profile algorithms of the Coastal Evolution Model. The model is initialized using 7 seafloor cores taken at in the nearfield of the ESGS, see APPENDIX-A. The closure depth solutions and elliptic cycloid profile solutions that determine the burial and erosion potential of the intake and discharge end-works are functions of the seabed sediment grain size (Jenkins and Inman, 2006). There is a unique solution for the volume of critical mass for any arbitrary selection of grain size in the bar-berm, D_1, and the shore-rise, D_2. Regional seafloor sediment characterization by USACE, (2006) for region around ESGS and RBGS has produced the grain size distribution shown in Figure 4.4. According to the boring logs in Appendix-A, the upper 20 feet of sediment cover can be characterized by this grain size distribution. Accordingly, the top 20 feet of seabed sediments are comprised of 82% sand sized sediment and 18% fines consisting of very fine sand, silts and clays. Below 20 feet from existing grade, lens of brown, blue, and gray clays are found, believed to be derived from ancient lagoon deposits that underlie the King Harbor breakwaters and adjacent potions of the shelf. In the top 20ft of sediment, median grain size is about 220microns, fairly typical of fine sand beaches found throughout the lower Southern California Bight. The wet bulk density of these seafloor sediments is 1.63 g/cm^3 with a water content of 47.4%. The sediments also contain about 3.38% organics, again associated with ancient lagoon deposits. These grain size values are inputs to the elliptic cycloid solutions (Equations (12) to (15)) after Jenkins and Inman (2006).

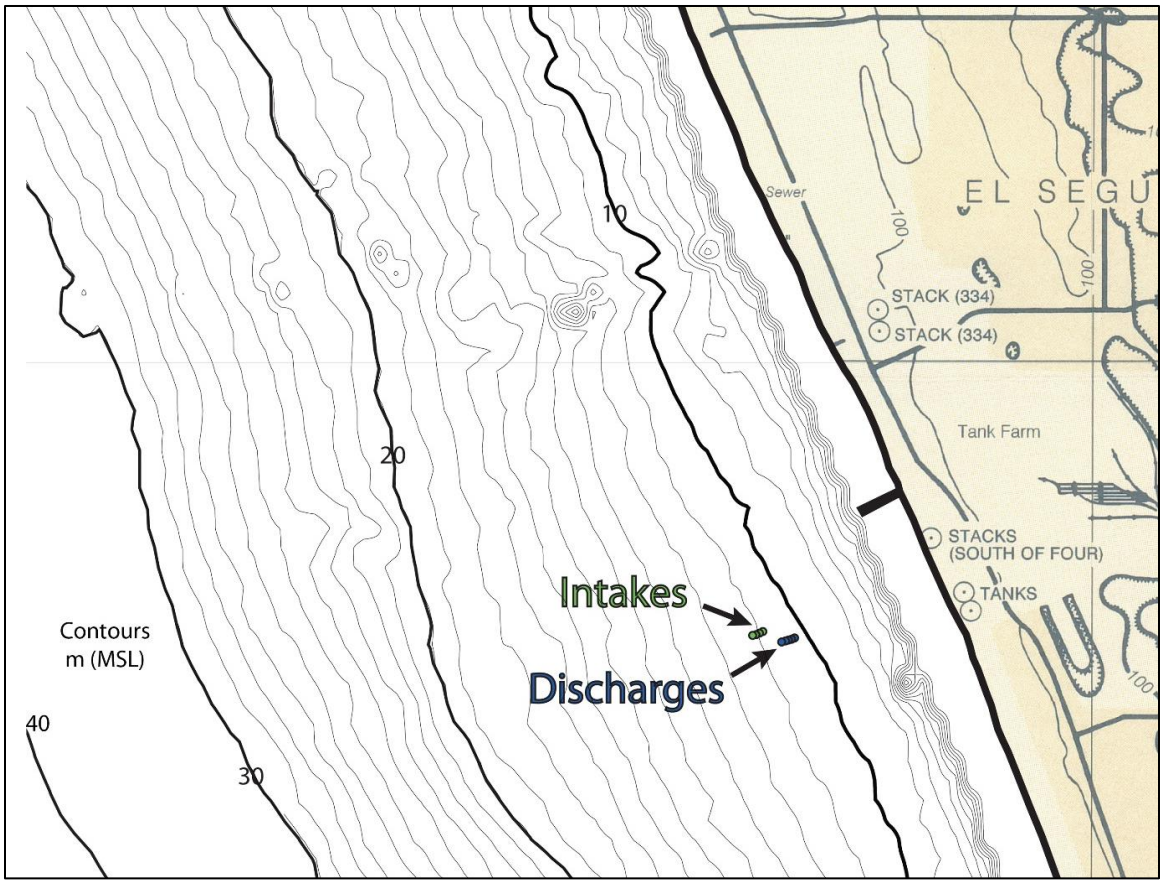

Figure 4.2: Nearfield bathymetric grid centered on the ESGS site for the West Basin Municipal Water District's proposed sea water desalination. Bathymetry from NOS with survey corrections by Tenera (2007).

El Segundo end of tunnel coordinates in UTM (m) are:

- Intake: 11S 367,576 m; E - 3,752,769 m N
- Discharge: 11S 367,720 m; E – 3,752,820 m N

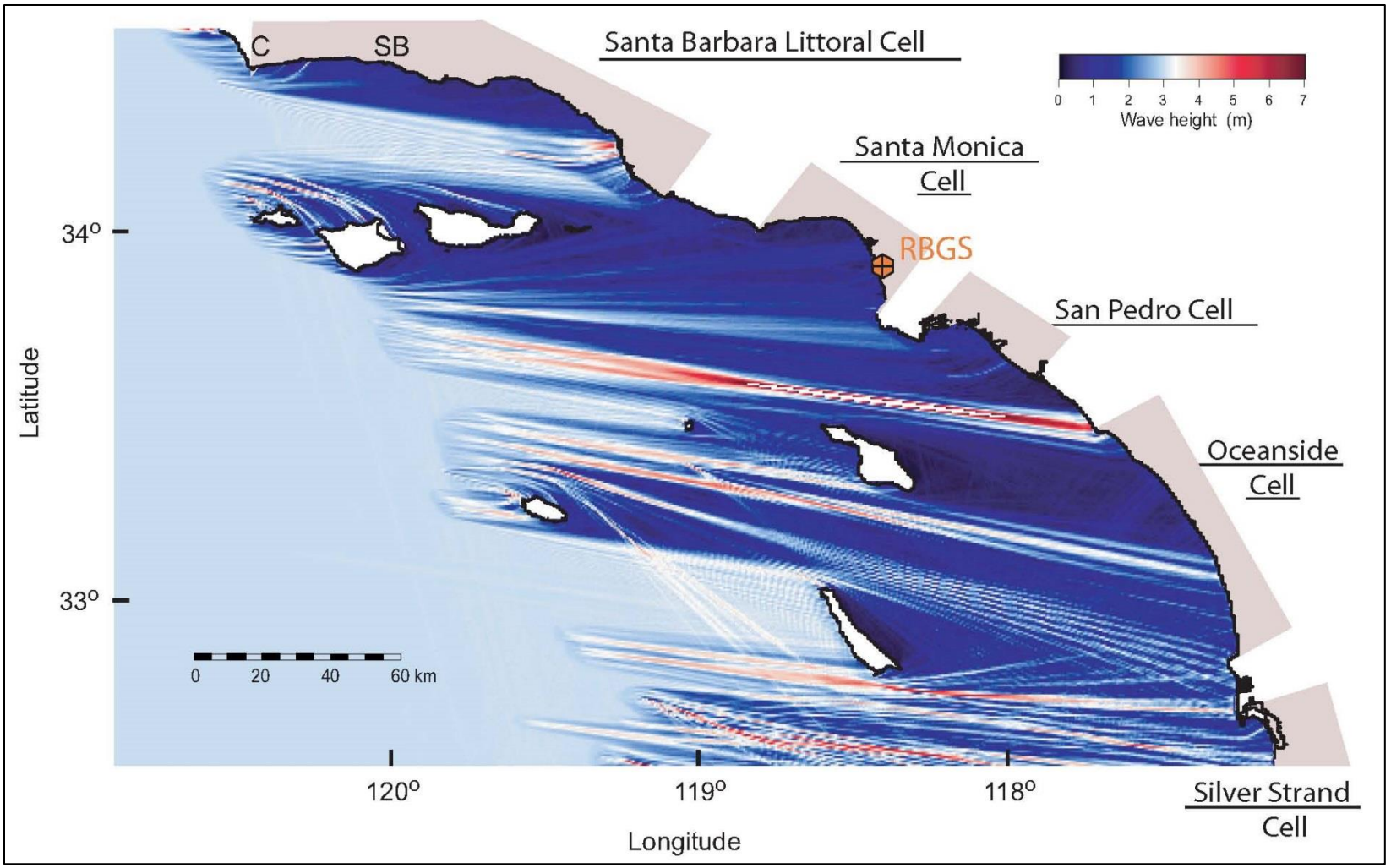

Figure 4.3: Far-field refraction/diffraction for broad-scale littoral sediment transport calculations in the Santa Monica Littoral Cell based on NOS digital bathymetry. Refraction/diffraction based on storm of 13 January 1993 with 3m deep-water significant wave heights and 15 sec periods approaching Southern California Bight from 285^0

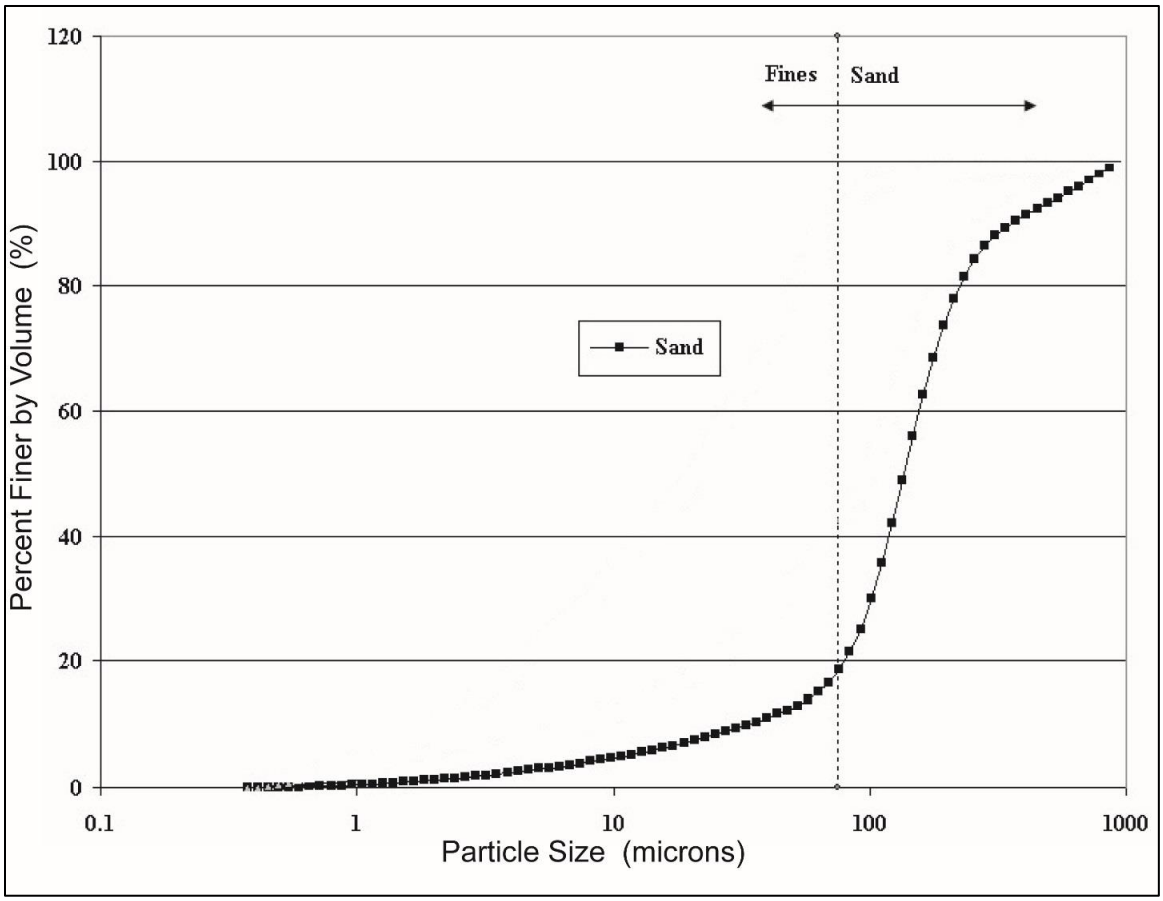

Figure 4.4: Sediment grain size distribution as measured by Coulter-Counter for Santa Monica Bay near the El Segundo and Redondo Beach project sites. (From USACE, 2006, APPENDIX-A).

4.3 Beach and Shore-rise Profiles

Non-Stationary bathymetry is the domain of seafloor inshore of closure depth that varies over time in response to beach erosion and accretion. It is measured periodically with beach and shore-rise profiling conducted by the US Army Corps of Engineers (USACE) in the neighborhood of the Chevron Groin and the Redondo King Harbor. These measurements are archived in the reports USACE, (1999 and 2001), and the profiles for the ranges relevant to the seabed stability around the ESGS and RBGS sites are plotted Figures 4.5. These measurements are used to calibrate the beach and shore-rise profile algorithms in the Coastal Evolution Model. Measured beach and shore-rise profiles across the south fillet beach at the Chevron Groin near the ESGS site are plotted in Figure 4.5 between June 1991 and September 1997. This is the down-drift beach at the groin and typically represents the most eroded profiles in the nearfield of the ESGS site; thereby capturing the worst case scenario at this site. These measurements are used to calibrate the beach and shore-rise profile algorithms in the Coastal Evolution Model.

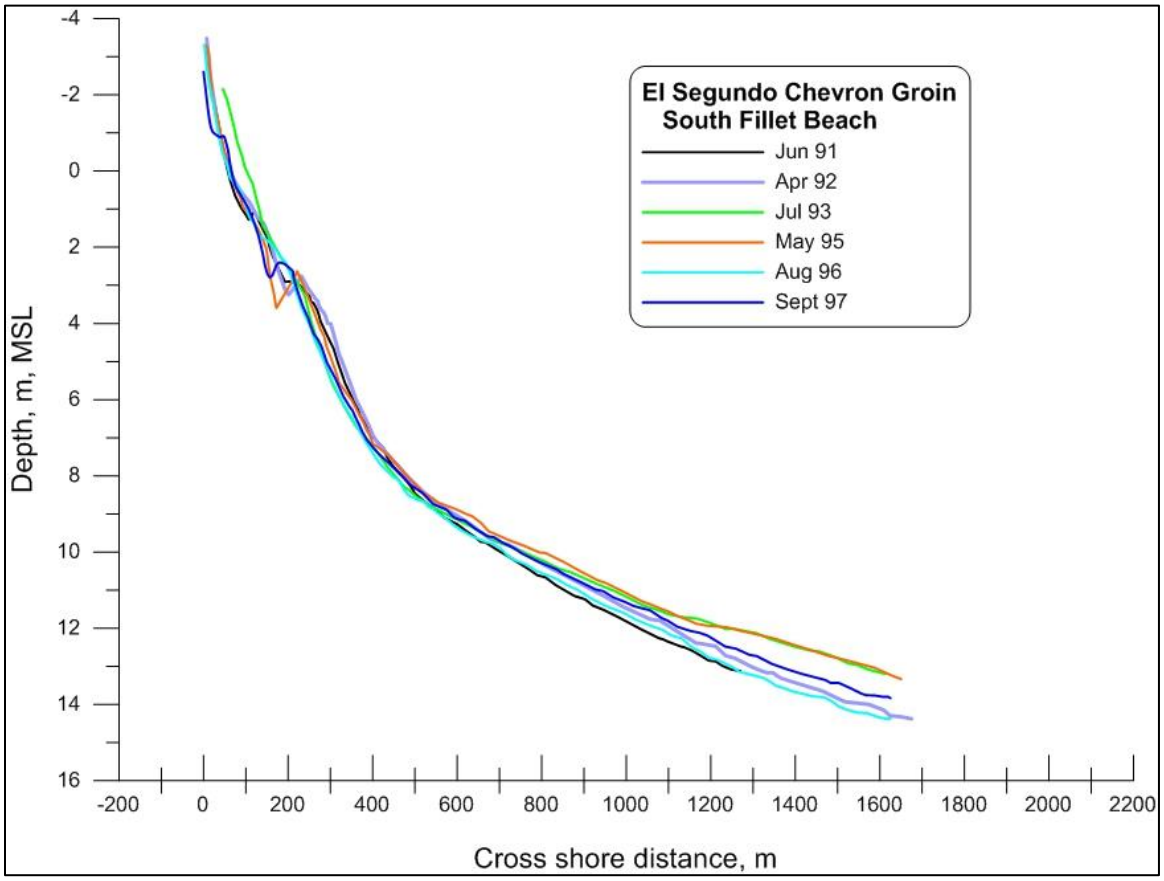

Figure 4.5: Measured beach and shore-rise profiles at the Chevron Groin near the ESGS site, (cf. Figure 4.1), monitored by the U.S. Army Corps of Engineers, Los Angeles District, between June 1991 and September 1997. Data from USACE, (1999 and 2001).

4.4 Sediment Flux from River Floods

River sediment flux is the most persistent source term in the sediment budget of the Santa Monica Littoral, and is due to the discharges from three major creeks: Calleguas Creek, Malibu Creek, and Ballona Creek, represented by the *J(t)* term in Equation (3). The USGS has published annual mean flow volumes since 1940 and daily event based runoff volumes for these creeks during water years 1997-98 and 1998-99 (USGS, 2000). The upstream drainage of these creeks has a combined area of 1,146 square kilometers. The annual mean flow volumes at the USGS gage stations on these creeks for the period of record of 1940-99 are listed in Inman and Jenkins, 1999. The peak flow event was in 1983, and no comparable floods have occurred since 1998.

The sediment yield data induced by rainfall variation is derived by applying sediment rating curves to the annual mean stream flow of the three major creeks of the Santa Monica Littoral Cell. The rating curves were derived in a two-step procedure [e.g., Brownlie and Taylor, 1981a&b]. This procedure utilized a limited amount of daily sediment flux measurements available under two separate USGS monitoring programs, namely: 1) the Hydrologic Benchmark Network; and 2) the National Stream Quality Accounting Network (USGS, 1997). Rather than seeking rating curves between annual flow volume and annual sediment flux per Brownlie and Taylor (1981a), better correlations are obtained between daily cumulative flow volume, (V_i, m^3/day) and daily sediment yield (J_i, tons/day), see Inman and Jenkins, (1999). These data were fitted to a power function $J_i = \xi Q^{\omega}$, where (ξ, ω) are statistically derived constants (per Equation (9)) that give daily estimates of sediment flux from the Calleguas Creek, Malibu Creek, and Ballona Creek over the period of record of the CEM simulations. For the Calleguas Creek, ξ = 4.13 x 10^{-9} and ω = 1.892; for the Malibu Creek, ξ = 5.04 x 10^{-9} and ω = 1.872; while for the Ballona Creek ξ = 2.14 x 10^{-9} and ω = 1.996. Sediment flux data for these three creeks are plotted in Figures 4.6 through 4.8. There it is shown that sediment flux from the Calleguas Creek and Malibu Creek, is an order of magnitude greater than that of the Ballona Creek, where annual mean sediment flux from the Calleguas Creek is *J* = 0.62 x 10^6 metric tons per year; and the Malibu Creek is *J* = 0.72 x 10^6 metric tons per year as compared to only *J* = 0.014 x 10^6 metric tons per year for the Ballona Creek. These values are used as sediment source inputs to the CEM sediment budget analysis for the Santa Monica Littoral Cell.

4.5 Sediment from Beach Disposal of Dredge Material

Another important input to the sediment source term *J(t)* in the CEM sediment budget (Equation (1)) is beach disposal of dredge material, otherwise referred to as *beach nourishment*. Beach nourishment has been especially active in the Santa Monica Littoral Cell for many years, principally due to beach disposal of dredge material from Marina Del Rey. With over 4,700 boat slips and a design depth of 20 feet, it is the largest man-made harbor in the United States. By law, the United States Army Corps of

Engineers (Corps) is responsible for keeping the Marina's entrance and main channels navigable and safe for all users.

As such, the Corps dredges sediment from the main channel an average of every three to five years and places on average 150,000 cubic yards (CY) on neighboring beaches. In 1999-2000, the Corps dredged 480,000 CY from the Marina to remove clean and contaminated sediment and restore, its design depth (of 20 feet) in many locations and fully opening both entrances. Although an additional 350,000 CY of dredging occurred in both 2007 and 2009, the Marina had not been fully dredged thereafter to eliminate the vast quantity of contaminated sediment. By fall 2011, both of the Marina's entrances, as well as a portion of the main channel were suffering from the buildup of approximately 1 million CY of sediment from the adjacent Ballona Creek and neighboring beaches. Over 760,000 CY of this sediment was contaminated with toxic chemicals, insecticides, chlordane, and heavy metals, such as arsenic and lead, due to waste and runoff from the Ballona Creek flood control channel. Though only 62% of this contaminated sediment was eventually removed, estimates to dispose of even this smaller amount at a hazardous waste landfill varied between $70.6 and $94.2 million.

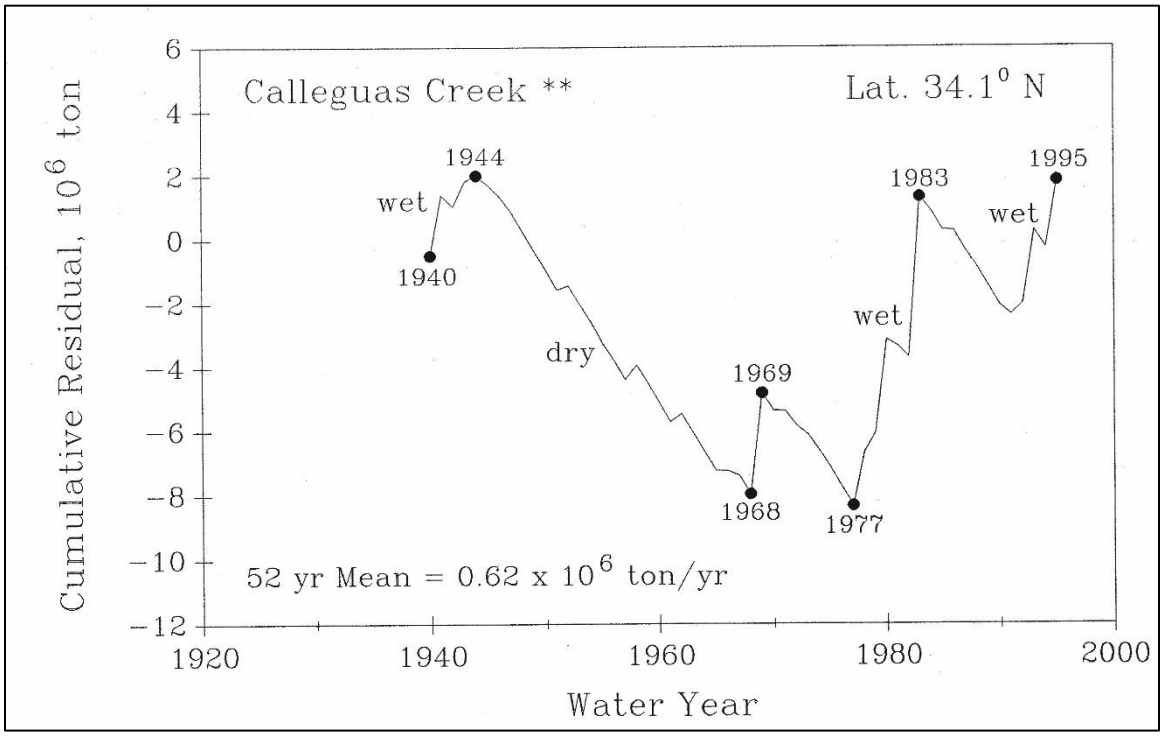

Figure 4.6: Cumulative Residual time series of sediment flux from the Calleguas Creek calculated using data from Inman and Jenkins, (1999) with a 52-year mean, 1945-1995.

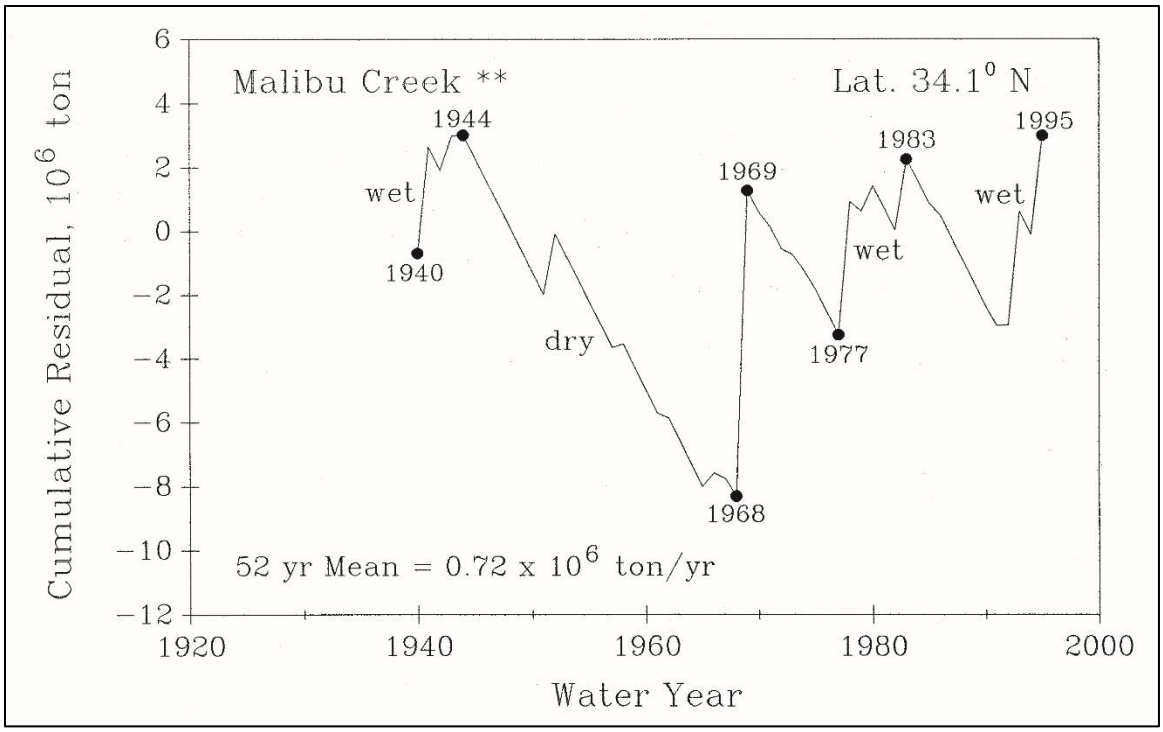

Figure 4.7: Cumulative Residual time series of sediment flux from the Malibu Creek calculated using data from Inman and Jenkins, (1999) with a 52-year mean, 1945-1995.

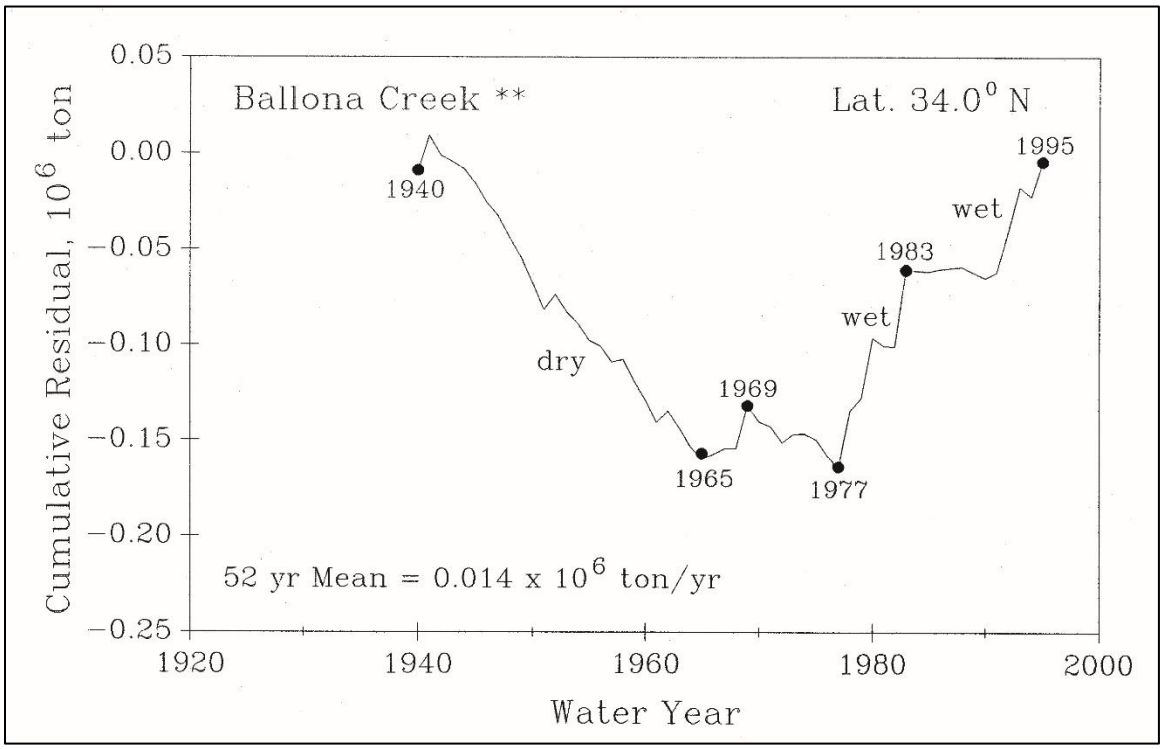

Figure 4.8: Cumulative Residual time series of sediment flux from the Ballona Creek calculated using data from Inman and Jenkins, (1999) with a 52-year mean, 1945-1995.

In October 2011, the Department of Beaches and Harbors and the U.S. Army Corps of Engineers began developing a Maintenance Dredging Project that eventually cleared the entrances of 777,000 total CY, with 471,000 CY of MDR contaminated sediment encapsulated in a pier construction project at the Port of Long Beach and 306,000 CY of clean sediment placed at both Redondo and Dockweiler beaches, as well as offshore at Redondo Beach for use in a future nourishment project. These dredge and beach disposal quantities are used as sediment source inputs to the CEM sediment budget analysis for the Santa Monica Littoral Cell.

4.6 Tides and Ocean Water Levels

The nearest ocean tide gage station is at Santa Monica Pier (NOAA # 941-0840). However, continuous ocean water level measurements are only available at this station after 1995. To fill the period of record prior to 1995 we use the tide gage records at Los Angeles (NOAA #941-0660). For the pre-1995 period we choose the Los Angeles tide gage in preference to the King Harbor tide gage due to the uncertainties associated with gage subsidence at King Harbor. The Los Angeles tide gage (NOAA #941-0660) was last leveled using the 1983-2001 tidal epoch. Elevations of tidal datums referred to Mean Lower Low Water (MLLW), in **METERS** are as follows:

- HIGHEST OBSERVED WATER LEVEL (11/13/1997) = 2.332 m
- MEAN HIGHER HIGH WATER (MHHW) = 1.624 m
- MEAN HIGH WATER (MHW) = 1.402 m
- MEAN TIDE LEVEL (MTL) = 0.839 m
- MEAN SEA LEVEL (MSL) = 0.833 m
- MEAN LOW WATER (MLW) = 0.276 m
- NORTH AMERICAN VERTICAL DATUM-1988 (NAVD) = 0.058 m
- NGVD29 = 0.700 m
- MEAN LOWER LOW WATER (MLLW) = 0.000 m
- LOWEST OBSERVED WATER LEVEL (12/17/1933) = -0.874 m

The Annualized Hydroperiod function, $H_{i,j}$, calculated from Equation (37) using the Los Angeles tide gage record (NOAA #941-0660) is plotted in Figure 4.9. This function is used for the determining the *SWL* inputs tot the total water level *TWL* calculations based on a 1% combined frequency of recurrence of extreme wave heights and high water levels.

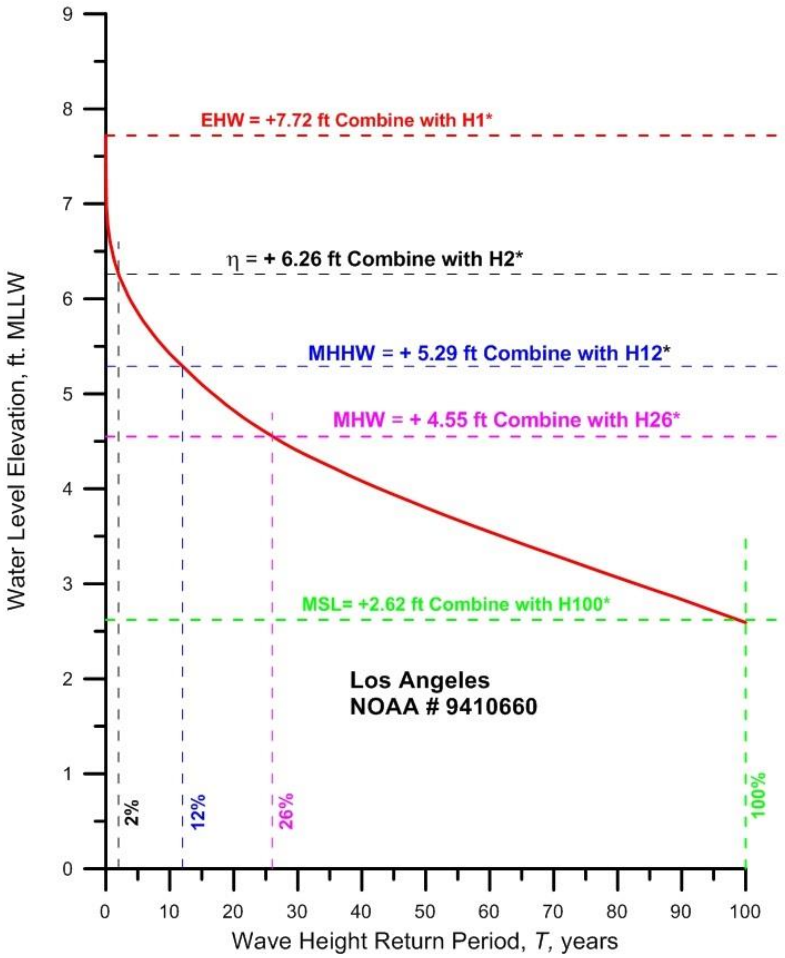

Figure 4.9: *Annualized Hydroperiod function, $H_{i,j}$*, for the 1% combined frequency of recurrence of extreme wave heights and water levels, (after Jenkins and Taylor, 2016).

4.8 Waves

Waves are the principle driving mechanism of mixing and current ventilation in the very nearshore region off the ESGS site. This wave dominated region consists primarily of the surf zone but extends seaward into the wave shoaling zone a few surf zone widths beyond the point of wave breaking. Waves are also the most difficult of the 8 controlling variables to get long unbroken records. The availability of wave data in the lower Southern California Bight is what limited the period of record for this long term model analysis to 1980-2004. Waves have been routinely monitored at several locations in the lower Southern California Bight since 1980 by the Coastal Data Information Program (CDIP, 2004).

In considering the wave climate of the Santa Monica Bay and Redondo Beach/El Segundo area, the sheltering effects of the Channel Island System must be taken into account. Figure 4.3 shows that only certain gaps or “wave windows” between the islands and intervening land masses will allow the high energy, long period swells of distant storms to reach RBGS and ESGS area. Because these island sheltering effects are

directionally dependent, it is not sufficient to use wave monitoring data that does not include wave direction. Wave energy and direction have been routinely monitored at several locations in the lower Southern California Bight since 1980 by the Coastal Data Information Program (CDIP, 2004). The nearest CDIP directional wave monitoring sites are:

Huntington Beach Array

- Station ID: 072
- Location: 33 37.9 North, 117 58.7 West
  Approximately 1 mile west of lifeguard headquarters at Huntington Beach, CA
- Water Depth: 10 m
- Instrument Description: Underwater Directional Array
- Measured Parameters: Wave Energy, Wave Period, Wave Direction

San Clemente

- Station ID: 052
- Location: 33 25.2 North, 117 37.8 West
  1000 ft NW of San Clemente Pier
- Water Depth (MLLW): 10 m
- Instrument Description: Underwater Directional Array
- Measured Parameters: Wave Energy, Wave Period, Wave Direction

San Pedro

- Station ID: 092
- Location: 33 37.07 North, 118 19.02 West
- Water Depth (MLLW): 457 m
- Instrument Description: Datawell Directional Buoy
- Measured Parameters: Wave Energy, Wave Period, Wave Direction

Santa Monica Bay

- Station ID: 028
- Location: 33 51.27 North, 118 37.98 West
- Water Depth (MLLW): 365 m
- Instrument Description: Datawell Directional Buoy
- Measured Parameters: Wave Energy, Wave Period, Wave Direction

Sunset Beach

- Station ID: 027
- Location: 33 42.30 North, 118 4.20 West
- Water Depth (MLLW): 8 m
- Instrument Description: Directional Array

- Measured Parameters: Wave Energy, Wave Period, Wave Direction

Begg Rock

- Station ID: 138
- Location: 33 22.80 North, 119 39.80 West
- Water Depth (MLLW): 110 m
- Instrument Description: Buoy
- Measured Parameters: Wave Energy, Wave Period, Wave Direction

These data sets possessed gaps at various times due to system failure and a variety of startups and shut downs due to program funding and maintenance. The undivided data sets were pieced together into a continuous record from 1980-2004 and entered into a structured preliminary data file. The data in the preliminary file represent partially shoaled wave data specific to the local bathymetry around each monitoring site. To correct these data to the nearshore of RBGS and ESGS, they are entered into a refraction/diffraction numerical code, back-refracted out into deep water to correct for local refraction and island sheltering, and subsequently forward refracted into the immediate neighborhood of RBGS and King ESGS. Hence, wave data off each monitoring site was used to hindcast the waves at RBGS and King Harbor.

The backward and forward refractions of CDIP data to correct it to RBGS and King Harbor were done using the numerical refraction-diffraction computer code, OCEANRDS. The primitive equations for this code are lengthy, so a listing of the FORTRAN codes of OCEANRDS appear in Jenkins and Wasyl (2005). These codes calculate the simultaneous refraction and diffraction patterns propagating over a Cartesian depth grid. A large outer grid (Figure 4.3) was used in the back refraction calculations to correct for island sheltering effects, while a high resolution inner grid (Figure 4.10) was used for the forward refraction over the local bathymetry around the Palos Verdes Peninsula and the RBGS and ESGS. OCEANRDS uses the parabolic equation method (PEM), Radder (1979), applied to the mild-slope equation, Berkhoff (1972). To account for very wide-angle refraction and diffraction relative to the principle wave direction, OCEANRDS also incorporates the high order PEM Pade approximate corrections modified from those developed by Kirby (1986a-c). Unlike the recently developed REF/DIF model due to Dalrymple, et al. (1984), the Pade approximates in "OCEANRDS" are written in tesseral harmonics, per Jenkins and Inman (1985); in some instances, improving resolution of diffraction patterns associated with steep, highly variable bathymetry such as found near the Redondo Submarine Canyon. These refinements allow calculation of the evolution and propagation of directional modes from a single incident wave direction; which is a distinct advantage over the more conventional directionally integrated ray methods which are prone to caustics (crossing wave rays) and other singularities in the solution domain where bathymetry varies rapidly over several wavelengths.

An example of a reconstruction of the wave field throughout the Bight is shown in Figure 4.3 using the back refraction calculation of the CDIP data from the San Clemente array. Wave heights are contoured in meters according to the color bar scale and represent 6 hour averages, not an instantaneous snapshot of the sea surface elevation. Note how the sheltering effects of Catalina and San Clemente Islands have induced longshore variations in wave height throughout the Southern California Bight. Figure4.11a shows the significant wave heights inside Santa Monica Bay, with corresponding periods and directions, resulting from the series of back-refraction calculations for the complete CDIP data set at Δt = 6 hour intervals over the 1980-2004 period of record. The data in Figure 4.11a are values used as the deep water boundary conditions on the nearfield grid (Figure 4.1) for the forward refraction computations into the RBGS and ESGS region (like those in Figure 4.10). The deep water wave angles in Figure 4.11c are plotted with respect to the direction (relative to true north) from which the waves are propagating at the deep water boundary of the nearfield grid (Figure 1.1). Inspection of Figure 4.11a reveals that a number of large swells lined up with the wave windows open to RBGS and ESGS during the El Niño's of 1980-83, 1986-88, 1992-95, and 1997-98. The largest of these swell events was the 1 March 1983 storm, producing 3.5-meter-deep water swells seaward of the Redondo Submarine Canyon. Due to the refraction effects of the Redondo Submarine Canyon, these waves shoaled to 6-meter wave heights in the vicinity of the ESGS and the Chevron Groin (Figure 4.10).

Figure 4.10 gives an example of the complete forward refraction pattern over the nearfield grid of the RBGS and ESGS region for the El Niño storm of 1 March 1983. Although the swells in deep water from this storm were 3.5 m high, we find in Figure 4.10 that the refraction effects over local bay bathymetry create areas to the south of the King Harbor and to the north of the Chevron Groin where heights increase to 6 m. In these areas, the bay and submarine canyon bathymetry has focused the incident wave energy and these regions of intensified wave energy are referred to as "*bright spots*." In this case the bright spot is caused by the narrowing of the shelf in the vicinity of the Redondo Submarine Canyon. The increased wave heights in these bright spots increase the dynamic and static wave set-up as well as the rms-breaking wave heights and run-ups along the bike trail revetment. This increases the local beach erosion which increases the water depth at the toe of the revetment, further increasing the wave run-up. Conversely, the dark areas in Figure 4.10 south of the ESGS South site and the north breakwater of King Harbor where wave heights have been diminished are termed "shadows," and represent areas of reduced run-up and lesser amounts of beach erosion. For the 1 March 1983 storm, the area around the RBGS Unit 5-6 discharge is indeed in a shadow zone, while the ESGS site is a "bright spot". In shadow zones adjacent to bright spots, wave-driven currents (sometimes referred to as mass transport) flow away from the bright spots and towards the shadow zones; thereby causing offshore flow in the form of rip currents.

Refraction patterns of the type shown in Figure 4.10 were generated for each of the 8,920 deep water wave events in Figure 4.11 between 1980 and the middle of 2004. The resulting arrays of local wave heights, periods and directions were throughput to CEM for continuous littoral cell analysis (divergence of drift).

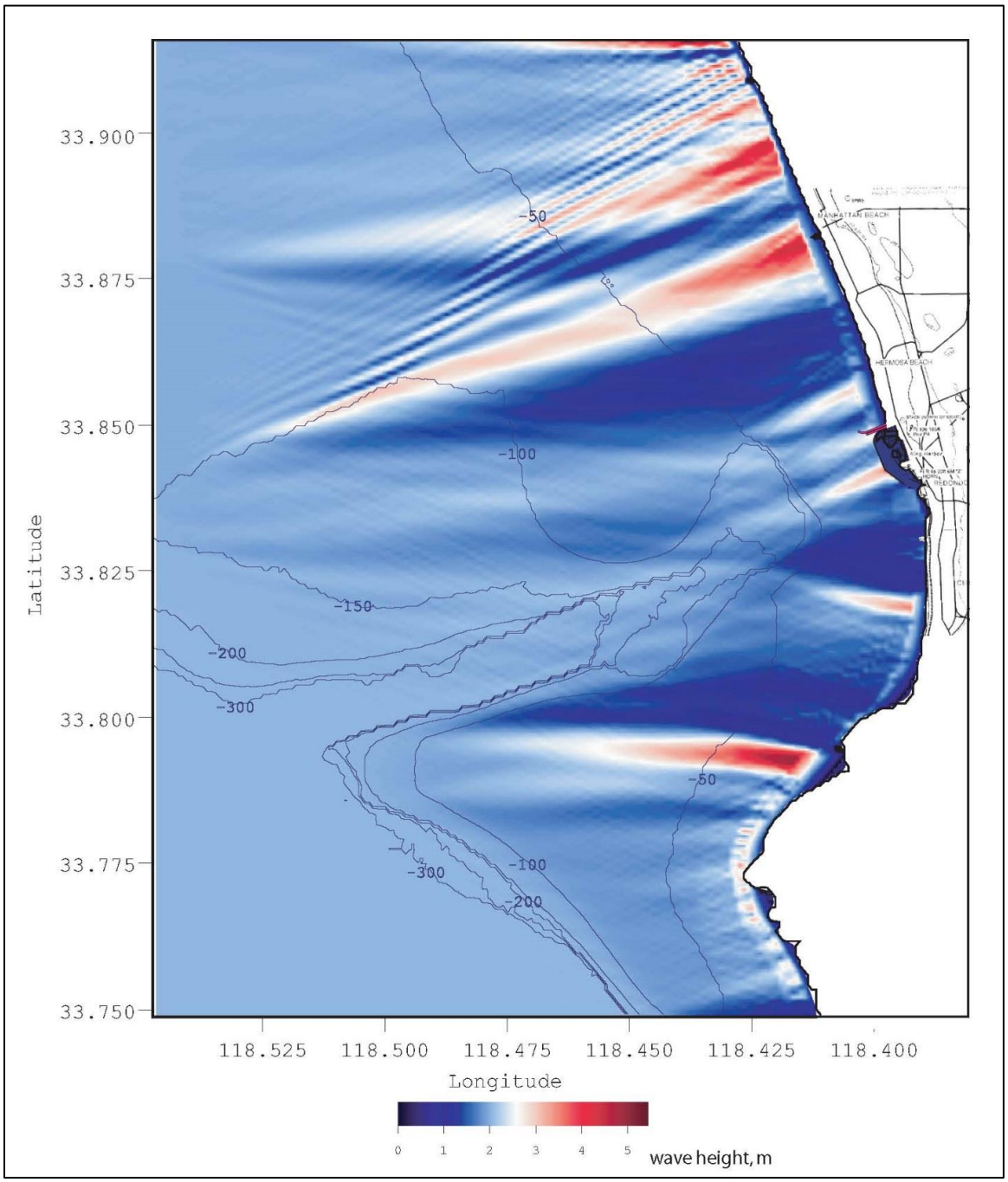

Figure 4.10: Refraction/diffraction pattern in the neighborhood of the ESGS site for the proposed West Basin Municipal Water District Ocean Water Desalination Project. Note the large wave shadow in the region between the Redondo King Harbor and the Chevron Groin. Refraction/diffraction calculations based on 100 year wave event from the 1 March 1983 storm.

5. Coastal Evolution Analysis of the Santa Monica Littoral Cell

The Coastal Evolution Model (CEM) was time-stepped through the 24-year period of record of input variables as detailed in Section 5, (January 1980 through July 2004); producing 8,920 daily solutions at 220 coupled control cells (cf. Figure 3.3 b) along a 19.8 km reach of coast between the Santa Monica Pier and the Redondo King Harbor. In the nearfield of the RBGS & ESGS, computational precision was increased by using the nested inner nearfield grid with 1 arc-second resolution among 238 coupled control cells along a 7.2 km reach of coast between Redondo King Harbor and the Chevron Groin. In the coarse outer grid, the control cells are assigned 90 m spacing along the coastline, and 30 m spacing in the high resolution inner grid. The keystone solutions in each control cell are: 1) the sediment volume flux, *dq/dt,* per unit length of shoreline (m^3/m/day), also referred to as the erosion-deposition flux; 2) the closure depth; and, 3) the critical mass envelope. The sediment volume flux, *dq/dt,* tells us whether the section of coast represented by a particular control cell is eroding (*dq/dt < 0*), or accreting through sediment deposition (*dq/dt > 0*). We use the sediment volume flux to assess the long-term seafloor stability of a particular Neodren™ or other sub-seabed intake site. Ideally an optimal sub-seabed intake site will neither erode nor accrete; and so, we look for the closest places to the RBGS & ESGS where, $dq/dt \to 0$.

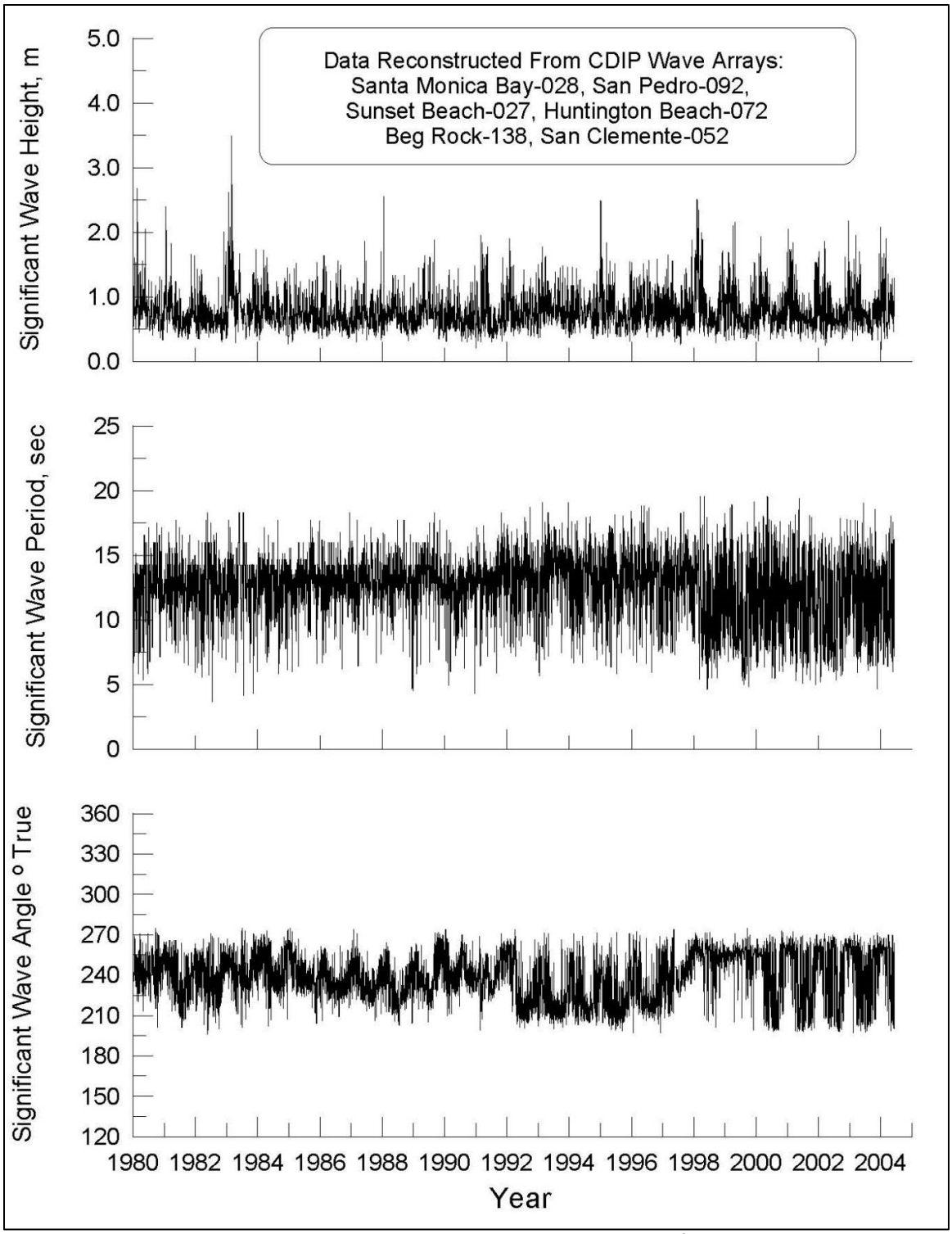

Figure 4.11: Wave data reconstructed from the far-field refraction/diffraction analysis of CDIP measurements. These data used as deep water boundary conditions on the nearfield sediment budget and divergence of drift calculations (see Section 5)

The sediment volume flux is calculated by the CEM in each control cell using Equation (1). The predominant term is the source term *J(t)*, and the largest sources are the average annual 1.3 million metric tons of deposition from the Calleguas and Malibu Creeks, and the beach-fill that has been placed on Santa Monica and Redondo beaches from dredging of Marina del Rey. However, beach fill sediments do not stay where they were initially deposited, and will propagate down-drift over time as a lump of sediment known as an *accretion/erosion wave*, see Figure 3.3a and Inman and Jenkins (2004c). The formulation of this down-drift migration of the accretion/erosion wave is given by the second term in Equation (1), the $V_l\ (dq/dy)$ term, known as *the advective term*. As the accretion/erosion wave migrates down-drift, it also spreads out laterally along the shore line and is reduced in amplitude by the action of the first term in Equation (1), referred to as the surf-diffusion term, $\varepsilon(\partial^2 q/dy^2)$. The initial placement of a large amount of sediment in a relatively small area, (whether that be a river delta after a flood or a receiver beach after placement of beach-fill), creates a large along-shore gradient in sediment volume, *dq/dy.* That gradient renders the sediment mass to be highly mobile under the influence of longshore currents, V_l, with additional spreading by surf diffusion. Longshore currents are generated when waves break at an angle to the shoreline, or when there is an along shore variation in wave height; where longshore currents flow down-coast in the direction of wave breaking and flow away from areas of high waves and towards areas of low waves. The formulation for the longshore transport rate of sediment, Q_L, due to the action of the longshore current, V_l, is taken from the work of Komar and Inman (1970) according to:

$$Q_L = K\left(C_n\, S_{yx}\right)_b \tag{38}$$

where Cn is the phase velocity of the waves; $S_{xy} = E\sin\alpha_b\cos\alpha_b$ is the along shore component of the onshore component of the radiation stress tensor; α_b is the breaker angle relative to the shoreline normal; $E = 1/8\rho g H_b^2$ is the wave energy density; ρ is the density of water; g is the acceleration of gravity; H_b is the breaking wave height; and, K is the transport efficiency equal to:

$$K = 2.2\sqrt{c_{rb}} \tag{39}$$

$$c_{rb} = \frac{2g\tan^2\beta_0}{H_b\sigma^2} \tag{40}$$

Here c_{rb} is the reflection coefficient which is calculated from the nearshore bottom slope, β_0 of the stationary bathymetry as determined from the break point coordinates and the position of the 0 MSL contour; and, σ is the radian frequency = 2π/T, where T is the wave period. The longshore transport velocity, $V_l = \overline{V_l(x)}$ is determined from the longshore current theories of Longuet-Higgins (1970), according to:

$$\overline{V_l}(x) = v_0\left(\frac{10x}{49X_b} - \frac{5}{7}\log\frac{x}{X_b}\right) \text{ if } 0 \le x \le X_b \quad \overline{V_l}(x) = v_0\frac{10}{49}\left(\frac{x}{X_b}\right)^{5/2} \text{ if } x > X_b \tag{41}$$

where:

$$v_0 = \frac{0.256\pi\beta}{C_D}\sqrt{gh_b}\,\sin\alpha_b$$

Here, X_b is the width of the surf zone derived from the coordinates of the break points (x_b, y_b) that were computed from the CEM refraction analysis. Solutions from Equations (38) to (41) give the highest rates of sediment flux in the neighborhood of the break point, $x = X_b$, where the longshore currents approach a maximum value of $\overline{V_l}(x) = v_0$. When the longshore transport rate is averaged over some extended length of time, t_0, the resultant is referred to as littoral drift $\overline{Q_L}$, where :

$$\overline{Q_L} = \frac{1}{t_0}\int_{t_0} KC_n S_{yx}\,dt \qquad (42)$$

The net sediment volume flux out of or into a control cell (erosion or deposition, respectively) that results from the action of the advective term in Equation (1) is related to the longshore transport rate Q_L by a functional known as the *divergence of drift*, $\nabla \bullet Q_L$, written as:

$$V_l \frac{dq}{dy} = \nabla \bullet Q_L \cong \int \frac{\partial Q_L}{\partial y}dy = KC_n \int \frac{\partial S_{yx}}{\partial y}dy \qquad (43)$$

Therefore, the net erosion or deposition of sediment in a control cell due to advective transport by longshore currents (divergence of drift) is proportional to the along shore gradient of the radiation stress tensor component, $S_{xy} = E\sin\alpha_b\cos\alpha_b$. Positive values of radiation stress gradient indicate depositional tendencies, while negative values indicate erosion. Ideally, for a sub-seabed intake site we seek sections of coast where the radiation stress gradient is small and trending to zero. These equations (38-43) relate divergence of drift to the longshore flux of energy at the break point which can be obtained directly from the refraction/diffraction solutions of the CEM, (e.g., Figures 4.10); and is proportional to the square of the near breaking wave height and breaker angle. By this formulation, the CEM calculates a local sediment volume fluxes for control cells in the far-field grid, and in the nearfield grid that are separated by great distances from the primary sources of sediment in the Santa Monica Littoral Cell, in particular beach fill sites at Marina Del Rey and Redondo Beach.

The advective (divergence of drift) term of Equation (1) is decisive to the sub-seabed intake siting analysis because it is the mechanism that spreads out the large volumes of river deposition and beach-fill over many kilometers of coastline in southern portion of the Santa Monica Littoral Cell between Santa Monica Pier and the Redondo King Harbor. Divergence of drift and surf diffusion are wave driven, and their magnitudes and variations from place to place in the Santa Monica Littoral Cell depend on the wave refraction/diffraction pattern of the general region, beginning with the initial approach of waves into the Southern California Bight from distant storms. Figure 4.3 shows CEM computations of the refraction/diffraction patterns of the 5 largest storms to enter the Southern California Bight during the 1998 El Niño winter. Many

areas of the Bight are sheltered from these waves by the break-water effect of the offshore islands (referred to as *island sheltering*); but there is a significant gap between Catalina Island and the Channel Islands that leaves the southern portion of the Santa Monica Littoral Cell open to waves from the west and north west, while waves approaching from southern hemisphere storms and Mexican hurricanes can freely travel inside of Catalina and San Clemente Islands to arrive at ESGS and RBGS.

Zooming in on local wave shoaling tendencies in the lower Santa Monica Littoral Cell, Figure 4.10 reveals that an abrupt narrowing of the continental shelf seaward of the near the Redondo Submarine Canyon, (creating a large dog-leg in the -40 m to – 250 m depth contours), gives rise to an inner beam of intensified wave energy (red bright spot), that doubles shoaling wave heights at the Chevron Groin and ESGS North and South sites. Further south of the ESGS South site, there is an area of greatly diminished wave energy (blue shadow zone) extending about a kilometer to the south of the ESGS property boundary. Additional bright spots in Figure 4.10 are found at numerous places north of the Chevron Groin and south of the Redondo King Harbor. These bright spots are consistent with the legacy surfing reputation of Redondo Beach.

The CEM ran 8.920 daily refraction calculations over the January 1980- July 2004 period of record, from which the littoral drift parameters of long-shore current, radiation stress, and radiation stress gradients were obtained for 220 coupled control cells along a 19.8 km reach of coast between Santa Monica Pier and the Redondo King Harbor. Model inputs for these calculations included CDIP monitored waves (cf Figure 4.11), grain size distributions after Figures 4.4 and APPENDIX-A, Calleguas Creek, Malibu Creek, and Ballona Creek sediment flux from, and beach disposal of dredge material from the Marina Del Rey Dredging Project (USACE, 1994; Shad and Ryan, 1996; Weigel, 2009; Gadd et al., 2009). These littoral drift parameters were averaged over the 24-year period of record and their variation along the coast is plotted in Figure 5.1 in terms of distance from the Redondo King Harbor. Dashed trend lines are also overlaid on these plots. Several striking trends are revealed. The variation of the longshore current is plotted in the upper panel of Figure 5.1. The dashed trend line indicates the long-term average longshore current is on the order of 25 cm/s to 35 cm/s, and is directed toward the south everywhere from the sediment sources of Calleguas Creek, Malibu Creek, and Ballona Creek and Marina Del Rey. The longshore current will move (advect) sediment (primarily beach sands) by two transport mechanisms: suspended load transport where sand moves in suspension in the water column; and bed load transport where sand moves in traction along the seabed. Abrupt decelerations in the longshore current indicate locations of chronic rip currents. This southerly persistence and the down-drift intensification indicates that, over time, the longshore current will induce potential transport of beach fill down-coast from Marina Del Rey receiver beaches, dispersing it across other portions of shore zone to the south. This is confirmed by the long-term average of the radiation stress in the middle panel of Figure 5.1. The radiation stress is proportional to the littoral drift, and its trend line is positive, indicating southward-

directed transport everywhere between the receiver beaches to the north, down-coast to Redondo King Harbor to the south. The dashed trend line indicates the long-term average radiation stress on the order of 250 N/m to 300 N/m. The alongshore continuity of the long-term average radiation stress indicates that the net littoral drift is a one-way, unidirectional transport stream, a *river of sand* so to speak, flowing away from sediment sources of the creeks and receiver beaches to the north, and flowing toward the Redondo King Harbor and the regional sediment sink a short distance offshore that is the Redondo Submarine Canyon.

The gradient of the radiation stress in the lower panel of Figure 5.1 adds another wrinkle to this transport mechanism. The radiation stress gradient is the dominant factor in determining the magnitude and sign of the divergence of drift. The trend line of the radiation stress gradient has a similar form as that for the longshore current, and is strongly negative immediately south of Marina Del Rey due to the capture of littoral drift sands by the marina's detached breakwater and groin system, causing the beaches south of the marina to be erosional (with negative radiation stress gradient). This underscores the need for the continuance of the Marina Del Rey Dredging Project because without the beach re-nourishment cycles under this program, the strong negative gradient of radiation stress south of the marina assures these beaches will experience loss. The condition for *loss* of these beaches occurs after they erode to the point to where the no longer retain enough sediment to meet the required critical mass, whence they can no longer support a profile at equilibrium (Jenkins and Inman, 2006). If that happens an *erosion wave* will develop and propagate southward, destabilizing other beaches of the Manhattan and Redondo Beach community (Inman and Jenkins, 2004c).

Of particular interest to the problem at hand is the feature in the long-term gradient in radiation stress (Figure 5.1) that trends negative immediately south of the Chevron Groin. It is here that the ESGS North and South sites are located. This negative divergence of drift is indicative of narrow, steeply sloping beaches with potential for episodic erosion. Further south of the ESGS sites, the gradient in radiation stress approaches zero along a 4,000 m section of coast in between the ESGS and RBGS facilities. This condition is referred to as *non-divergent littoral drift* and indicates a stable, steady-state condition that is neither erosional nor depositional. To the south of this area, the gradient in radiation stress turns positive at the Redondo King Harbor breakwater system while the longshore current is turned offshore by the deflection action of the breakwater, resulting in offshore deposition in and around the harbor entrance.

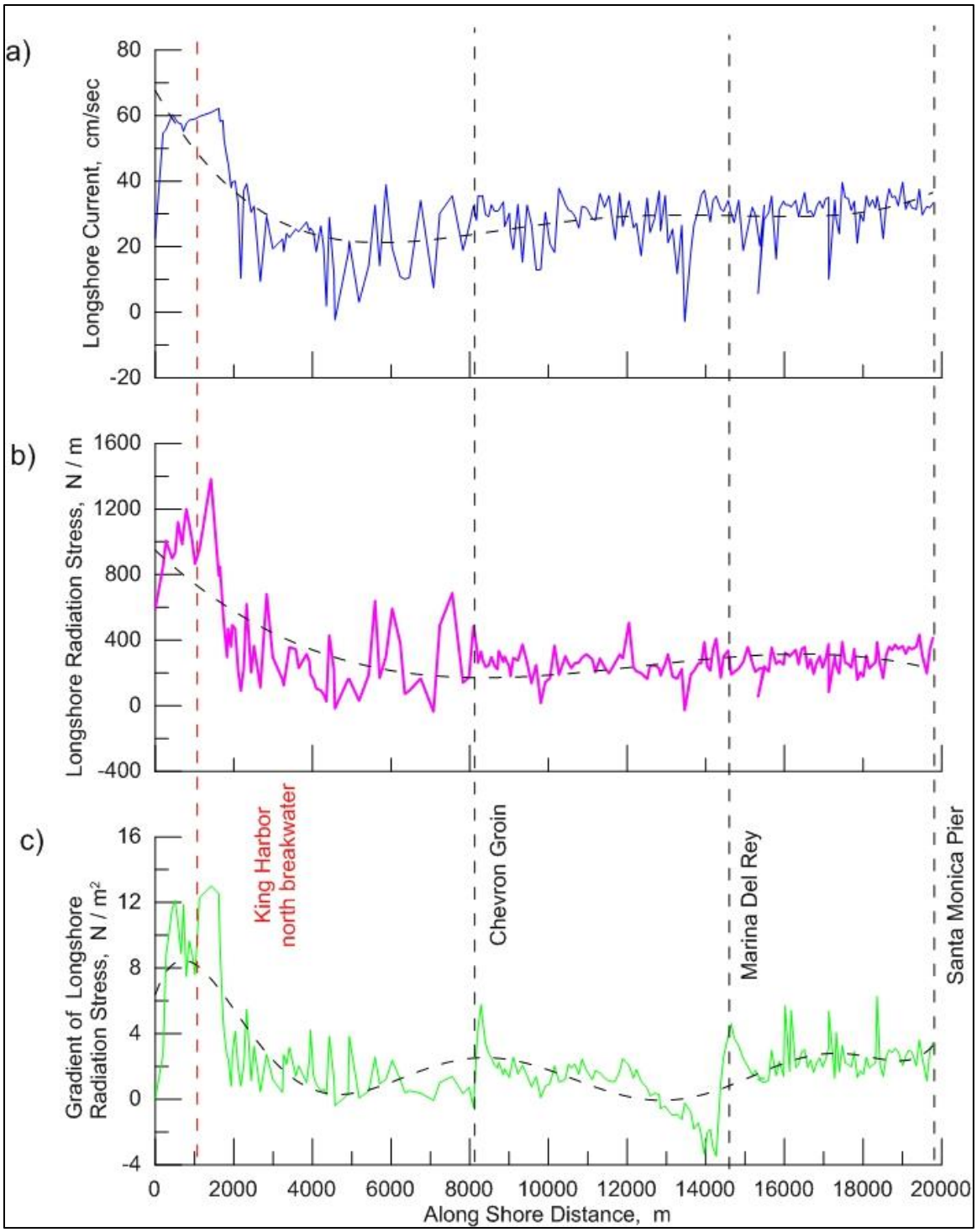

Figure 5.1: Littoral drift parameters at 220 locations between the Santa Monica Pier and Redondo King Harbor, calculated by the calibrated CEM and averaged over the 24-year period of record (1980-2004). Upper panel: longshore current (positive toward the south, negative toward the north). Middle panel: Radiation stress (positive toward the south, negative toward the north). Lower panel: gradient of longshore radiation stress (positive values are depositional and negative values are erosional).

With this insight, we now turn to CEM solutions using the high-resolution inner grid with 238 coupled control cells along a 7.2 km reach of coast between the Chevron Groin and Redondo King Harbor. In this inner grid we perform the more complex calculations for sediment volume flux solutions to Equation (1) for the complete sediment budget. Divergence of drift with its radiation stress gradient factor is only one of 4 terms contributing to sediment volume flux solution. Figure 5.2 gives the solution for the daily sediment volume flux between the Chevron Groin and Redondo King Harbor averaged over the 24-year period of record (1980-2004). Inspection of Figure 5.2 reveals the sediment volume flux trends to zero over a 4000 m reach of coast south of the Chevron Groin, indicating that the section of coast fronting the ESGS North and South sites, is stable with minimal erosional or depositional tendencies; (also indicating that the Chevron Groin is functioning as designed for stabilizing the shoreline). Although the beaches are narrow and steep in front of the ESGS North and South sites, the zero trending sediment volume flux suggests the same amount of littoral drift that arrives at the northern edge of the ESGS North Site also exits this region at the southern edge of the ESGS South site. Nowhere else is this stable condition found within 7 km to the north or to the south of the RBGS & ESGS facilities. North or south of the ESGS sites, there are erosional and depositional regions, interspersed at the cross-over points by very short segments of coastline with zero sediment volume flux. However, these cross-over coastal segments between depositional and erosional areas do not embrace sufficient coastline length for a usable desalination facility site. Also, the magnitudes of the non-zero sediment volume fluxes in these neighboring erosional or depositional areas are significant. When factored over 20 years, these non-zero sediment volume fluxes accumulate to 2,000 m^3 to 4000 m^3 per meter of coast, on the order of all the total sediment volume in a critical mass envelope.

Fortuitously, the beach profile characteristics at the two potential ESGS sites are approximately represented by the historic US Army Corps of Engineers survey ranges at the Chevron Groin, cf. Figures 4.5. These surveys provide very high confidence to the CEM solutions for beach slopes, closure depth and critical mass that provide essential inputs to the TWL wave overtopping calculations in Section 6 to follow. Based on 8,290 solutions over the 1980-2004 simulation period, the CEM calculates in Figure 5.4 that bottom profile perturbations caused by shoaling waves at the ESGS site near the Chevron Groin were found to cease seaward of the -15 m MSL depth contour, referred to as *closure depth*. In addition, the critical mass envelope is relatively thin at the Chevron Groin (Figure 5.5) due to the stabilization action of the groin.

The critical mass determines the volume of sediment cover that can be potentially eroded by the action of seasonal and episodic profile change or shoreline recession. The critical mass of sand on a beach is that required to maintain equilibrium beach shapes over a specified time, usually ranging from seasons to decades. The critical mass envelope in Figure 5.5 indicates that sand level variations due to beach profile changes are no more than 3.3 m across the bar-berm beach profile at the ESGS sites,

and no more than 1.5 m across the shore rise profile off shore. This fortuitous sediment transport behavior is a long term trend, but extreme event storms such as Figure 4.10 indicate episodes of erosion from hot spots in the refraction pattern are possible, although not persistent. Overall, however, the beach and shore rise sedimentary shoaling and run up slopes are stable, although moderately steep.

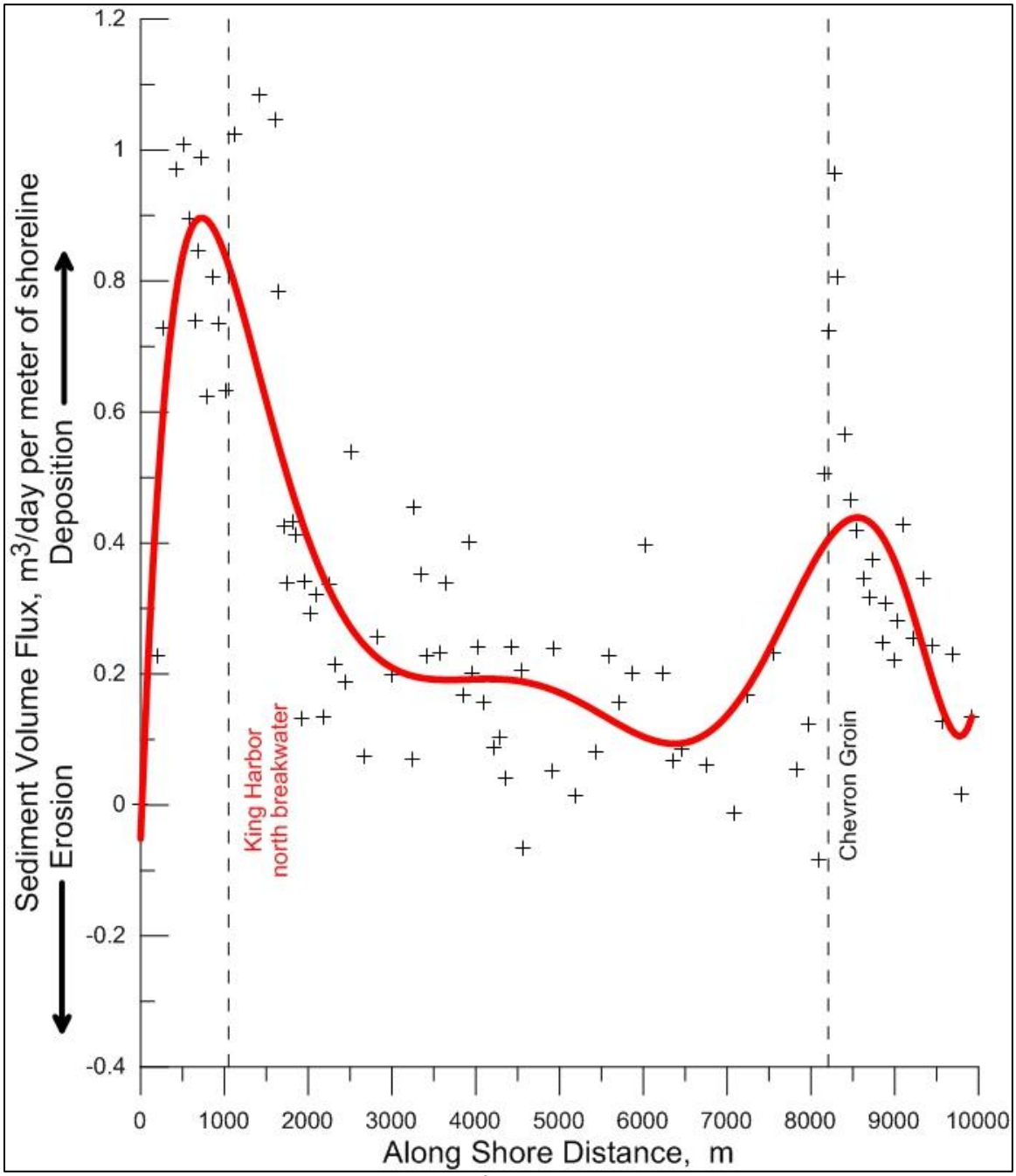

Figure 5.2: Daily sediment volume flux, *dq/dt*, calculated by the calibrated CEM from Equation (1) and averaged over the 24-year period of record (1980-2004) for the reach between the Chevron Groin and Redondo King Harbor in the southern end of the Santa Monica Littoral Cell.

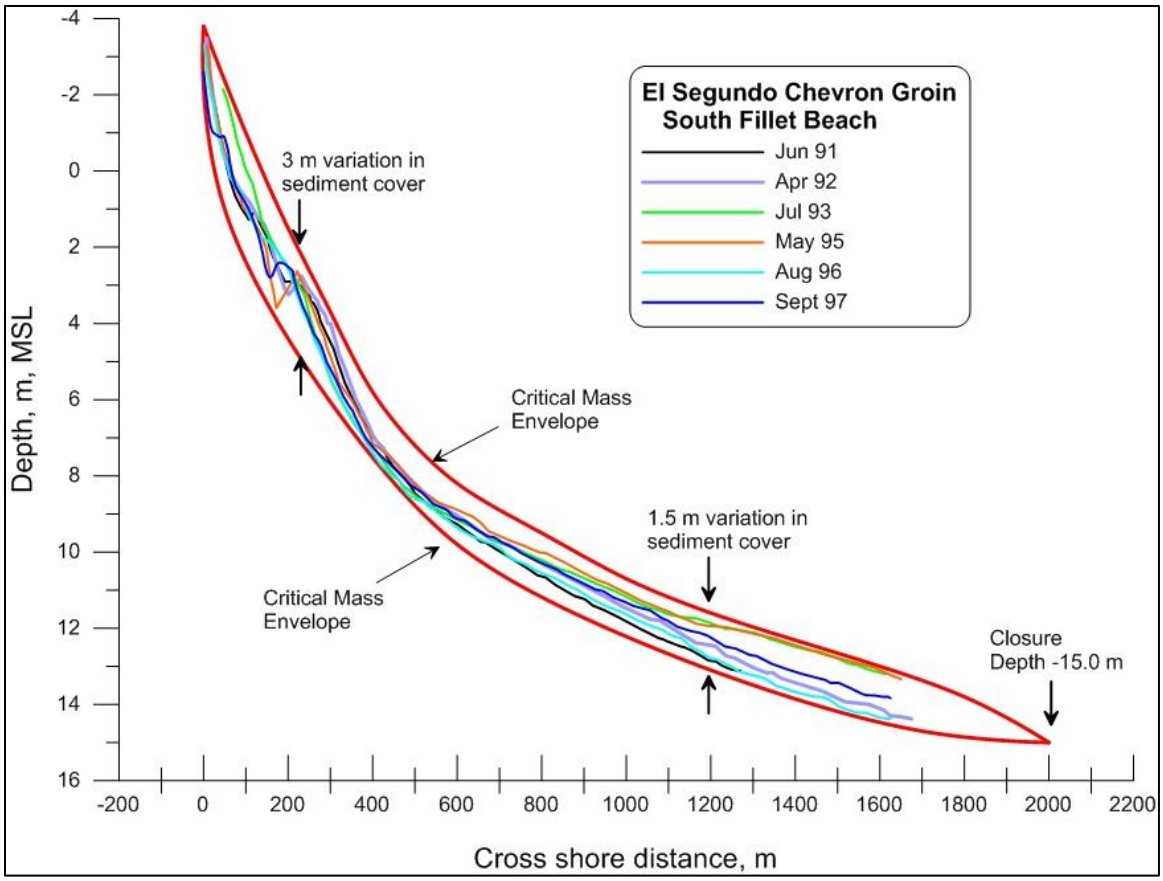

Figure 5.3: Critical mass envelope at historic Chevron Groin survey range, El Segundo, calculated by the calibrated CEM sediment budget based on the 24-year period of record CDIP monitored waves, Calleguas, Balona and Malibu Creek sediment flux APPNEDIX-A, and beach disposal of dredge material from the Marina Del Rey Dredging Project, (USACE, 1994 Measured beach profiles from Gadd et al., 2009. Closure depth = -15 m MSL calculated from Equation (7). Critical mass volume = 2,941 m^3 per meter of shoreline calculated from Equation (13).

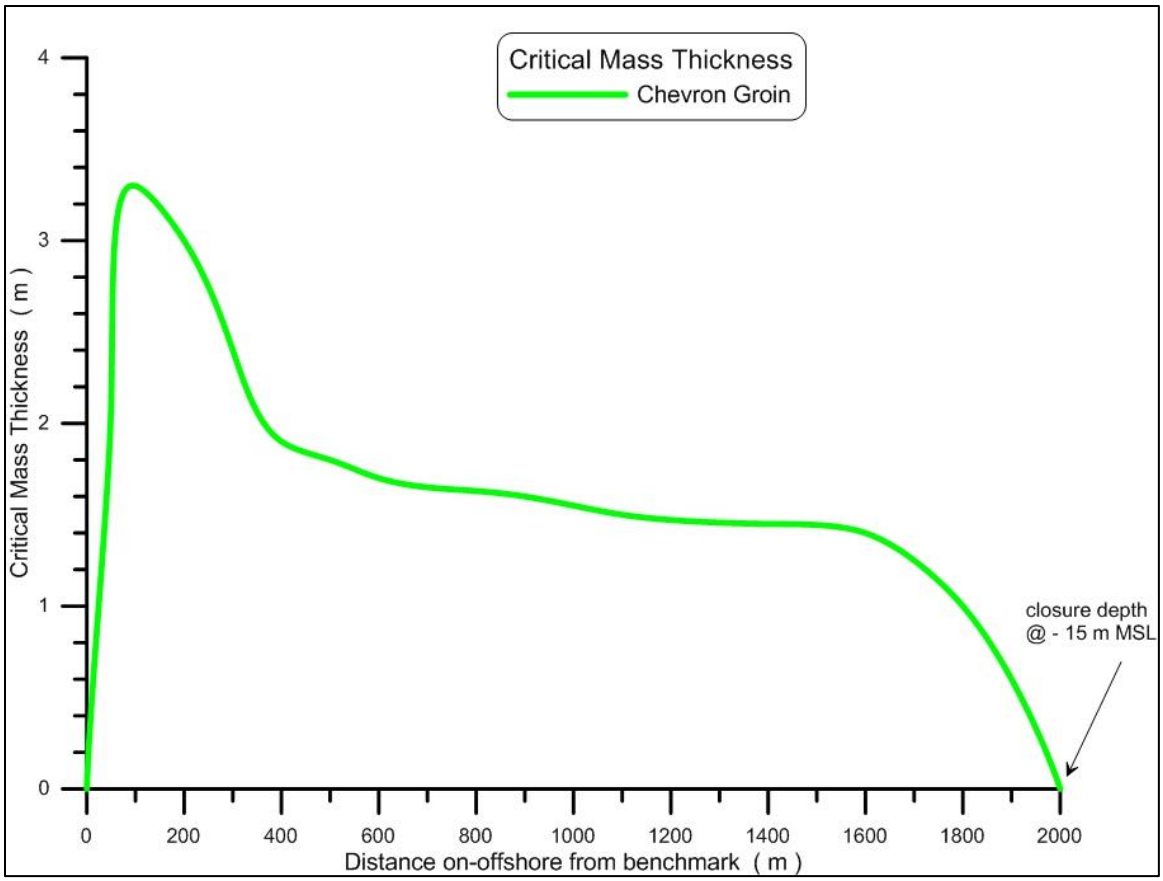

Figure 5.4: Thickness of critical mass envelope at historic Chevron Groin survey range, El Segundo, calculated by the calibrated CEM sediment budget based on the 24-year period of record CDIP monitored waves, Calleguas, Balona and Malibu Creek sediment flux APPNEDIX-A, and beach disposal of dredge material from the Marina Del Rey Dredging Project, (USACE, 1994 Measured beach profiles from Gadd et al., 2009. Closure depth = -15 m MSL calculated from Equation (10). Critical mass volume = 2,941 m^3 per meter of shoreline calculated from Equation (16).

6. Coastal Hazards Wave Run-up and Tsunami Analysis

Extreme wave and tsunami run-up, and overtopping were analyzed for the ESGS North and ESGS South sites being proposed for with the West Basin Desalination Project. Due to the bike trail revetment and narrow beach with moderately steep profile immediately south of the Chevron Groin (Figures 5.5 and 6.1), the TAW method (Section 3.9) is best suited for assessing potential flooding and inundation due to extreme wave run up and Tsunami run-up. Hand calculation are given as a lowest order estimate of total water level at both sites, followed up by more exact calculations using the CEM software described in Section 3. Both hand calculations and CEM solutions are given for present sea level and for two extreme scenarios (maximum and minimum) of future sea level rise.

6.1 ESGS North

Due to its previous use for Units 3 and 4, virtually the entire ESGS North Site is a level pad at approximate elevation Z = +23 ft MLLW. The important features with respect to a coastal hazards analysis site is the presence of a sea wall immediately landward from the bike trail, Figure 6.2. The elevation of the crest of this sea wall ranges from h_c = +28 ft MLLW at the north end rising slightly to h_c = +29 ft MLLW at the south end which is bounded by a fence along the boundary with the ESGS site. Other significant shoreline fortifications are the bike trail itself which is perched atop a rip-rap revetment at elevation Z = +22 ft MLLW at the north end of the sea wall; and at elevation Z = +23 ft MLLW at the south end of the sea wall. The revetment fortifies a low bluff that boarders the back beach, (Figure 6.3). The average beach slope at the toe of the revetment is m_{TAW} = 0.065.

6.2 ESGS South

Virtually the entire ESGS South site is an elevated level pad that was the site of the previous fuel-oil tanks. From this pad, which is at approximately elevation Z = +41 ft, a vegetated slope falls away to the west to a berm at Z = + 25 ft MLLW. The berm then slopes down to the existing bike trail below whose road bed is at Z = +23 ft MLLW. This slope was recently planted and landscaped as part of NRG's redevelopment project for Units 5, 6, and 7. Also as part of that redevelopment project a landscaped berm at elevation Z = +25 ft MLLW was constructed at the south boundary bordering on 45th Street. Significant shoreline fortifications are the bike trail itself which is perched atop a rip-rap revetment at elevation Z = +22 ft MLLW at the north end of the sea wall and elevation Z = +23 ft MLLW at the south end of the ESGS property. The revetment fortifies a low bluff that boarders the back beach, (Figure 6.3). There is little change in beach widths and slopes along both the ESGS North and ESGS South sites (Figure 6.1); and so, the average beach slope at the toe of the revetment at the ESGS South site is also taken as: m_{TAW} = 0.065.

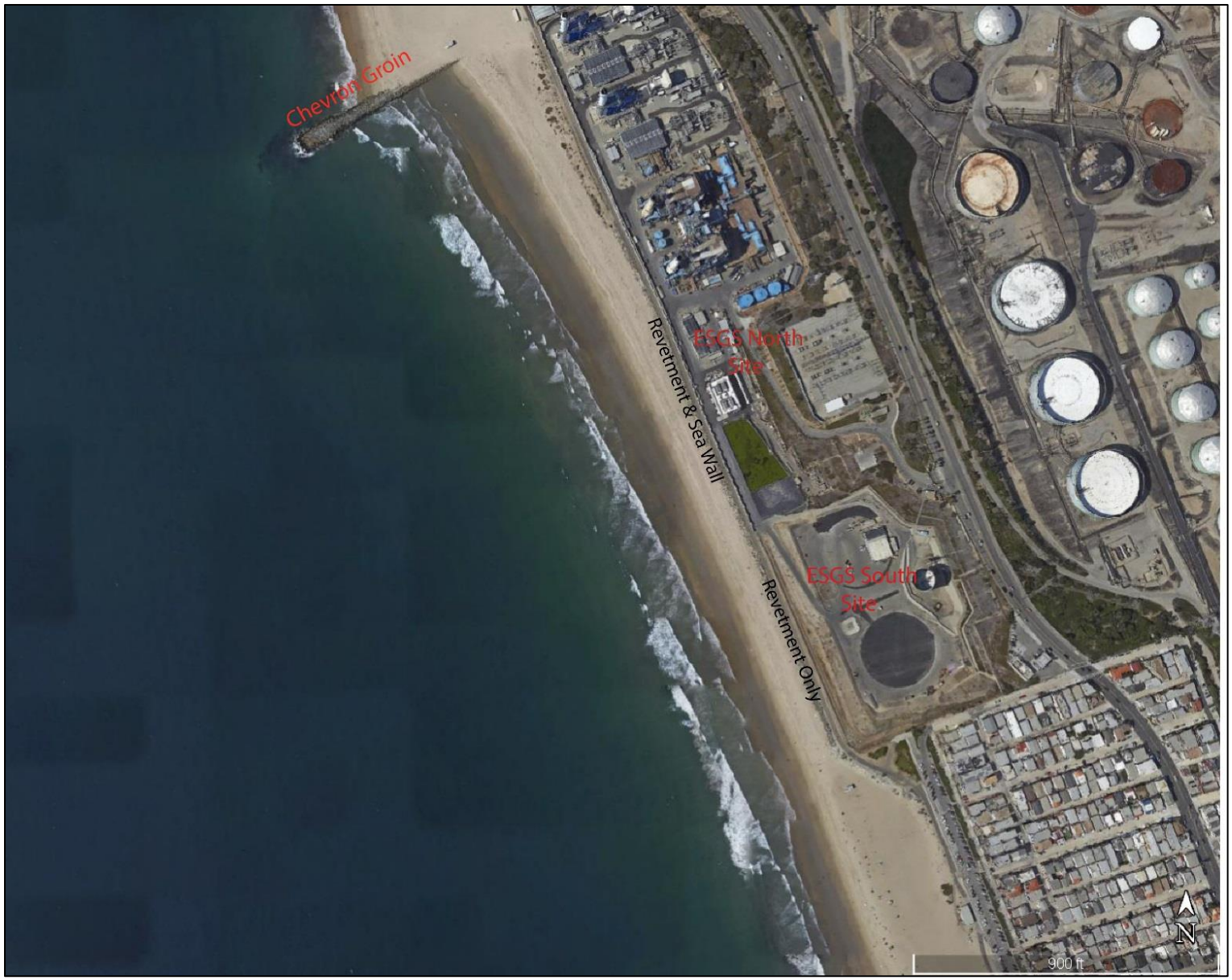

Figure 6.1: Aerial Image showing beach width variations south of the Chevron Groin. Note uniformly narrow beach in front of the bike trail revetment at the ESGS North and ESGS South sites.

Figure 6.2: Sea wall at the ESGS North Site, crest elevation = + 29 ft MLLW

Figure 6.3: Bike trail perched atop a rip-rap revetment at ESGS site; crest elevation Z = +22 ft to + 23 ft MLLW

6.3 Extreme Wave TWL Hand Calculation

Since the beach widths, slopes and bike trail revetment crest elevations are essentially the same at both the ESGS North and ESGS South sites, the same total water level (TWL) results can be expected for both sites. The TWL calculation by the TAW method begins with determining the root mean square of the breaking significant wave height $(H_b)_{rms}$. From Figure 4.10, the 1% highest design wave has a wave height of H_0' = 19.7 ft, a peak period of T_P = 17 s, a wave length of $L_0 = gT_P^2 / 2\pi$ = 1,479.8 ft. The wave phase speed (celerity) is $C_0 = gT_P / 2\pi$ = 87.05 ft/s, and the still water level is *SWL* = 2.62 ft MLLW. The $(H_b)_{rms}$ is determined using Equation (8) in Section 2.5:

$$(H_b)_{rms} = 0.714\left(\frac{\kappa}{g}\right)^{1/5}\left(\frac{H_0'^2 C_0}{2}\right)^{2/5} = 16.66 \text{ ft} \quad (44)$$

Where κ is the breaker criterion equal to 0.78. The static wave setup at the SWL shoreline is:

$$\overline{\eta}_0 = 0.189(H_b)_{rms} = 3.15 \text{ ft} \quad (45)$$

The local water depth, h, at the toe of the sea wall relative to SWL is nil, whence the static wave setup at the toe of the sea wall is:

$$\overline{\eta}(h) = \overline{\eta}_0 \quad (46)$$

The static wave setup reduction factor, γ_η is then a ratio of the static wave setup at the toe to the static wave setup at the SWL shoreline, or:

$$\gamma_\eta = \frac{\overline{\eta}(h)}{\overline{\eta}_0} = 1.0 \quad (47)$$

This reduction factor is then applied to the DIM static wave setup to compute a depth-adjusted static wave setup at the toe of the engineered barrier,

$$\overline{\eta}' = \gamma_\eta \overline{\eta} = 3.15 \text{ ft} \quad (48)$$

The Iribarren number of the 100-year storm wave incident on the steeply sloping beach surface is:

$$\xi_0 = \frac{m_{TAW}}{\sqrt{H_0' / L_0}} = 0.563 \quad (49)$$

The steep slope of the back-beach area that fronts the bike trail produces very little dissipation of the wave run-up, so that the standard deviation of the wave run-up oscillations, σ_2 is large:

$$\sigma_2 = 0.3\xi_0 (H_b)_{rms} = 2.81 \text{ ft} \quad (50)$$

which represents only 32% of the incident wave height. With such a large standard deviation, the run-up spectra becomes very broad, and $\nu = \left[2\sigma_2 / (H_b)_{rms}\right]^{1/2}$ = 0.581, whence Gamma approaches the broad spectrum limit: $Gamma \rightarrow 1.0$. With this *Gamma* value, the dynamic wave setup can be calculated as:

$$\eta_{rms} = 4.0\left(\frac{H_0'}{26.2}\right)^{0.8}\left(\frac{T_P}{20.0}\right)^{0.4}\left(\frac{m_{TAW}}{0.01}\right)^{0.2} = 4.34 \text{ ft} \quad (51)$$

The 2-percent Dynamic Water Level ($DWL_{2\%}$) is thus calculated as:

$$DWL_{2\%} = \overline{\eta}' + 2\eta_{rms} + SWL = 14.37 \text{ ft NAVD} \quad (52)$$

From Figures 4.5 and 5.3, the sand level at the toe of the bike trail revetment is at +14 ft MLLW. Hence the water depth at the toe of the revetment due to $DWL_{2\%}$ is h_{toe} = 0.37 ft. The bore height post- wave breaking, H_{m0}, is depth- limited and is calculated using a breaker index of 0.78, whence $H_{m0} = 0.78 h_{toe}$ = 0.29 ft. For the purposes of worst-case assessments, we assume smooth run-up surfaces, normally incident waves, and plane sloping revetment, whence the influence coefficients approach unity, $\gamma_r = \gamma_b = \gamma_\beta \rightarrow 1.0$, and we calculate the 2-percent wave run-up on the face of the sea wall using the following TAW formulation:

$$R_{2\%} = 1.77 H_{m0}\, \xi_{0m} = 0.476 \text{ ft} \quad (53)$$

Where the Iribarren number based on wave parameters at the toe of the revetment is:

$$\xi_{0m} = m_{TAW} / \left(H_{m0} / L_m\right)^{0.5} = m_{TAW} T^{1/2} g^{1/4} / (0.883 h_{toe}^{1/4}) = 0.926 \quad (54)$$

Ultimately, the incident wave run-up at the toe of the bike trail revetment using TAW, $R_{2\%}$, is statistically combined with the reduced dynamic wave setup, and added to SWL and static wave setup to yield the total water level, TWL, or:

$$TWL = SWL + \overline{\eta}' + 2.0\sqrt{\eta_{rms}^2 + \left(\frac{R_{2\%}}{2}\right)^2} = 14.46 \text{ ft MLLW (present sea level)} \quad (55)$$

Thus, at present sea level, the incident wave run-up at the toe of the bike trail revetment, $R_{2\%}$, makes only a minor contribution to the dynamic water level; and with a the bike trail road surface at Z = 23 ft MLLW the ESGS North and South sites are adequately protected against overtopping by the 1% extreme wave event. However, unlike DIM calculations on low-steepness beaches, the TAW calculations for TWL do not simply linearly superimpose on the increment of sea level rise. This is because the incident wave run-up at the toe of the bike trail revetment slope, is dependent on the water depth at the toe of the revetment, h_{toe}. At 2065 sea levels, the still water level and dynamic water level will probably range somewhere between:

At 2065 sea level, low estimate:

SWL = 2.62 ft MLLW + 0.58 ft = 3.20 ft MLLW

$DWL_{2\%} = \overline{\eta}' + 2\eta_{rms} + SWL$ = 3.15 ft + 8.68 ft + 3.20 ft NAVD = 15.06 ft NAVD

h_{toe} = 0.95 ft

$\xi_{0m} = m_{TAW} T^{1/2} g^{1/4} / (0.883 h_{toe}^{1/4})$ = 0.732

$H_{m0} = 0.78 h_{toe}$ = 0.74 ft

$R_{2\%} = 1.77 H_{m0} \xi_{0m}$ = 0.960 ft

At 2065 sea level, high estimate:

SWL = 2.62 ft MLLW + 2.92 ft = 5.54 ft MLLW

$DWL_{2\%} = \overline{\eta}' + 2\eta_{rms} + SWL$ = 3.15 ft + 8.68 ft + 5.46 ft NAVD = 17.37 ft MLLW

h_{toe} = 3.29 ft

$\xi_{0m} = m_{TAW} T^{1/2} g^{1/4} / (0.883 h_{toe}^{1/4})$ = 0.569

$H_{m0} = 0.78 h_{toe}$ = 2.57 ft

$R_{2\%} = 1.77 H_{m0} \xi_{0m}$ = 2.588 ft

Thus, at future sea levels in 2065, the total water level, TWL at the HWY 101 sea wall in Carlsbad, CA, could vary between:

$$TWL = SWL + \overline{\eta}' + 2.0\sqrt{\eta_{rms}^2 + \left(\frac{R_{2\%}}{2}\right)^2}$$ = 15.08 ft MLLW (2065 sea level, low estimate) (56)

$$TWL = SWL + \overline{\eta}' + 2.0\sqrt{\eta_{rms}^2 + \left(\frac{R_{2\%}}{2}\right)^2}$$ = 17.75 ft MLLW (2065 sea level, high estimate) (57)

Therefore, even the high estimate of sea level in 2065 the *TWL* of the extreme design wave will not exceed the crest height of the bike tail (at h_c = +22 ft to +23 ft MLLW), and consequently no overtopping rates can be anticipated at either the ESGS North or ESGS South sites. With a sea wall behind the bike trail (crest height at h_c = +28 ft MLLW) the pad for the ESGS North Site (at Z = +23 ft MLLW) appears to be extremely well protected against overtopping and flooding by the 1% extreme wave event even when superimposed on the highest predicted sea level for the next 50 years.

6.4 TWL Calculations Using CEM Computer Software

Calculations of *TWL* using the *Coastal Evolution Model (CEM)* software (Section 3) proceed by the same series of steps outlined in Section 6.3. The only differences here are in the populating of the input files for the beach profiles in Figures 4.5 and 5.3. This beach profiles show that sand elevations near the toe of the bike trail revetment can

drop as low as + 7.37 ft MSL during erosional episodes. The tidal datum data in Section 4.6 indicate that + 7.37 ft MSL = +10.1 ft MLLW. Therefore, the beach profile measurements in Figure 4.5 suggest sand levels at the toe of the revetment may be as much as 6.6 ft lower than what was assumed in the hand calculations in Section 5.1.1. This leads to lower beach slope values, m_{TAW} , and deeper water depths across the run-up surfaces that result in higher wave run-up at the toe of the sea, $R_{2\%}$. Moreover, the plane constant-slope assumption used in Section 4.1.1 does not apply and m_{TAW} and $R_{2\%}$ must be solved iteratively using the finite differencing techniques incorporated in the ***CEM*** software.

Table-6.1 compares the hand calculations for total water level and overtopping based on the plane constant slope beach assumption used in Section 6.3 vs the iterative calculation from the *CEM* software that accounts for the complex beach profiles of the eroded states of the Chevron Groin and ESGS North and South sites (cf. Figures 4.5 and 5.3). Inspection of Table-6.1 reveals that accounting for the spatial complexity of shoaling and run-up on the eroded beach profiles in front of the ESGS North and South sites does indeed produce higher total water levels (TWL) on the bike trail revetment slopes for all present and future sea level scenarios. However, the crest elevation of the bike trail is still sufficiently high that only minor overtopping of about 0.4 ft to 1.4 ft occurs, and only then, during the most extreme future sea level rise scenario under CAT-OPC design guidance. The overtopping of the bike trail, however, is blocked by the sea wall at the ESGS North site, whose crest elevation is at h_c = +28 ft MLLW. Similarly, the vegetated berm and slopes at the ESGS South prevent this small amount of overtopping of the bike trail from reaching the desalination facilities construction pad at Z = +41 ft MLLW. Hence both sites are protected against overtopping and flooding by the 1% extreme wave event, even when superimposed on the highest predicted sea level for the next 50 years.

The overtopping rates on the bike trail during the 2065 sea level rise scenario are only about 0.004 cfs per lineal ft, which would only limit casual pedestrian activity in the vicinity of the over-pour flows according to EurOtop Manual guidance.

Table-6.1: Comparison of Total Water Level (*TWL*) and Overtopping Rates (*q*) for Hand vs. Software Computations at the ESGS North and ESGS South sites for the proposed West Basin Municipal Water District Ocean Water Desalination Project

Sea level Scenario	*TWL by Hand	**TWL by Software	*Overtopping Rate by Hand	**Overtopping Rate by Software
present	14.38 ft MLLW	19.77 ft MLLW	0.0 cfs/ft	0.0 cfs/ft
2065, low	15.00 ft MLLW	20.91 ft MLLW	0.0 cfs/ft	0.0 cfs/ft
2065, high	17.67 ft MLLW	23.42 ft MLLW	0.0 cfs/ft	0.004 cfs/ft

*Based on constant slope beach inferred from Google Earth Imagery
**Based on complex measured beach profiles that account for erosion per Figure 24 and freeboard $R_c = h_c - SWL$ = + 23 ft MLLW – SWL.

6.5 Tsunami Run-up and Inundation

Tsunami induced erosion, run-up, and inundation were analyzed for the Chevron Groin bottom profiles (Figures 4.5) and shoreline fortifications associated with the bike trail revetment, sea wall and vegetated berms at the ESGS North and South sites. Tsunami induced TWL's were calculated assuming present conditions and two future scenarios including sea level rise. The tsunami scenario is based on a 2m high solitary wave approaching the ESGS site from 165 degrees true, as could be anticipated for a catastrophic tsunami event arising from a major landside on the East side of San Clemente Island. The local refraction/diffraction pattern from the solitary wave is calculated in Figure 6.4. Inspection of Figure 6.4 reveals the tsunami wave height begins to increase in about 50 m of water depth due to shoaling. Due to refraction effects from the offshore bathymetry, a very powerful bright spot (area of focusing of tsunami energy) forms along the shores of the ESGS North and South sites where tsunami surge heights reach about 8m! Because the tsunami wave begins shoaling in much deeper water than typical storm-induced waves, it causes seabed scour and erosion to occur out to very deep water depths. The critical mass thickness computed by the CEM in Figure 6.5 for this tsunami shoaling scenario reveals that seabed erosion occurs offshore to depths of -54 m MSL; and the volume of eroded sediment can be as high as 8,663 m^3 per meter of shoreline. Figure 6.5 also shows that a tsunami of this magnitude is capable of eroding as much as 9 ft to 13 ft of seabed offshore, to depths of -176 ft (53.7 m) MSL, and could erode as much as 12 ft of beach sediment cover in a single tsunami wave breaking event.

Tsunami run-up and TWL inundation calculations using the CEM software are given in Tables 6.2 and 6.3. These tables that the bike trail will be overtopped by several feet of tsunami run-up at both sites for both present and future sea levels. At the ESGS North site, the overtopping will be blocked by the sea wall, but the over-pour flows will be free to flow around the southern flank of the sea wall and cause flooding of the pad on which the desalination facility is built, which is at Z = +23 ft MLLW, the same elevation as the bike trail. It should also be noted that the crest elevation of the sea wall is just marginally adequate to prevent overtopping at the high estimate of 2065 sea levels. At the ESGS South site, tsunami overtopping of the bike trail will run up on the vegetated slopes and berms that border the facilities construction pad, reaching peak run-up elevations of + 27.9 ft MLLW. However, the facilities construction pad is at + 41 ft MLLW, and hence the site elevation of the desalination facilities at the ESGS South site will be sufficiently high to avoid flooding by tsunami run up, even for the highest forecasted sea levels for 2065.

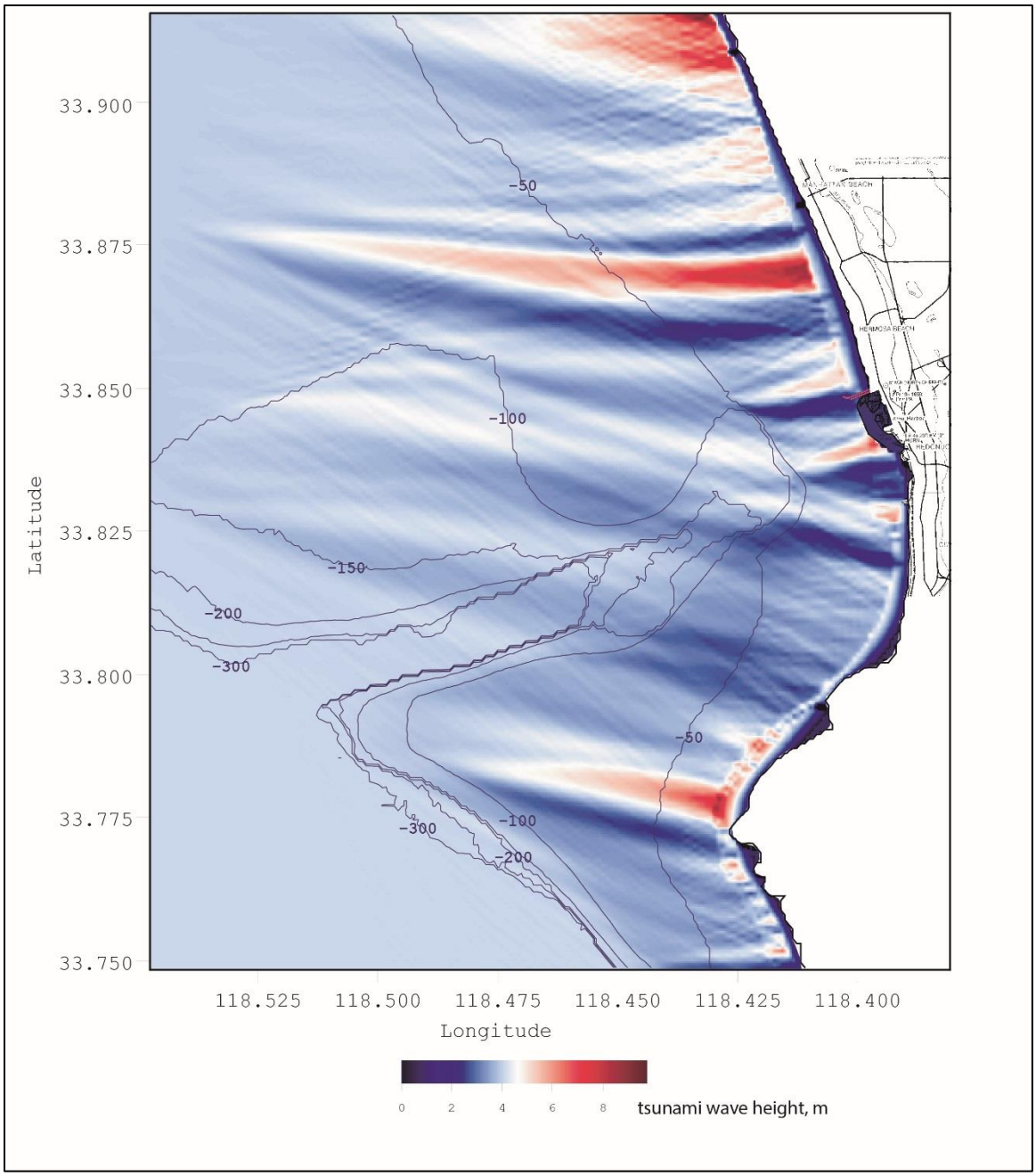

Figure 6.4: High resolution refraction/diffraction computation for a 2m high solitary tsunami wave approaching ESGS North and South sites from 165 degrees true.

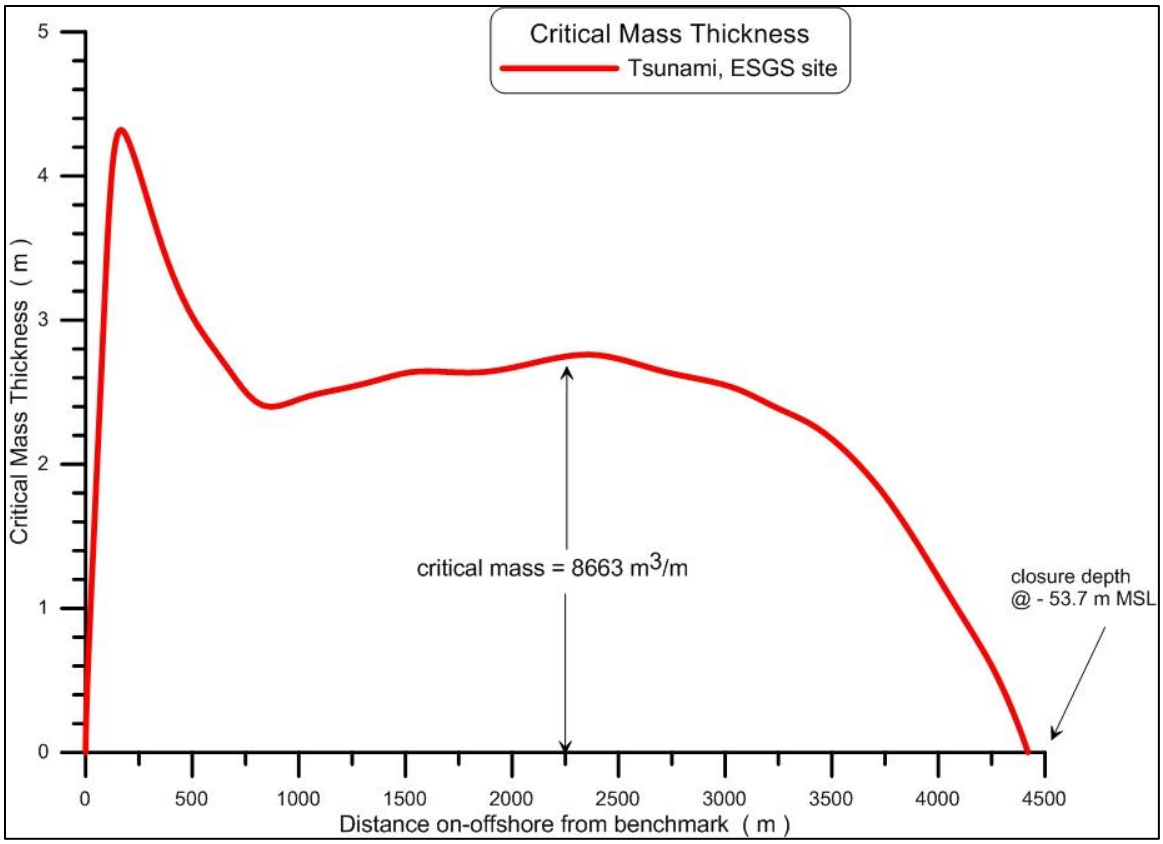

Figure 6.5: Tsunami-Induced thickness of critical mass envelope in the nearshore and inner shelf region off the ESGS North and South sites, calculated by the calibrated CEM sediment budget based a 2m high solitary tsunami wave approaching Chevron Groin from 165 degrees true. Closure depth = -53.7 m MSL; critical mass volume = 8,663 m^3 per meter of shoreline.

Table 6.2: Tsunami TWLs and Mean Run-up Slopes at ESGS North, (bike trail elevation + 22 ft MLLW, sea wall crest +29 ft MLLW).

Scenario	Mean Run-up Slope	vertical wall reduction factor, γ_v	dq/dt Beach Erosion Rate $m^3/m/day$	Site Elevation (ft, MLLW)	Tsunami TWL (ft, MLLW)
Present	0.065	1.0	-8663	23.0	25.0
2065, low	0.071	1.0	-8663	23.0	25.7
2065, high	0.160	1.0	-8663	23.0	28.8

Table 6.3: Tsunami TWLs and Mean Run-up Slopes ESGS South, (bike trail elevation + 23 ft MLLW, construction pad elevation +41 ft MLLW).

Scenario	Mean Run-up Slope	vertical wall reduction factor γ_v	dq/dt Beach Erosion Rate $m^3/m/day$	Site Elevation (ft, MLLW)	Tsunami TWL (ft, MLLW)
Present	0.065	1.22	-8663	41.0	24.3
2065, low	0.071	1.22	-8663	41.0	24.9
2065, high	0.160	1.22	-8663	41.0	27.9

7. Conclusions

Extreme wave and tsunami run-up, and overtopping were analyzed for the ESGS North and ESGS South sites being proposed for with the West Basin Desalination Project. Hand calculation are given as a lowest order estimate of total water level at both sites, followed up by more exact calculations using the Coastal Evolution Model (CEM) software. Both hand calculations and CEM solutions are given for present sea level and for two extreme scenarios (maximum and minimum) of future sea level rise. Accounting for the spatial complexity of shoaling and run-up on the eroded beach profiles in front of the ESGS North and South sites produced the highest total water levels (TWL) on the bike trail revetment slopes that front both sites for all present and future sea level scenarios. However, the crest elevation of the bike trail is sufficiently high that only minor overtopping of about 0.4 ft to 1.4 ft occurs, and only then, during the most extreme future sea level rise scenario under CAT-OPC design guidance. The overtopping of the bike trail, however, is blocked by the sea wall at the ESGS North site, whose crest elevation is at h_c = +28 ft to + 29 ft MLLW. Similarly, the vegetated berm and slopes at the ESGS South prevent this small amount of overtopping of the bike trail from reaching the desalination facilities construction pad at +41 ft MLLW. Hence both sites are protected against overtopping and flooding by the 1% extreme wave event, (aka, the 100-year storm) even when superimposed on the highest predicted sea level for the next 50 years.

Site vulnerabilities to extreme tsunami were found to be more problematic, although the modeled tsunami scenario associated with a seismic induced land side on the east side of San Clemente Island has never been recorded throughout the Holocene to present. Tsunami run-up and TWL inundation calculations using the CEM software indicate that the bike trail will be overtopped by several feet of tsunami run-up at both sites during both present and future sea levels. At the ESGS North site, the overtopping will be blocked by the sea wall, but the over-pour flows will be free to flow around the southern flank of the sea wall and cause flooding of the pad on which the desalination facility is proposed to be built, which is at elevation +23 ft MLLW. At the ESGS South site, tsunami overtopping of the bike trail will run up on the vegetated slopes and berms that border the facilities construction pad, reaching peak run-up elevations of + 27.9 ft MLLW. However, the facilities construction pad is at + 41 ft MLLW, and hence the site elevation of the desalination facilities at the ESGS South site will be sufficiently high to avoid flooding by tsunami run up, even for the highest forecasted sea levels for 2065.

The West Basin Desalination Project proposes no structures that would influence wither sediment transport or wave shoaling, breaking and run-up processes. Therefore, the project causes no impacts to the adjacent shoreline due to sea level rise, or wave induced erosion from wave diffraction and reflection from the major components of the desalination project and associated structures.

8. References

Allen, J.B., T.J. Tseng, R.C. Cheng, K.L. Wattier, 2008, “Pilot and demonstration-scale research evaluation of under-ocean floor seawater intake and discharge”, *Proceedings, AWWA Water Quality Conference,* and Cincinnati, Ohio, pp. 16–20.

Brownlie, W. R. and Taylor, B. D., 1981a, "Coastal sediment delivery by major rivers in southern California, Sediment Management of Southern California Mountains, Coastal Plains, and Shorelines, Part C," California Institute of Technology, Pasadena, CA, Environmental Quality Laboratory Report No. 17-C, 314 pp.

Brownlie, W. R. & B. D. Taylor, 1981b, "Sediment management of southern California mountains, coastal plains and shoreline, Part C," Coastal Sediment Delivery by Major Rivers in southern California, California Institute of Technology, Pasadena, CA, Environ. Quality Lab. Report 17-C, 314 pp.

Borthwick S.A., Corwin, C. and R. Liston, 2001, “Wild Fish Entrainment at the Red Bluff Research Pumping Plant, Upper Sacramento River, California,” U. S. Bureau of Reclamation Red Bluff Fish Passage Program, Annual Rpt. December, 2001, 79 pp

CDP (2006), “Waste Discharge Permit Requirements, Order R9-2006-0065.

CDIP (2001), "Coastal data information program," *SIO Reference Series*, 01-20 and http://cdip.ucsd.edu.

CDIP, 2004, “Coastal Data Information Program” http://cdip.ucsd.edu/

CRWQCB, 2000, Waste discharge requirements for the AES Redondo Beach Generating Station, NPDES No. CA-0000370, Order No. 00-083.

Coudrain-Ribstein, A., Gouze, P., and de Marsily, G. (1998). Temperature-carbon dioxide partial pressure trends in confined aquifers. *Chemical Geology* 145, 73-89.

Dehwah, A. H., and T.M. Missimer, 2013, “Technical feasibility of using gallery intakes for sweater RO facilities, northern Red Sea coast of Saudi Arabia: The King Abdullah Economic City site, Desalin. Water Treat. http://dx.doi.org/10.1080/19443994.2013.770949.

Delhomme, J., Labregre, D., Rogala, J., and D. McCann, 2005, “Horizontal wells: a solution for desalination feed water intake and brine disposal”, *Proceedings, International Desalination Association World Congress on Desalination and Water Reuse,* Singapore, 2005.

Driscoll, F., G., 1986, *Groundwater and Wells, 2nd edition*, Johnson Division, St. Paul, Minnesota, 1986.

EPRI, 2003, *Fish Protection at Cooling Water Intakes: Status Report*, EPRI, Palo Alto, CA, 1999. TR-114013.

EPRI. 2003. Laboratory evaluation of wedgewire screens for protecting early life stages of fish at cooling water intakes. Prepared by Alden Research Laboratory, Inc. EPRI Report No. TR-1005339.

Farinas, M., and L.A. Lopez, 2007, "New and innovative sea water intake system for the desalination plant at San Pedro del Pinatar", *Desalination*, vol.203, pp.199–217.

Foster, M.S., Cailliet, G.M., Callaway, J., Raimondi, P. and Steinbeck, J. 2012. Mitigation and Fees for the Intake of Seawater by Desalination and Power Plants. Report to State Water Resources Control Board, Sacramento.

Geosyntec, 2013, "Feasibility Assessment of Shoreline Subsurface Collectors Huntington Beach Seawater Desalination Project Huntington Beach, California", Tech Rpt WR1794, submitted to Poseidon Resources, 79 pp.

Graham, J. B., 2004, "Marine biological considerations related to the reverse osmosis desalination project at the Applied Energy Sources, Huntington Beach Generating Station," Appendix-S in REIR, 2005, 100 pp.

Hunt, H., 2002, "American experience in installing horizontal collector wells", *Chapter 2 Riverbank Filtration: Improving Source Water Quality*, Kluwer Academic Publishers, pp.29–34.

Inman, D. L., S. A. Jenkins, 1996, "Wave climate cycles and coastal engineering practice," *Coastal Eng., 1996, Proc. 25th Int. Conf., (Orlando)*, Amer. Soc. Civil Eng., Vol. 1, Ch. 25, p. 314–327.

Inman, D. L. & S. A. Jenkins, 1999, "Climate change and the episodicity of sediment flux of small California rivers," *Jour. Geology,* v. 107, p. 251–270. http://repositories.cdlib.org/sio/cmg/2/

Inman, D. L. & S. A. Jenkins, 2002, "Scour and burial of bottom mines, a primer for fleet use," *University of California, San Diego*, Scripps Institution of Oceanography, SIO Reference Series 02-8, text, fig. & appen. 100 pp. http://repositories.cdlib.org/sio/reference/02-8/

Inman, D. L. & S. A. Jenkins, 2004a, "Climate patterns in the coastal zone," p. 301–305 in M. Schwartz, ed., *Encyclopedia of Coastal Science*, Kluwer Academic Publishers, Dordrecht, Netherlands. http://repositories.cdlib.org/sio/cmg/3/

Inman, D. L. & S. A. Jenkins, 2004b, "Energy and sediment budgets of the global coastal zone," p. 506–514 in M. Schwartz, ed., *Encyclopedia of Coastal Science*, Kluwer Academic Publishers, Dordrecht, Netherlands. http://repositories.cdlib.org/sio/cmg/5/

Inman, D. L. & S. A. Jenkins, 2004c, "Accretion and erosion waves on beaches," p. 1–4 in M. Schwartz, ed., *Encyclopedia of Coastal Science,* Kluwer Academic Publishers, Dordrecht, Netherlands. http://repositories.cdlib.org/sio/cmg/6/

Jenkins, S. A. and J. Wasyl, 2004, "Hydrodynamic modeling of source water make-up and concentrated seawater dilution for the ocean desalination project at the AES Huntington Beach Generating Station," Appendix- C in REIR, 2005, 298 pp.

Jenkins, S. A. and J. Wasyl, 2005, "Coastal evolution model," Scripps Institution of Oceanography Tech Report No. 58, 179 pp + appendices. http://repositories.cdlib.org/sio/techreport/58/

Jenkins, S. A. and D. L. Inman, 2006, "Thermodynamic solutions for equilibrium beach profiles", *Jour. Geophys. Res.,* v.3, C02003, doi:10.1029/2005JC002899, 2006. 21pp.

Jenkins, S. A., Inman, D.L., Michael D. Richardson, M.D., Thomas F. Wever, T.F.and J.Wasyl, 2007, "Scour and burial mechanics of objects in the nearshore", IEEE Jour.Oc.Eng, vol.32, no. 1, pp 78-90.

Jenkins, S. A., 2007, "Receiving Water Dilution Analysis for the West Basin Municipal Water District Redondo Beach Temporary Ocean Water Desalination Demonstration Facility" submitted to MWH America, 113 pp.

Jenkins, S. A. and J. Wasyl, 2008, "Wedge-Wire Intake Screen Flow Analysis for the West Basin Municipal Water District Redondo Beach Temporary Ocean Water Desalination Demonstration Facility", submitted to MWH Americas, 28 September 2008, 47 pp.

Jenkins, S. A. and J. Wasyl, 2014 "Oceanographic and Sediment Transport Analysis of Optimal Siting of a Seabed Infiltration Gallery (SIG) at the Huntington Beach Desalination Facility", prepared for Poseidon Resources, submitted to the Independent Science and Technology Advisory Panel (ISTAP), California Coastal Commission, 78 pp.

Jones, A. T., 2008, "Can we reposition the preferred geological conditions necessary for an infiltration gallery? The development of a synthetic infiltration gallery", *Desalination* vol. 221, pp.598–601.

Kawaguchi, A., 2007, "Findings from the site visit to the Fukuoka Desalination Plant," MWH Technical Memorandum, 4 October, 2007, 6 pp.

Kessler, T. J., and Harvey, C. F. (2001). The global flux of carbon dioxide into groundwater. *Geophysical Research Letters* 28(2), 279-282.

LePage, S., 2004, "Salinity tolerance investigation: supplemental report for the Huntington Beach Desalination Project", submitted to Poseidon Resources, 29 pp.

Los Angeles County Department of Regional Planning (LADRP). 2012. Marina del Rey Land Use Plan: A Component of the Los Angeles County Local Coastal Program. Accessed at http://planning.lacounty.gov/view/marina_del_rey_land_use_plan/in June 2013.

Malfeito, J., 2006, "San Pedro del Pinatar desalination plant: first year of operation with A horizontal drilled intake*", Proceedings, International Desalination Association Desalination and Water Reuse International Forum and Exposition,* Tianjin, China, Sept. 6–8, 2006.

Malfeito, J. and A. Jimenez, 2007, "Horizontal drains for seawater desalination experience of Cartagena", *Proceedings, American Membrane Technology Conference and Ex- position*, Las Vegas, Nevada, 2007.

Macpherson, G. L. 2009. CO2 distribution in groundwater and the impact of groundwater extraction on the global C-cycle. *Chemical Geology* 264, 328-336.

Missimer, T., 1997, "Technical evaluation of Ranney collectors for raw water supply to seawater reverse osmosis treatment facilities", *Proceedings, International Desalination Association World Congress on Desalination and Water Reuse*, Madrid, Spain, vol. 1, pp. 439–454

Missimer, T., 2009, *Water Supply Development, Aquifer Storage, and Concentrate Disposal for Membrane Water Treatment Facilities, 2nd edition,* Schlumberger Limited, Sugar Land, Texas.

Missimer, T., Ghaffour, N., Dehwah, H., Rachman, R., Maliva, R., and G. Amy, 2013, "Subsurface intakes for seawater reverse osmosis facilities: Capacity limitation, water quality improvement, and economics", *Desalination*, vol. 322, pp 37-51.

MBC Applied Environmental Services, 2002, "National pollutant discharge elimination system 2002 receiving water monitoring report AES Redondo Beach L.L.C. Generating Station Los Angeles, California," prepared for AES Redondo Beach L.L.C., 62 pp. + appens.

MBC Applied Environmental Services, 2003, "National pollutant discharge elimination system 2003 receiving water monitoring report AES Redondo Beach L.L.C. Generating Station Los Angeles, California," prepared for AES Redondo Beach L.L.C., 63 pp. + appens.

MBC Applied Environmental Services, 2004, "National pollutant discharge elimination system 2004 receiving water monitoring report AES Redondo Beach L.L.C.

Generating Station Los Angeles, California," prepared for AES Redondo Beach L.L.C., 62 pp. + appens.

MBC Applied Environmental Services, 2005, "National pollutant discharge elimination system 2005 receiving water monitoring report AES Redondo Beach L.L.C. Generating Station Los Angeles, California," prepared for AES Redondo Beach L.L.C., 70 pp. + appens.

MBC Applied Environmental Services, 2006, "National pollutant discharge elimination system 2006 receiving water monitoring report AES Redondo Beach L.L.C. Generating Station Los Angeles, California," prepared for AES Redondo Beach L.L.C., 73 pp. + appens.

NCDC, 2004, National Climate Data Center Document Library: http://www4.ncdc.noaa.gov/ol/documentlibrary/datasets.html

NGDC, 2013, *National Geophysical Data Center*, available from the URL: (http://www.ngdc.noaa.gov/mgg/gdas/gd_designagrid.html)

NOAA, 2013, National Oceanic and Atmospheric Association (NOAA), Verified/Historical Water Level Data, URL: http://www.opsd.nos.noaa.gov/data_res.html

NOAA, 2010, National Oceanic and Atmospheric Association (NOAA), National Data Buoy Center. URL: http://ndbc.noaa.gov/

Osborne, R.H., Darigo, N.J., and R.C. Scheidman, 1983, "Potential Offshore Sand and Gravel Resources of the Inner Continental Shelf of Southern California," California Department of Boating and Waterways, Sacramento, California, 302 p., 31 tables, 69 figures.

Pankratz, T., 2014, "WDR visits Fukuoka" *Water Desalination Report*, vol. 50, no. 2.

Peters, T. and D. Pinto, E. Pinto, 2007, "Improved seawater intake and pre-treatment system based on Neodren technology", *Desalination*, vol.203, pp. 134–140.

Peters, T. and D. Pinto, 2010," Seawater intake and partial pre-treatment with Neodren results from investigation and long-term operation", *Desalin. Water Treat*., vol. 24, pp.117–122.

SEIR, 2010, "Subsequent Environmental Impact Report Sea Water Desalination Project at Huntington Beach," #2001051092, City of Huntington Beach, prepared by Dudek Consulting, May, 2010, 9 sections + append.

SIO, 2005, "Shore Stations Program", Scripps Institution of Oceanography, University of California, San Diego 9500 Gilman Drive, La Jolla, California 92093-0218, http://shorestation.ucsd.edu/active/index_active.html

U.S. Army Corps of Engineers (USACE), 1993, "Existing State of Los Angeles County Coast," US Army Corps of Engineers, Los Angeles District, Tech Rpt 93-1, 335 pp.

U.S. Army Corps of Engineers (USACE), 1999 (unpublished). *Chapter 4.-Beach Width and Profile Volumes,* Coast of California Storm and Tidal Waved Study-Los Angeles Region, Prepared by Coastal Frontiers Corporation for the Los Angeles District, 108 pp. + appen.

U.S. Army Corps of Engineers (USACE), 2001, "California Storm and Tidal Waves Study Los Angeles Region", Stage 3, Design Documentation Report, August 2001.

USGS, 1997, "USGS Digital Data Series DDS-37 at INTERNET URL," http://wwwrvares.er.usgs.gov/wgn96cd/wgn/wq/region18/hydrologic unit code.

Voutchkov, N., 2005, "Thorough study is key to large beach-well intakes, *Desalin. Water Reuse Q*. vol.14, no. 1, and pp.16–20.

Wang S., E. Leung, R. Cheng, T. Tseng, D. Vuong, D. Vuong, D. Carlson, J. Henson, S.Veerapaneni, 2007, "Under sea floor intake and discharge system", *Proceedings, International Desalination Association World Congress on Desalination and Water Reuse*, Maspalomas, Gran Canaria, Spain, October 21–26, 2007, IDAWC/MP07-104, 2007.

Wang, S., J. Allen, T. Tseng, R. Cheng, D. Carlson, J. Henson, 2009, "Design and performance update of LBWD's under ocean floor seawater intake and discharge system", *Alden Desalination Intake/Outfall Workshop*, October 16 2009.

APPENDIX A:
Sediment Characterization from Borings at the ESGS and RBGS Sites

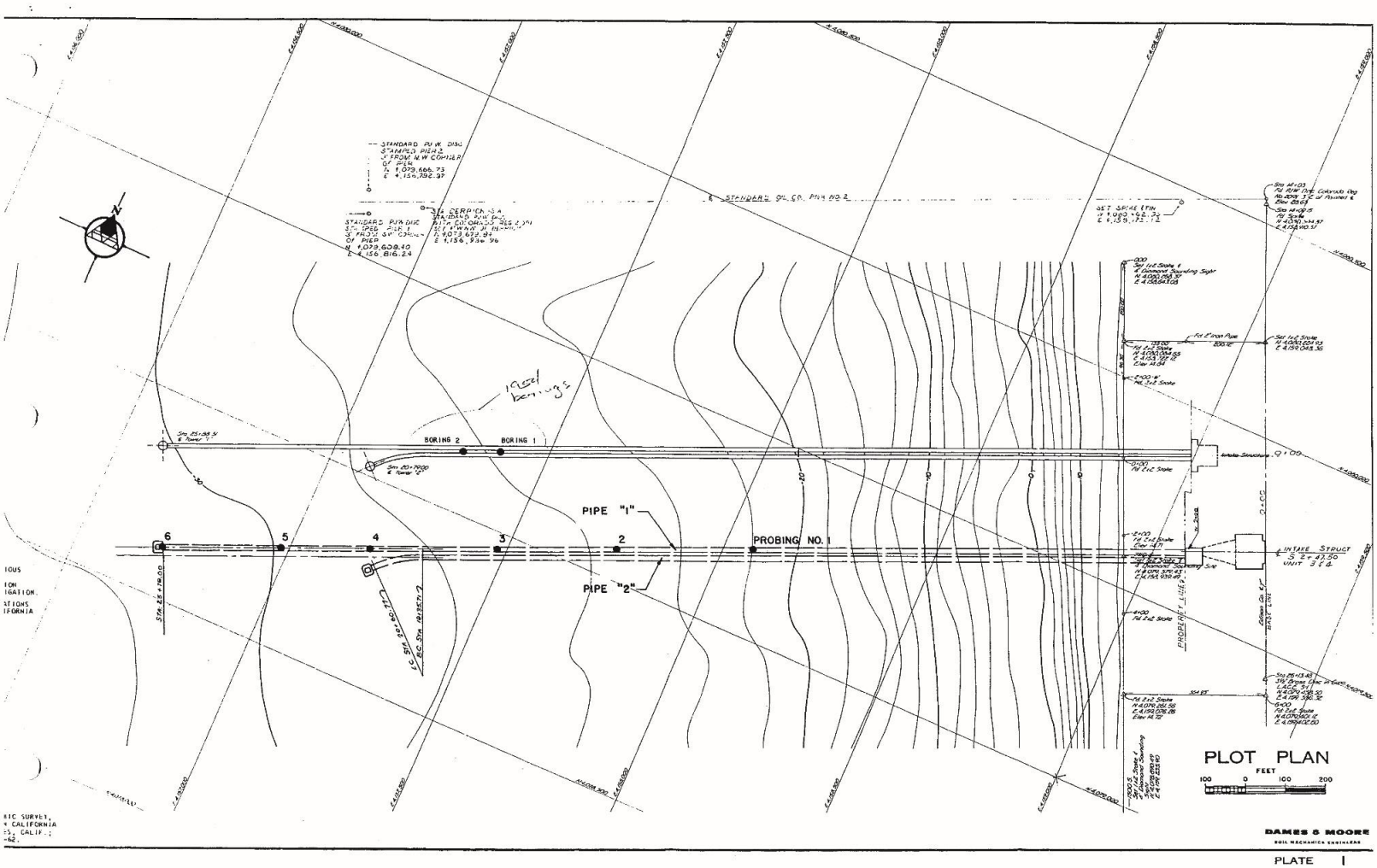
BORING 2
BORING 1
PIPE "1"
PIPE "2"
PROBING NO. 1
6
5
4
3
2
PLOT PLAN
FEET
100 0 100 200
DAMES & MOORE

PLATE 1

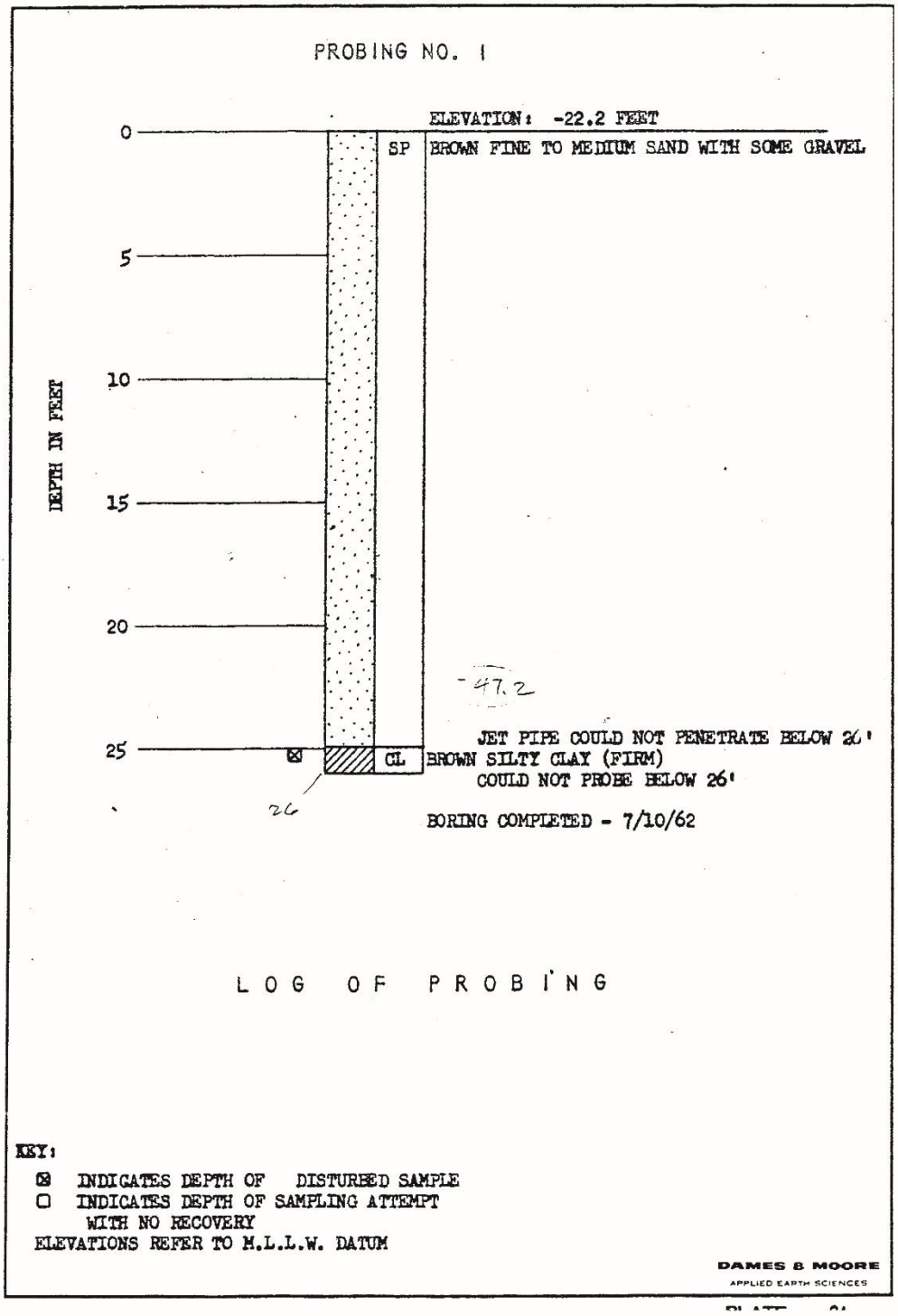
PROBING NO. 1
ELEVATION: -22.2 FEET
0
5
10
15
20
25
DEPTH IN FEET
SP
BROWN FINE TO MEDIUM SAND WITH SOME GRAVEL
-47.2
JET PIPE COULD NOT PENETRATE BELOW 26'
CL
BROWN SILTY CLAY (FIRM)
COULD NOT PROBE BELOW 26'
26
BORING COMPLETED - 7/10/62
LOG OF PROBING
KEY:
⊠ INDICATES DEPTH OF DISTURBED SAMPLE
□ INDICATES DEPTH OF SAMPLING ATTEMPT WITH NO RECOVERY
ELEVATIONS REFER TO M.L.L.W. DATUM
DAMES & MOORE
APPLIED EARTH SCIENCES
REVISIONS
BY DATE
Calif. Edison Co.
FILE 377-027
BY A.M. DATE 1-17-64
CHECKED BY

REVISIONS BY DATE

FILE 377-027 Alec Edson Co.

BY J.A.M. DATE 7-17-62 CHECKED BY

PROBING NO. 2

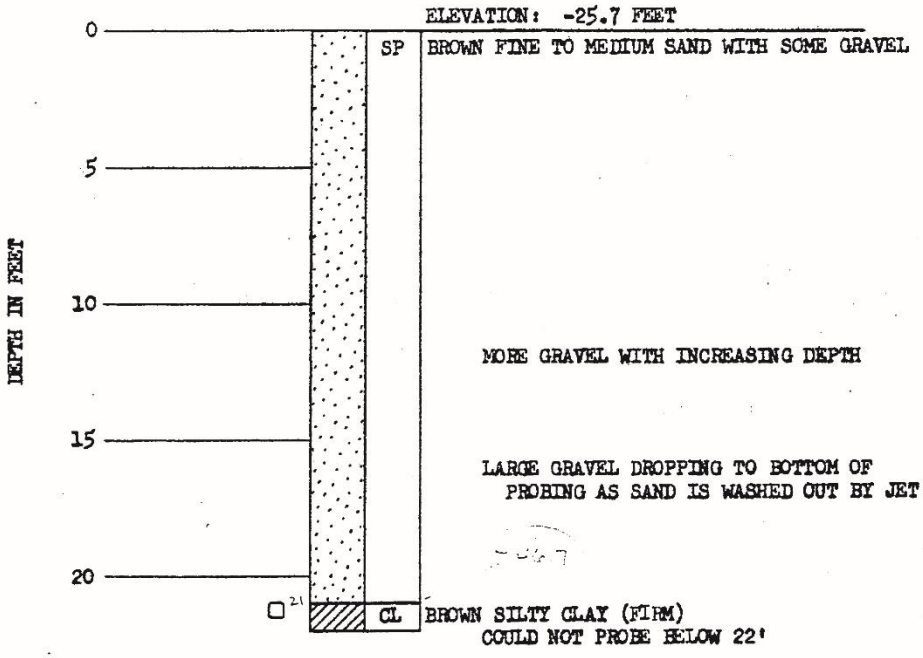

LOG OF PROBING

DAMES & MOORE
APPLIED EARTH SCIENCES

REVISIONS BY DATE

FILE 377-02 Calif Edison Co.

BY R.A.M. DATE 7-17-62
CHECKED BY

PROBING NO. 3

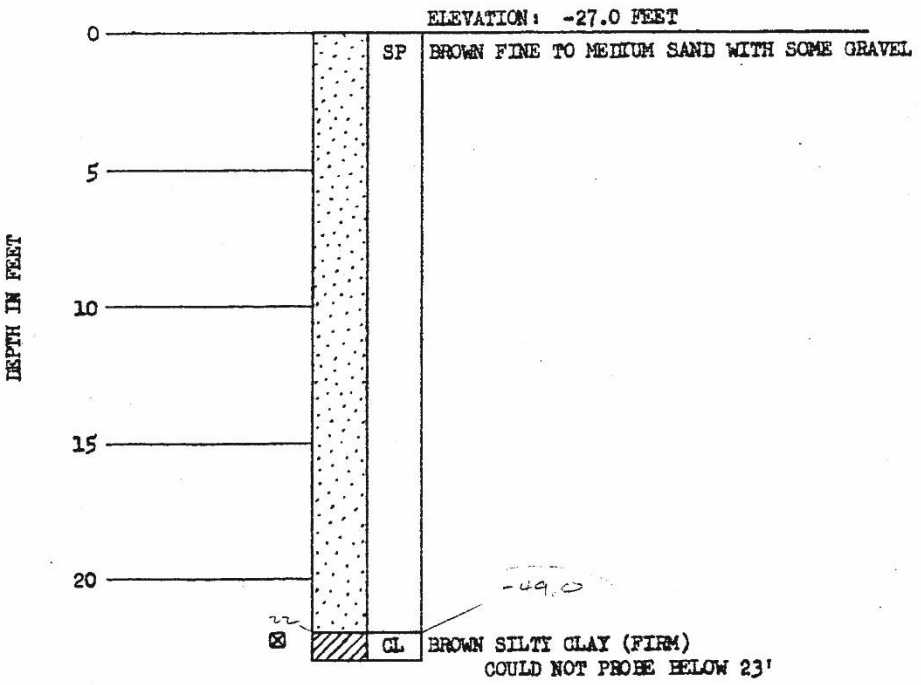

L O G O F P R O B I N G

DAMES & MOORE
APPLIED EARTH SCIENCES

REVISIONS BY DATE

FILE 377-022 Calif. Edison Co.

BY R.A.M. DATE 7-17-62 CHECKED BY

PROBING NO. 4

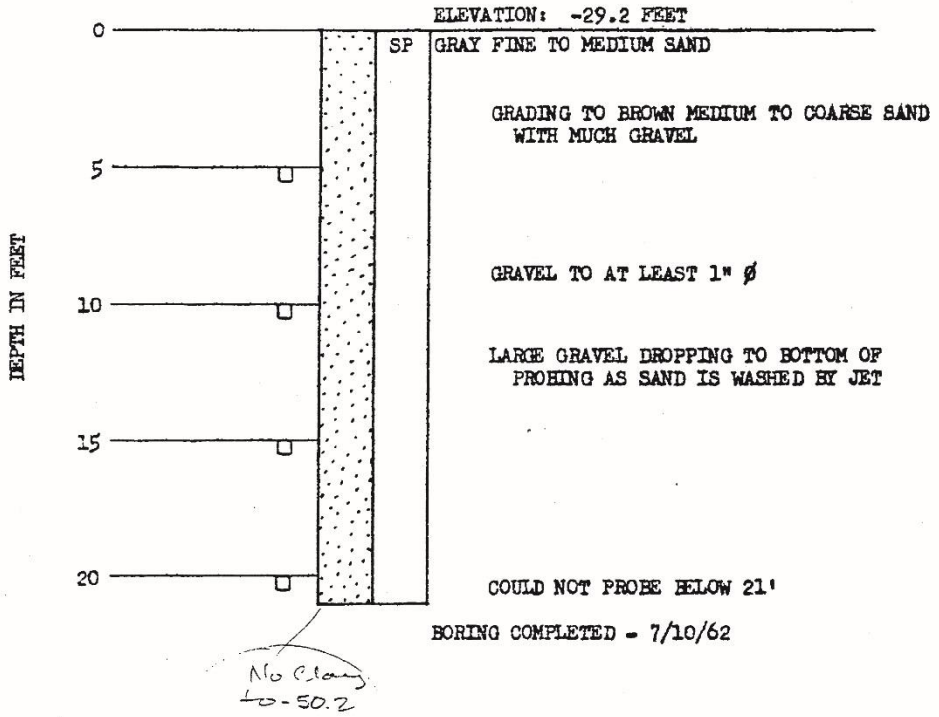

LOG OF PROBING

DAMES & MOORE
APPLIED EARTH SCIENCES

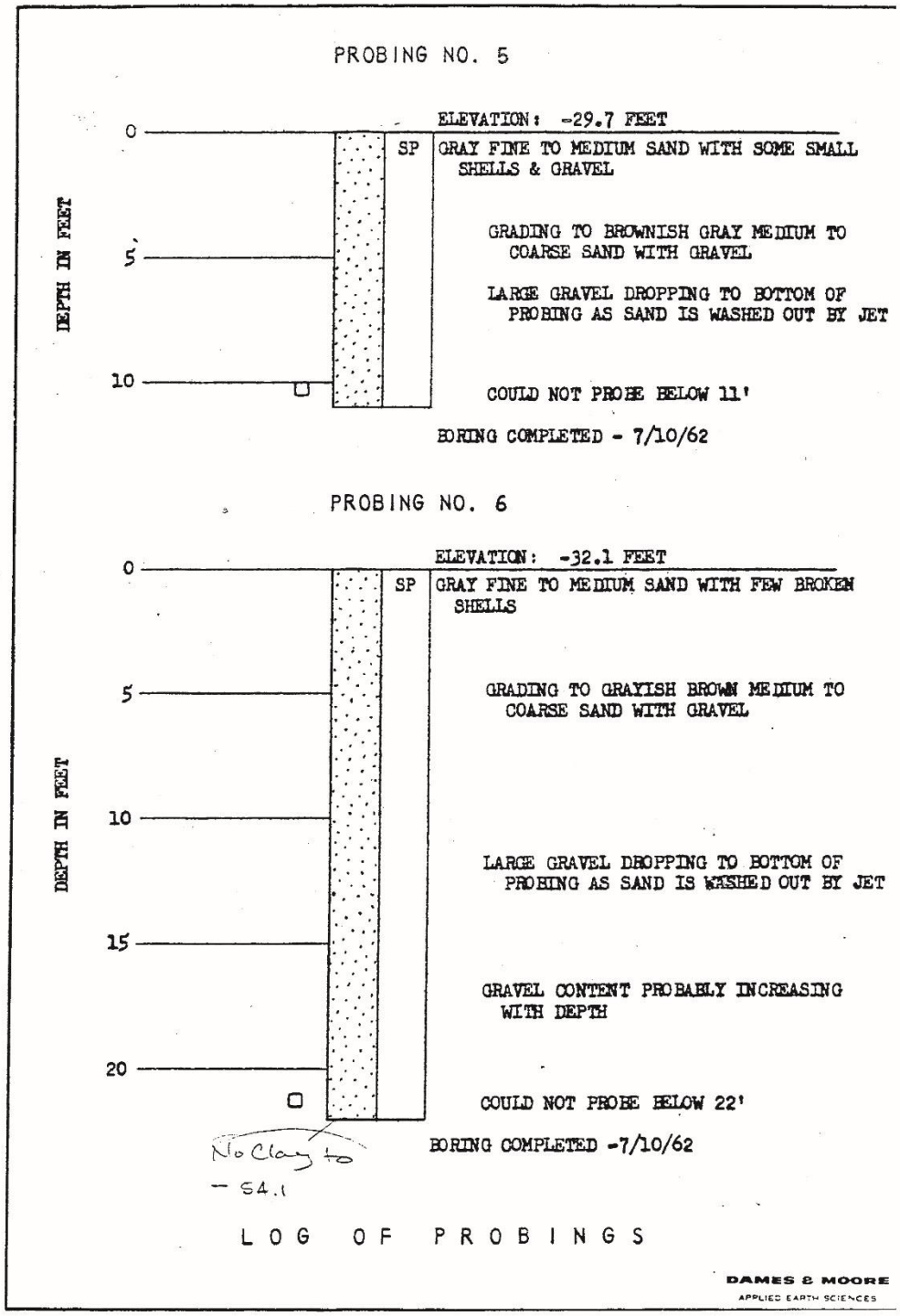
PROBING NO. 5
ELEVATION: -29.7 FEET
DEPTH IN FEET
0
5
10
SP
GRAY FINE TO MEDIUM SAND WITH SOME SMALL SHELLS & GRAVEL
GRADING TO BROWNISH GRAY MEDIUM TO COARSE SAND WITH GRAVEL
LARGE GRAVEL DROPPING TO BOTTOM OF PROBING AS SAND IS WASHED OUT BY JET
COULD NOT PROBE BELOW 11'
BORING COMPLETED - 7/10/62
PROBING NO. 6
ELEVATION: -32.1 FEET
DEPTH IN FEET
0
5
10
15
20
SP
GRAY FINE TO MEDIUM SAND WITH FEW BROKEN SHELLS
GRADING TO GRAYISH BROWN MEDIUM TO COARSE SAND WITH GRAVEL
LARGE GRAVEL DROPPING TO BOTTOM OF PROBING AS SAND IS WASHED OUT BY JET
GRAVEL CONTENT PROBABLY INCREASING WITH DEPTH
COULD NOT PROBE BELOW 22'
BORING COMPLETED -7/10/62
No Clay to -54.1
LOG OF PROBINGS
DAMES & MOORE
APPLIED EARTH SCIENCES
REVISIONS BY DATE
FILE 377-027 ALF, EDISON CO.
BY D.A.M. DATE 7-17-62
CHECKED BY

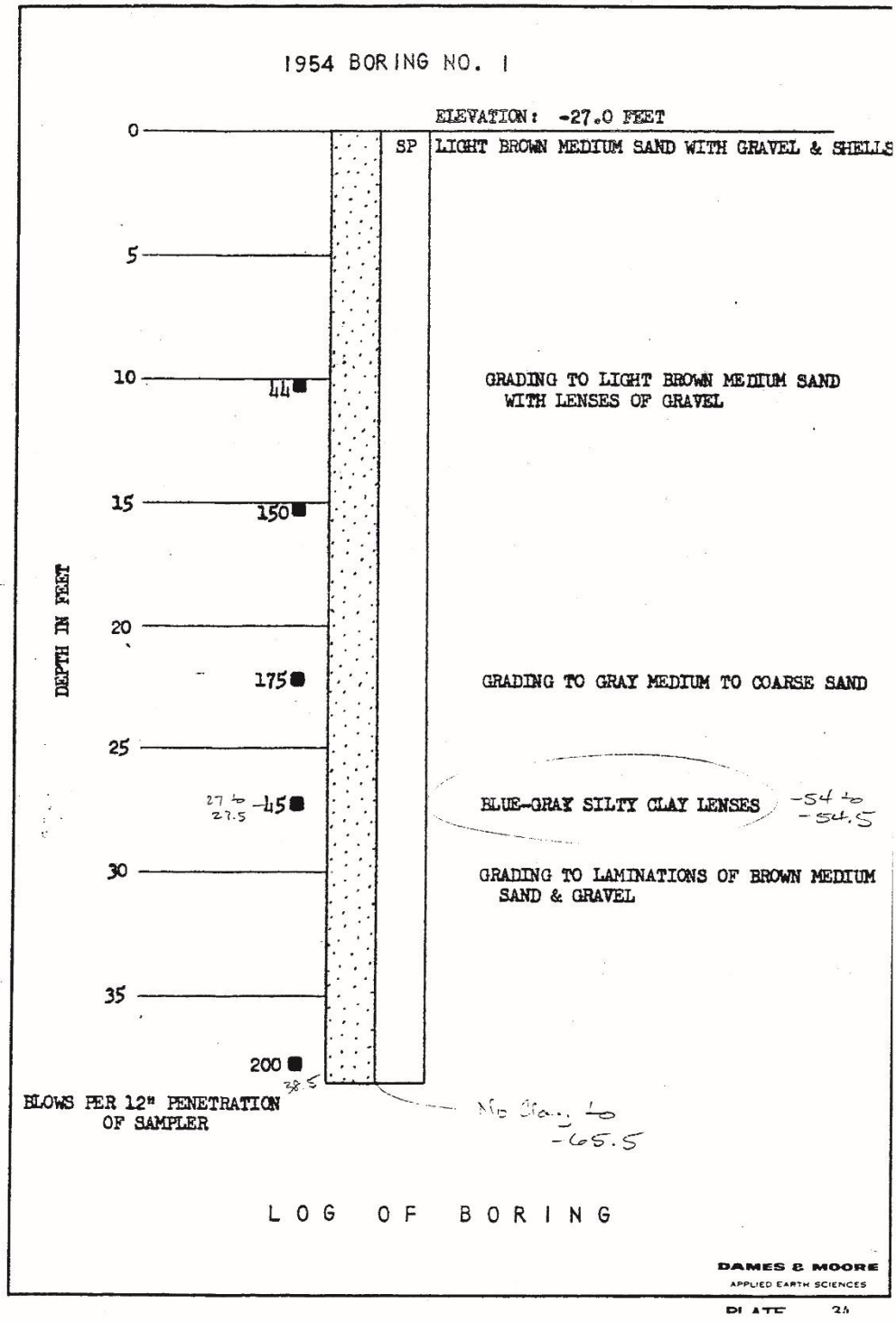
1954 BORING NO. 1
ELEVATION: -27.0 FEET
SP
LIGHT BROWN MEDIUM SAND WITH GRAVEL & SHELLS
GRADING TO LIGHT BROWN MEDIUM SAND WITH LENSES OF GRAVEL
GRADING TO GRAY MEDIUM TO COARSE SAND
BLUE-GRAY SILTY CLAY LENSES
-54 to -54.5
GRADING TO LAMINATIONS OF BROWN MEDIUM SAND & GRAVEL
No Sample to -65.5
DEPTH IN FEET
0
5
10
15
20
25
30
35
44
150
175
27 to 27.5
45
200
38
BLOWS PER 12" PENETRATION OF SAMPLER
LOG OF BORING
DAMES & MOORE
APPLIED EARTH SCIENCES
REVISIONS
BY DATE
CALEDISON CO.
FILE 23770-07
BY J.A.M. DATE 12-4-62
CHECKED BY

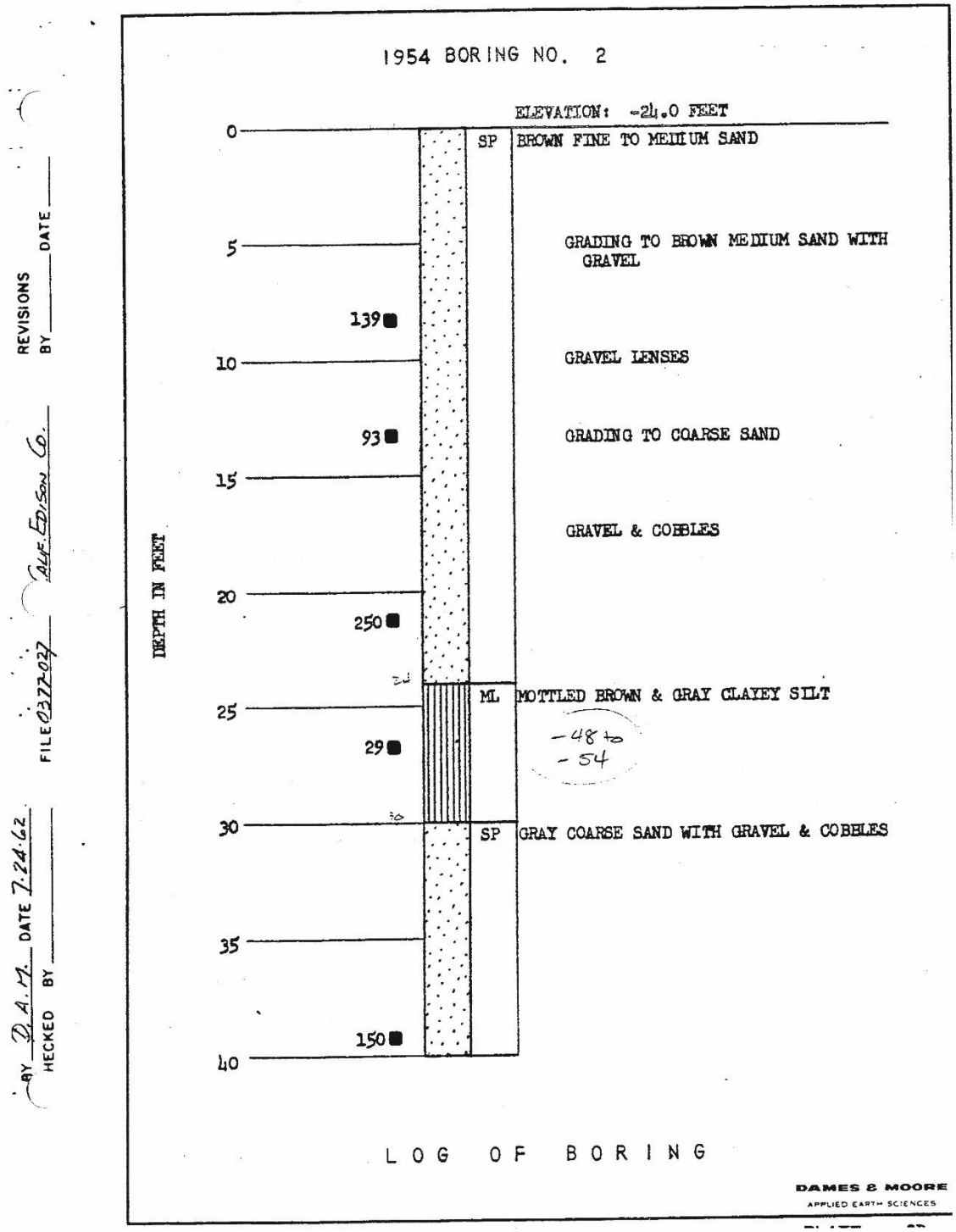
1954 BORING NO. 2
ELEVATION: -24.0 FEET
DEPTH IN FEET
0
5
10
15
20
25
30
35
40
139
93
250
29
150
SP
BROWN FINE TO MEDIUM SAND
GRADING TO BROWN MEDIUM SAND WITH GRAVEL
GRAVEL LENSES
GRADING TO COARSE SAND
GRAVEL & COBBLES
ML
MOTTLED BROWN & GRAY CLAYEY SILT
-48 to -54
SP
GRAY COARSE SAND WITH GRAVEL & COBBLES
LOG OF BORING
DAMES & MOORE
APPLIED EARTH SCIENCES
REVISIONS BY DATE
FILE 0377-027 Alle Edison Co.
BY D.A.M. DATE 7-24-62
CHECKED BY